THE WEAR OF MATERIALS IN AN ASH CONDITIONER

Alan Cuddon

A Dissertation submitted to the Faculty of Engineering, of the University of Cape Town, in fulfilment of the requirements for the Degree of Master of Science in Engineering.

Department of Materials Engineering
University of Cape Town
January 1989

For my family, in appreciation
of their patience and help

DECLARATION

I declare that this dissertation is my own unaided work except where due acknowledgement is made to others. It is submitted to the Department of Materials Engineering, University of Cape Town for the degree of Master of Science in Engineering. It has not been submitted for any degree or examination to any other university.

Signature removed

Signed by candidate

Alan Cuddon

31st day of January 1989

ABSTRACT

The abrasive nature of fly ash handled in large coal-fired power stations results in unacceptable material and maintenance costs in ash-water mixing plant.

Wear testing has been carried out in situ using a variety of generic materials. A ranking order of wear performance has been established both as a function of material and operating costs, and it has been demonstrated that impressive cost savings can be effected by the use of ceramic-coated steel mixing blades. The performance of such composites has been found to be sensitive to the design and method of application.

To optimise materials selection, a family of tungsten carbide-cobalt cermets together with a number of structural ceramics were tested in situ. The modes of wear can be related to material constitution. By ranking the performance of these candidate materials, value based materials selection and design for use can be applied.

ACKNOWLEDGEMENTS

The author wishes to express his gratitude to the following people and organisations :

Associate Prof. C Allen of the Department of Materials Engineering, University of Cape Town for his supervision and insight during this programme of work.

Mr. L Fourie of EID, Eskom for his assistance with the running of in situ tests.

Mr. E Olsen of Didier-Furnace Services, for providing ceramic materials and helpful advice.

To Boart Hardmetals, Springs for supplying WC-Co test materials and helpful advice.

Mr. P Terblanche of ITC, Wadeville for his discussions, encouragement and provision of ceramic test materials.

To Dynamic Ceramic, U.K. for supplying ceramic test materials.

To the Photographic Section of EID, Eskom.

To Mrs. Marie Cuddon, my mother for typing this manuscript.

To Mrs.H. Böhm for her help with the SEM analyses and for tracing the drawings as well as Mr. B. Greeves and Mr. J. Petersen for photographic assistance.

To Mr. W Morrison for sample preparation.

To Lethabo Power Station for their involvement in the programme of work.

To Eskom for financial support of the programme of work and permission to publish the manuscript.

LIST OF FIGURES

Figure 4.8 Loss of a tile from a blade due to mechanical damage during cleaning the conditioner after a period of service.

Figure 4.9 (a) The design which provided the most satisfactory performance after 6600 hours of service.
(b) A schematic diagram of final design for ceramic protective cappings on steel mixing blades. The middle segments lock against the outer segments, which are fixed to the blade by means of welded inserts. All segments are attached to the blades by means of epoxy adhesive.

Figure 5.1 Test blade showing positioning of test grades and references.

Figure 5.2 Detail of test and reference piece geometry.

Figure 5.3 (a) Orientation of wear tracks on a blade tip.
(b) Positioning of test pieces to account for orientation of wear tracks.

Figure 5.4 Variation in wear intensity as a function of position across the test blade periphery.

Figure 5.5 Cumulative volume losses with respect to test time for test pieces. Note the presence of incubation and steady state regimes. All test grades displayed trends falling within the shaded area. All trends have equivalent gradients in the steady state region.

Figure 5.6 Steady state wear rates for the reference pieces as a function of position along the blade periphery.

Figure 5.7 Relative wear resistance values for the test materials normalised against the reference material, S20.

Figure 5.8 Steady state wear rates for the test materials as a function of volume percent Co binder.

Figure 5.9 Relation between steady state wear rates for the test materials as a function of bulk material hardness.

Figure 5.10 Effect of carbide grain size on steady state wear rates.

Figure 5.11 Effect of mean free path between carbide grains on steady state wear rates.

Figure 5.12 Influence of abrasive hardness on the abrasive wear behaviour of homogeneous and heterogeneous materials.

Figure 5.13 Influence of cobalt content and grain size on the toughness of WC-Co alloys as determined by transverse rupture tests.

Figure 5.14 Retarded binder removal in a low binder content WC-Co alloy having high contiguity.

Figure 5.15 Significant binder removal in a high binder content WC-Co alloy having poor contiguity.

CONTENTS

CHAPTER I

INTRODUCTION

Coal fired power stations in the local power utility, Eskom, generate electricity through the combustion of finely milled coal, called pulverized fuel. This combustion results in the production of large quantities of fly ash and smaller quantities of boiler coarse ash. In most modern stations ash is continuously removed from the generating units and transported to ash heaps via a sequence of sliding and rolling conveyors. The condition of the ash is below its water saturation level.

Fly ash constitutes the major proportion of the ash and originates as small airborne particles which are separated from the flue gas by passing through electrostatic precipitators. Once the fly ash is precipitated, the ash free flue gas is removed via induced draught fans to the chimneys. The fly ash is removed by en masse conveyors from below the precipitators and taken to a dry fly ash bunker. These conveyors consist of mechanical pin and link type construction and slide on rails. Flights welded to the links scrape the fine ash along a duct towards a removal end. (Fig. 1.1)

Dry fly ash then gravity feeds through the fly ash bunker into a water blender, termed an ash conditioner. The flow of ash is controlled by a sliding gate. The ash conditioner consists of an enclosed bin which houses two parallel and adjacent shafts, each with a number of aligned blades which mix the ash with water when the shafts rotate. (Fig. 1.2) Ash is continuously fead through the conditioner and exits onto roller conveyor belts through a chute.

Each power generating unit has a set of these ash removal systems which are interchangeable between adjacent units in the advent of maintenance or stops due to faults.

These conveyor belts convey the conditioned ash towards a transverse conveyor belt running the length of the station and collecting ash from each unit.

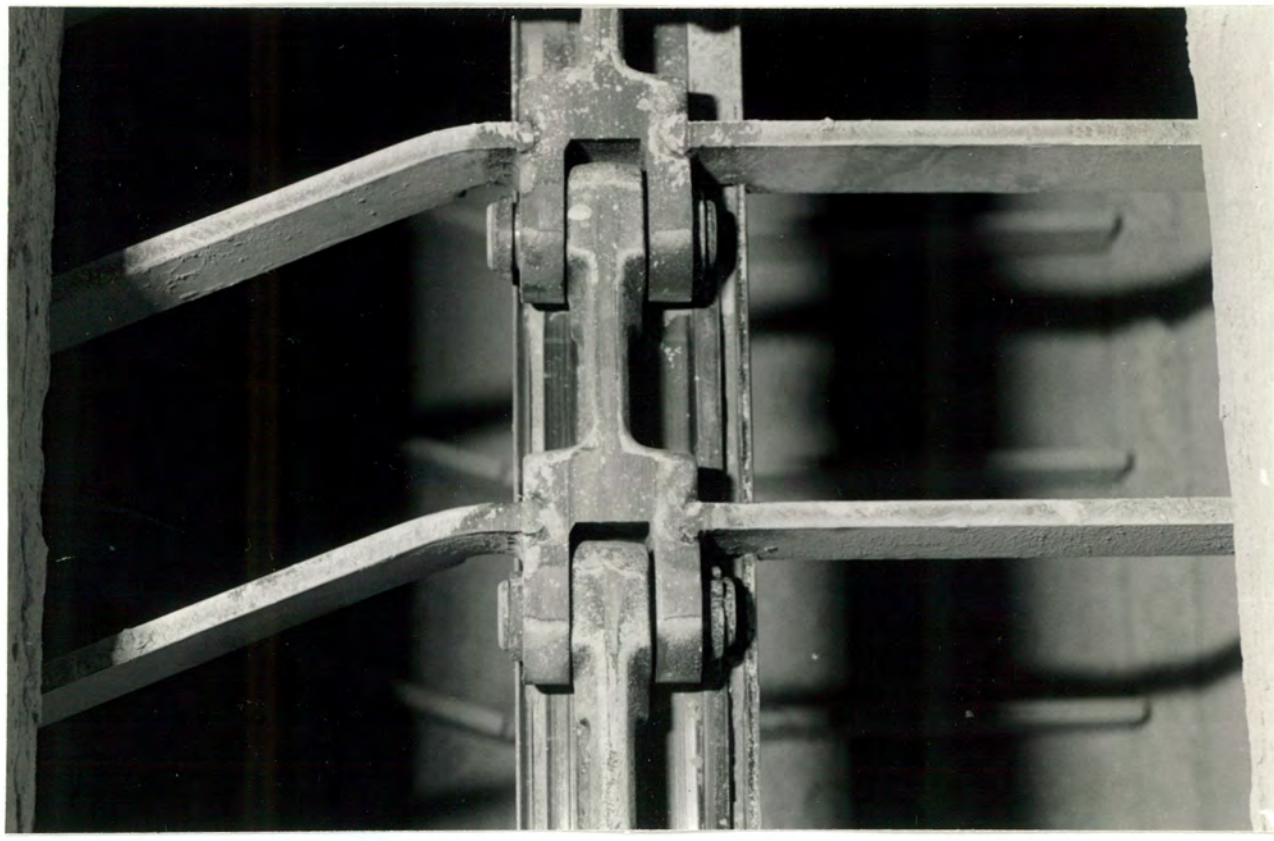

Figure 1.1 En masse conveyor removing fly ash in an ash duct. Take note of abrasion on the rail located under the links.

Figure 1.2 Ash conditioner showing positioning of mixing blades located on counter rotating shafts.

Coarse ash, collected from below the boiler, joins the fly ash along this transverse conveyor line. Coarse ash which collects at the bottom of the burner fired boilers is removed by means of a mechanical conveyor which is submerged in water which seals the bottom of the boiler off from the atmosphere. This conveyor consists of a dual chain driven arrangement of scrapers. The scrapers are suspended between the chains at equidistant spacings to each other. The ash is removed from the submerged deck by the scraper conveyor which transports the ash out of the bath and up a drainage slope. At this point the ash is deposited on a conveyor belt which transports the coarse ash to the transverse conveyor belt running the length of the station. Figure 1.3 illustrates the working principle of the submerged scraper conveyor, viewed here on the return side of the drainage deck, after having dumped the ash. The chains are gear driven by means of hydraulically powered sprockets and shaft. (Fig.1.4)

Located at the end of each conveyor belt are two sets of belt cleaners which remove adhered ash and water. These consist of scrapers which are held against the belt surface on a sprung arm, tangential to the belt. This arrangement is located at the removal end of each belt. (Fig. 1.5)

It has been reported [1] that wear of these items illustrated in figs. 1.1 through to 1.5 is a source of considerable down time and replacement costs. It was considered that attention should be given to correct material selection for these components based upon the testing and evaluation of materials in situ.

The frame of reference for this programme is that locally produced materials should be given preference and that design of application for the various materials be simple and robust.

Aims and Objectives

The overall aim of this programme of work is to minimise wear of ash handling plant and to reduce operating costs through an understanding of the factors which control the mechanisms of wear.

Figure 1.3 Return side of the drainage deck of a submerged scraper conveyor. Flights are suspended between two parallel running chains. Flights are seen moving over a surface lined with alumina tiles.

Figure 1.4 Sprocket used for driving the chains in a submerged scraper conveyor.

Figure 1.5 (a) Belt cleaning scraper, on a sprung arm held tangential to a conveyor belt.

(b) Scraper blade

The specific objectives of the work were to:

(a) Evaluate a range of potential materials for use in ash conditioning plant through in situ testing.
(b) Ascertain mechanisms of wear.
(c) Relate wear performance to material constitution.
(d) Produce a ranking order of wear resistance based on cost.

CHAPTER 2

REVIEW OF LITERATURE ON ABRASIVE WEAR

In general terms, the Oxford Dictionary defines **wear** as :

"Injure surface of, partly consume or obliterate, damage, attenuate or alter, by rubbing or use".

The term **abrasive** can be defined as:

"substance capable of rubbing or grinding down, tending to graze the skin".

These descriptions can conjure many ideas and thoughts and can be used to fit a persons understanding of abrasive wear.

A more specific description is desirable as a technical reference. For example the DIN standard on wear, DIN 50 320 (1979) describes wear as follows:

"Wear is the progressive loss of substance from the surface of a solid body due to contact and relative motion of a solid, liquid or gaseous counterbody".

Further to this, DIN 50 320 describes abrasion as a distinct wear mechanism :

"Abrasion is the removal of material by ploughing and/or microcutting processes".

The more technical description from the DIN standard, identifies a system as being responsible for a particular result, namely material removal. The standard then specifies the mechanism of removal. Clearly this description infers that when studying wear, the observer is actually looking at a system, which comprises of the surface of the material being removed, the

agents and their state causing material removal and the mechanisms of material removal. These basic components of a particular wear system interact with each other and determine the process behaviour. Hence it would be futile to separate these components in an effort to gain understanding of a particular process.

The role of material constitution and how it interacts in a wear system varies as the parameters determining the wear process diverge. Most work to date has concentrated on the effect of particular material properties on wear resistance for example hardness, toughness and strain accommodation. Moore [2], however states that a full understanding of how material properties influence abrasive particle contact and material removal, in different wear environments, is required before suitable materials selections can be made.

From this one begins to realise that many models are oversimplifications of a very complex dynamic process. Rabinowicz [3] for instance, proposed a simple equation for the volume removal during abrasion by a conical abrasive particle:

$$\frac{W}{s} = \frac{2 \tan a}{\pi} \frac{F}{H}$$

where W is the volume loss due to wear
s is the sliding distance of the cone
a is the angle between the cone face and material
H is the hardness of the wearing surface

This model assumes that all material is removed from the groove generated, in a single pass. Frequently material will be plastically pushed to the edges of the groove in ductile materials. Thus the model can not account for a material response where ploughing, or the plastic displacement of material to the edges of a wear groove, occurs to some extent. Furthermore the model suggests that hardness is the only controlling material property. No account is taken of fracture toughness, strain accommodation, ductility and phase transformations, all of which can play a role in an abrasive wear process. [4]

In practice material hardness does have a major influence on wear. However, since it is a single material parameter it can not account for the total wear process as it excludes plastic flow and fracture susceptibility of materials, which as mentioned often assist in determining the mode and rates of material removal.

In the classic findings of Kruschov and Babichov [5] a linear relationship was found to exist between wear resistance and hardness of various pure, annealed materials. A linear relationship, while less sensitive to hardness, was found for heat treated steels of specified carbon contents. As carbon content increased so did wear resistance. However Mutton and Watson [6] found that for heat treated steels a non linear relationship between wear resistance and material hardness occurred.

Richardson [7] takes not only the hardness of the material into account but also the hardness of the abrasive. (Fig. 2.1) Wear occurs at a low or high level depending on the hardness of the abrasive particles to the hardness of the surface being worn. The behaviour exhibits a transition from a lower to a higher level of wear in a narrow hardness interval corresponding to a situation where the two opposed surfaces in contact have about the same hardness. For a heterogeneous material e.g. cemented carbide, the interval is broader as an integrated result of the different constituents.

Clearly microstructure is an important issue. Mutton and Watson [6] found that in two-phase alloys containing hard brittle particles and in single-phase alloys of high ductility the mechanisms of groove formation was fundementally different for identical test procedures. Moore [2] summarises the role of microstructure in abrasive wear into two major effects. Both effects are clearly system interactions and determined by mutual responses. The first is when microstructure influences bulk properties, including the initiation of cracks. This occurs when the size of microstructural features are smaller than the depth of indentation of abrasive particles. The second is when microstructural features become effective as discrete components and their individual properties assume increasing importance. This is generally the case when the size of microstructural features is about equal to or larger than the depth of indentation of abrasive particles.

This can be used convincingly as a qualitative proposal for the transition from a high wear level to a low wear level as the hardness of the abrasive is "increased" for abrasion on a particular material. In the hard abrasive region (high wear level), indentation of abrasive particles is significant and large in relation to microstructural features. In the soft abrasive region, indentation is less significant and of the order of size of microstructural features resulting in the discrete responses of individual constituents in two phase materials. However once again this argument is open to criticism as it is not possible to alter abrasive hardness of naturally occurring abrasives without changing density and particle geometry.

Support is given by some recent work by Hokkirigawa and Kato [8] who elucidate this behaviour by means of some lateral thinking. Instead of increasing the hardness of abrading particles and thereby changing other particle characteristics, the load on a relatively hard hemispherical indentor was simply increased to provide increased depth of penetration and increased angle of attack. Angle of attack can be described as the angle between the abrading particle and material surface. It was found that as the degree of penetration and angle of attack increased, by sliding the loaded indentor, the degree of wear increased. This was explained by observing a change from a ploughing to a microcutting mechanism. (Fig. 2.2) However damage to relatively soft abrasive particles which often occurs was not accounted for in this study. Nevertheless a qualitative argument is provided which contributes to understanding the effect of material - abrasive interaction on the mechanism of wear.

Mulhearn and Samuels [9] and Murray et al [10] found the existence of a critical attack angle below which no cutting; only ploughing occurs. This angle was found to vary greatly from one material to another. Not only would this vary for different materials but also for different abrasive particles which have different strengths and therefore different abilities to penetrate a wearing surface for a particular set of particle dynamics. It is also easily visualised that the angle of attack is also sensitive to particle geometry. For instance as a spherical particle penetrates the surface, the angle of attack increases, whereas for a conical indentor on which the cited work is based, the angle remains constant for increasing penetration.

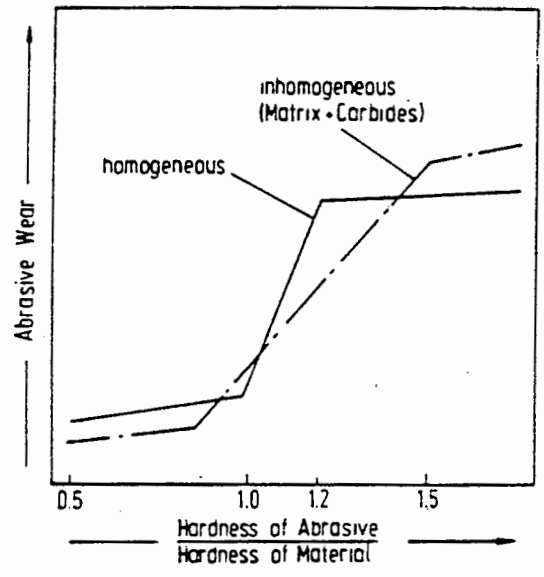

Figure 2.1 Abrasive wear as a function of increasing abrasive hardness for homogeneous and heterogeneous materials.

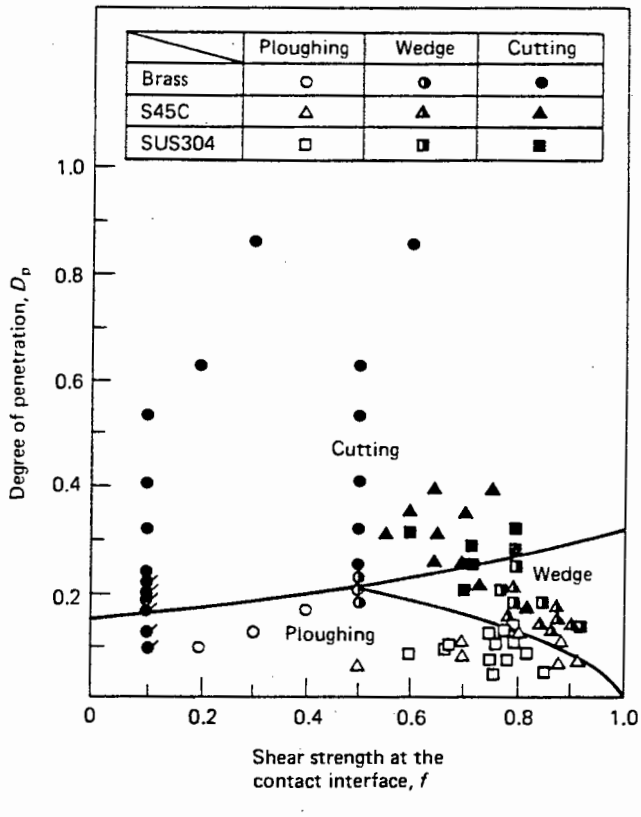

Figure 2.2 Transition in abrasive wear mechanisms as a function of increasing penetration for shear strength at the contact interface between a hemispherical sliding rider and material surface. [8]

At this stage it is necessary to clearly describe ploughing and microcutting features. These features are well illustrated by Zum Gahr [11] who states that ideally ploughing due to a single pass of one abrasive particle does not result in any detachment of material from a wearing surface. A prow is formed ahead of the abrading particle and material is continually displaced sideways to form ridges adjacent to the groove produced. Volume loss can however occur owing to the action of many abrasive particles or the repeated action of a single particle. Material may be ploughed aside repeatedly by passing particles and may break off by low cycle fatique. Pure microcutting results in a volume loss by chips equal to the volume of the wear grooves. Microcracking occurs when highly concentrated stresses are imposed by abrasive particles, particularly on the surface of brittle materials. In this case, large wear debris are detached from the wearing surface owing to crack formation and propagation. Microploughing and microcutting are the dominant processes on ductile materials while microcracking becomes important on brittle materials. (Fig. 2.3)

However once again microstructure is an important consideration in view of the above discussion. For instance in brittle materials having a pronounced granular structure as opposed to an amorphous structure, microcracking is more confined and limited to an order of grain size. Cracking may accumulate to form lateral cracks which can sometimes be described by fracture mechanics models. This is however not always the case as poor correlation often exists between toughness given by K_{Ic} and wear performance for ceramics, as the scale of fracture for K_{Ic} determination are in the order of size of indentations, whereas fracture due to a wear event is frequently in the order of grain sizes. These were the findings of Ajayi and Ludema. [12]

The contribution of fracture to increased wear is dependent on the size of wear grooves and on the mechanical properties and microstructure of the material. Zum Gahr [11] has rationalised this behaviour, for wear by a hard abrasive by plotting the relation between fracture toughness and abrasive wear resistance of metals and ceramics. (Fig. 2.4) As fracture toughness increases, wear resistance increases to a maximum, which tends to

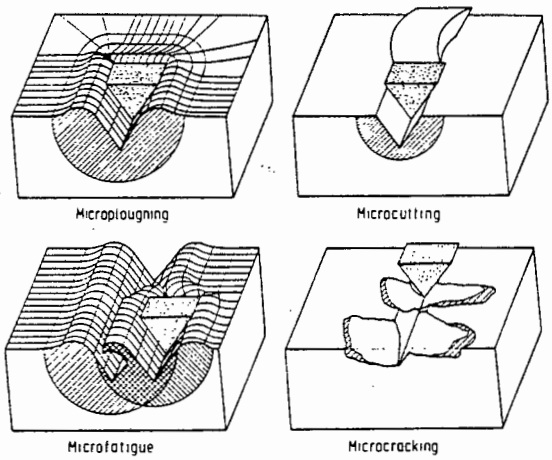

Figure 2.3 Schematic illustration of abrasion mechanisms resulting from physical interactions between abrasive particles and the surface of materials. [11]

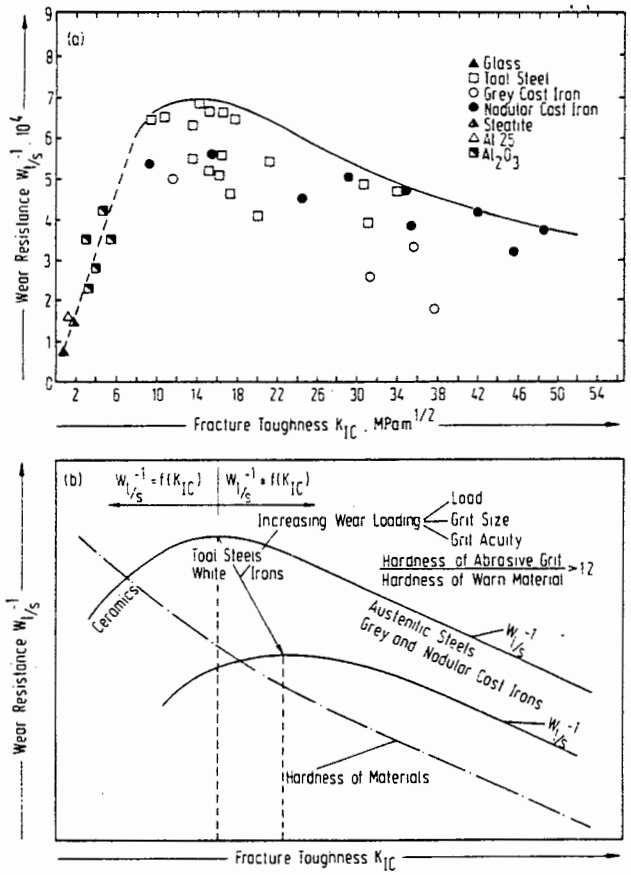

Figure 2.4 Relation between fracture toughness and abrasive wear resistance of different metallic and ceramic materials: (a) experimental data (b) schematic illustration [11].

a higher fracture toughness value for increasing groove size i.e. increasing applied load and for abrasive particle size. The dependency of wear rate on fracture toughness decreases as hardness decreases. Clearly as hardness is further compromised, wear resistance decreases. This suggests a compromise between hardness and toughness to be beneficial.

The designer should not loose track of this last comment as this to a large degree determines the versatility of materials employed.

Moore and Douthwaite [13] determined that high strains measured at worn surfaces occur due to a hydrostatic stress system being set up ahead of and below abrading particles. This stress increases the ductile stress and strain to fracture by suppressing ductile fracture processes. It is therefore expected that the wear of ductile materials is controlled by their strain hardening behaviour. Moore, Richardson and Attwood [14] observed that the worn surfaces of ductile materials, reached, by the above mechanism, a limiting strength, which is dependent on the metallurgical structure of the metal and the addition of substitutional elements. It is suggested that the limiting process is fracture and that the hydrostatic stress system imposed by the wear process inhibits the onset of fracture until some local fracture criterion is established.

Hence it is probable that ploughing is largely attributed to a high degree of strain hardening and high fracture toughness, inherent in a particular material. This would imply that cutting would occur in materials having a low capacity for strain hardening and low fracture toughness. However it is common knowledge that the two mechanisms often occur simultaneously, even though one may predominate. Hence these findings can not be used to solely describe wear behaviour in metals.

A number of other interactive phenomena are also common in abrasive wear, which include stress induced phase transformations from austenite to martensite at wear surfaces having sufficient energy. This imparts high hardness to the surface (martensite) while maintaining a tough inner core (austenite). These materials are particularly effective in resisting severe impact. Similar mechanisms occur in grinding media made of high chrome white cast irons, where the austenitic matrix at the surface

transforms to martensite. This can however enhance the propogation of cracks existing in the carbides, to extend beyond the carbide boundaries resulting in higher wear rates.

Interaction between an abrasive wear system and a corrosive environment are common in mineral transport equipment, Noël [15]. Barker and Ball [16] propose that abrasion and corrosion are synergistic since the kinetics of corrosion are influenced by abrasion. The effects of the frequency of abrasive and corrosive actions are different for steels of different levels of chromium. Low chromium steels are reported to perform better under low frequency of wear events, whereas steels with higher chromium levels resist wear better when wear events are frequent and periods between events brief. Noël [15] found that abrasion accelerates the rate of corrosive attack in metals because of the localised zones of high energy which are anodic with respect to underlying zones of lower energy. It was also found that by increasing the abrasion load, only a small incremental increase of volume loss due to corrosion arose. Hence for applications where abrasive-corrosive wear occurs continuously under high loads in a corrosive medium, the proportional effect of corrosion can become negligible. For applications which involve low loads and frequent abrasion, the proportional effect can become dominant.

Three types of corrosion behaviour at an abraded surface were identified by Barker and Ball [16]. Steels having low chromium content show general corrosion immediately after abrasion and have no induction period. Steels with intermediate levels of chromium content have short induction periods prior to localised corrosion action. High chromium steels (12 weight percent chromium and above) passivate immediately after an abrasive action and have infinite induction periods, and only loose material by pitting corrosion. Thus an increase in the alloying content, and in particular chromium, improves the corrosion resistance by increasing the induction period and decreasing the rate of volume loss from an abraded surface. (Fig. 2.5) A minimum chromium level of eight percent is required in order to reduce the weight loss due to corrosion.

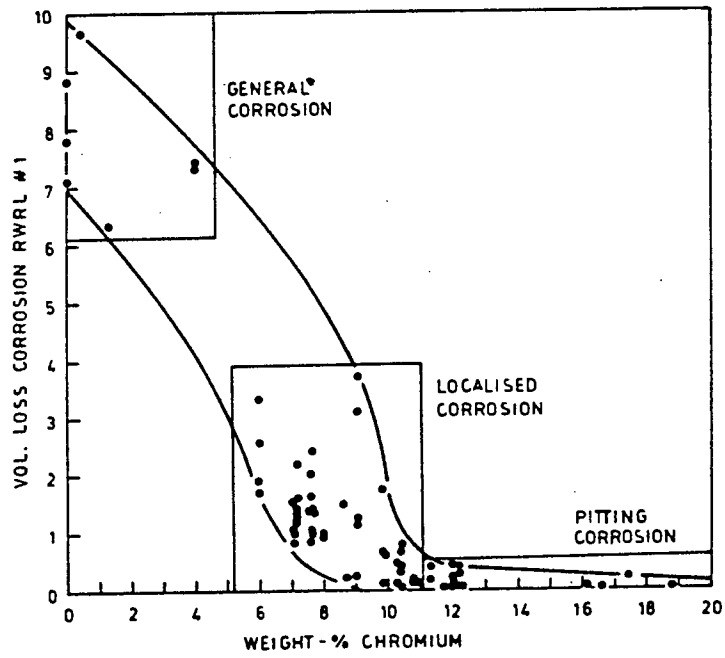

Figure 2.5 Volume loss due to corrosion of an abraded surface as a function of chromium content. Three types of corrosion are indicated.

In conclusion it is clear that wear is best dealt with in a systematic fashion in order to establish any benefit. Attempts to explain wear processes in terms of simplified models have shortcomings and are open to continued criticism. In this regard great care must be excercised in any attempt to isolate a system parameter and determine its effect on wear performance. A more lucid approach is to establish performance by relating the wear process in a wear system to material constitution, abrasive characteristics and mechanisms of degradation. This realisation lays the groundwork on which this programme of work is based.

CHAPTER 3

IN SITU TESTING OF GENERIC MATERIALS IN AN ASH CONDITIONER: INITIAL STUDIES

Introduction

The most meaningful method of collecting data by which materials can be ranked for wear resistance is to perform wear testing in situ. Consequently the ash conditioning plant at Lethabo Power Station was selected for this initial study.

An ash conditioner is shown schematically in Figure 3.1. It consists of two worm mixing shafts which move the fly ash-water mixture through the containment bin. Each shaft has twenty-five mixing blades set at an angle of 18.5° to the axis. This helix angle is designed to allow for sufficient residence time for complete mixing of the ash and water. The blades are normally manufactured from roller quenched and tempered medium carbon steel and have a maximum peripheral speed of 1.6 m/s. The throughput of the hot (70°C) ash-water mixture averages 150 tons per hour. The moisture content of the mixture can be varied between 8 and 25 per cent. The effluent water used has a pH between 9 and 11 and contains highly variable concentrations of sulphate, nitrate, chloride and hydroxide ions.

The ash particles vary in size from less than 1 micrometer up to 250 micrometers diameter. Fifty per cent of the particles by mass are finer than 10 micrometers in diameter, with some 5 per cent of particles being greater than 180 micrometers in diameter. (Fig. 3.2)

The ash itself is extremely abrasive being composed mainly of spherical glass particle shells and sphere aggregates. (Fig. 3.3) Quartz is the only identifiable phase being present as single grains [17], which may be encapsulated in glass shells. These grains still retain signs of sharp edges and conchoidal fractures, indicating that they survive the combustion process. Mullite [$3(Al_2O_3).2(SiO_2)$] and to a lesser extent phases of iron oxides are present as directional crystals in clear glass spheres.The ash has a hardness of approximately 1200 HV, essentially due to the glass spheres and quartz grains.

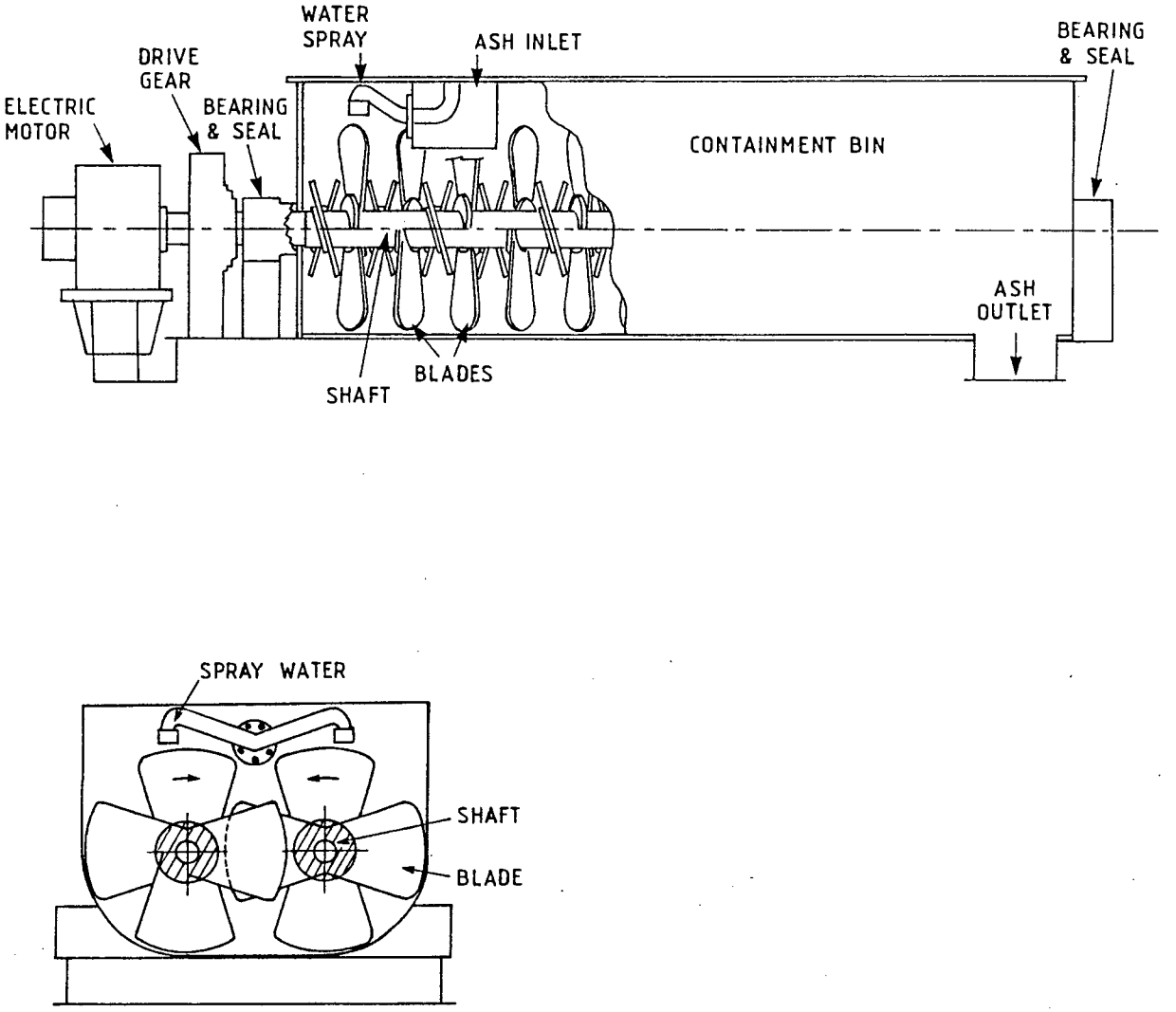

Figure 3.1 Schematic side and end views of an ash conditioner.

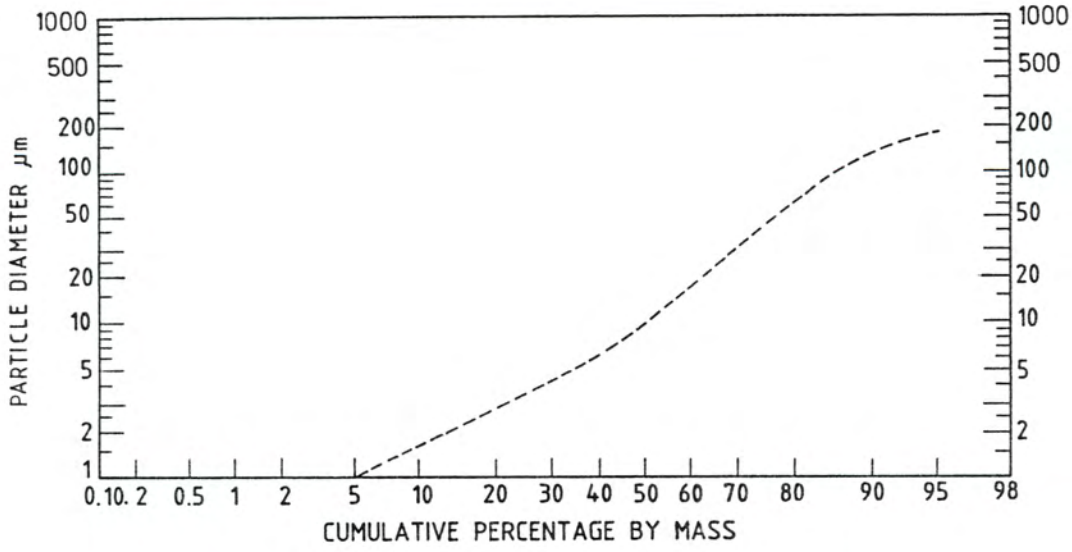

Figure 3.2 Particle size distribution of a representative fly ash sample taken at Lethabo Power Station.

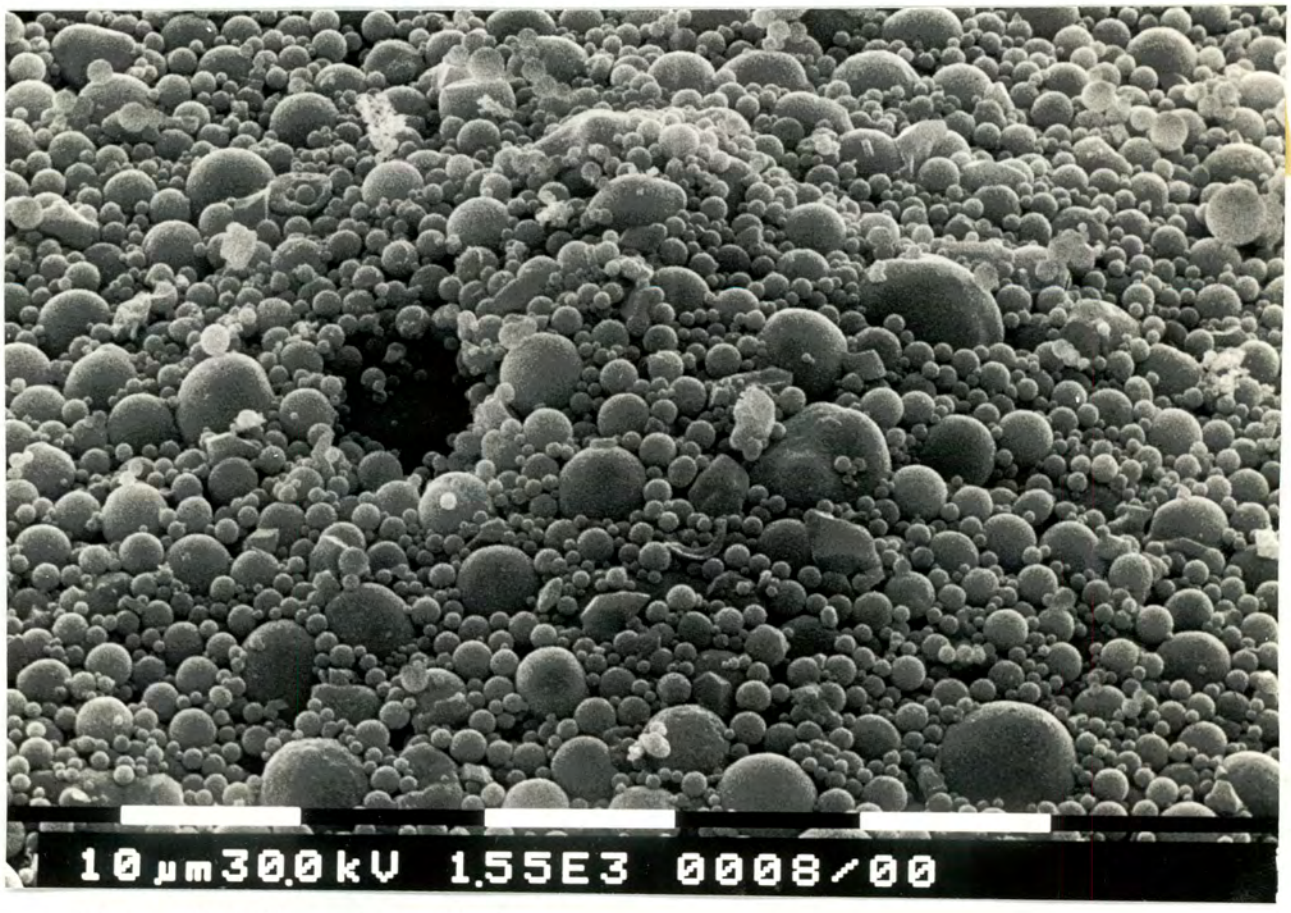

Figure 3.3 Fly ash particles.

The aggressive nature of the ash-water mixture results in rapid wear of the steel mixer blades, and lifetimes as low as three months have been reported. [18].

Initial observations of worn blades showed that wear occurred predominantly at the blade tip. (Fig. 3.4) The worn blade depicted has been in service for 2000 hours and is shown on top of an unused blade. Inspection of the mixer revealed that ash was encrusted on the inside surface of the bin. As the blades move across this encrusted layer, additional ash is compacted between the blade tip and the encrustation giving rise to three body type abrasive wear of the metal blades. Figure 3.5 shows typical ploughing and grooving of the metal surface associated with this abrasive wear process. Conversely, the blade faces are largely protected by adhering ash and experience little wear.

It was also noted that wear of the blades varied as a function of their position in the ash conditioner. Digitising of the worn profiles of the blades and calculating the area lost for a period of service provided an indication of the wear gradients in the mixer. It can be seen in figure 3.6 that the material loss from the mixer blades rose to a maximum in the mid-section of the mixer, being much lower at the entrance and exit points.

The reason for this variation in blade wear is considered to be due to the abrasion stress levels to which the metal is subjected. Near the inlet position there is little compaction of the loose ash-water mixture against the bin wall, with the result that the contact stress between the abrasive particles and the moving blade tip is low. However as the ash advances through the conditioner, it becomes more compacted and encrusted on the sides of the bin, resulting in progressively greater contact stresses between the blades and the ash mixture, with consequent higher wear rates. The fall in wear rate from the mid-section to the bin exit can be attributed to a lowering of the back pressure on the blades as the mixture moves more freely. At the exit point little wear is experienced.

Figure 3.4 Extent of mixer blade wear after 2000 hours in service.

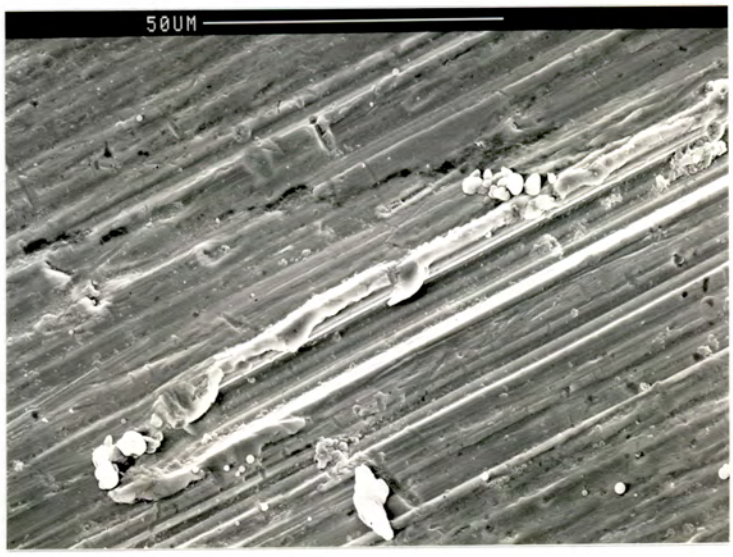

Figure 3.5 Typical ploughing and grooving on abraded service of steel blade tip, showing corrosion pitting.

Table 1
Description of materials.

Material	*Condition*	*HV30*	*Chemical composition*					*Structure*
			C%	*Cr%*	*Mn%*	*Si%*	*Other*	
Alloy A	HRA	160	0,03	11,0	0,8	0,35	0,3 Ti	Ferrite and martensite
AISI 304	HRA	185	0,03	18,0	1,3	0,35	8,0 Ni 0,1 Mo	Austenite
Alloy B	RQT	410	0,25		0,6	0,3	0,6 Mo	Tempered martensite
Alloy C	RQT	190	0,50		0,9	0,20		Ferrite and pearlite
Alloy C	Q	490	0,50		0,9	0,20		Martensite
Alloy C	Boronised	2 000*	0,50		0,9	0,20		Iron boride case; ferrite and pearlite core
Alloy D	RQT	570	0,30	0,8	1,6	0,7	0,7 Ni	Tempered martensite
Alloy E	Weld overlay	680	0,43	5,2	1,1	0,25	1,2 Mo	Martensite, austenite and carbides
Alloy F	Weld overlay	625	4,2	36,5	0,8	1,5		Complex primary chromium carbides in eutectic austenite
Alloy G	Overlay plate	650	3,5	31,0	0,8			Complex primary chromium carbides in eutectic austenite
Alumina bead impregnated filled epoxy		1 800	85 % Al_2O_3 bead in SiC filled epoxy					Granular alumina beads, SiC powder, epoxy resin
Alumina tiles		2 000	90 % Al_2O_3					Sintered granular

*On surface only
RQT — Roller quenched and tempered
HRA — Hot rolled and annealed
Q — Quenched in oil from 850 °C

Table 2
Results of abrasion testing.

Material	*RWR*	*Cost index**
Alloy A	0,73–0,82	1,83–1,62
AISI 304	0,79–0,98	2,44–1,97
Alloy B	0,90–0,94	1,44–1,38
Alloy C ROT	1,00	1,00
Alloy C Q	1,24–1,36	0,92–0,84
Alloy C boronised	1,63–1,97	2,29–1,89
Alloy D	1,02–1,15	1,36–1,20
Alloy E	1,56–1,82	1,08–0,92
Alloy F	1,78–2,12	0,95–0,80
Alloy G	3,95–4,05	0,48–0,45
Alumina bead filled epoxy	3,76–5,94	0,63–0,41
Alumina	11,74	0,16

* Costs as at November 1987

3.1 Test design

It was clear from initial observations, that due cognisance should be taken of the positional wear gradient in the conditioner in any assessment of wear performance. Consequently, it was decided to adopt an approach in which only half of the twenty-five blades on each drive shaft would be replaced by candidate materials, the remainder being standard blade material. The reference blades were positioned at odd intervals and the test blades at even intervals in the test numbering system shown in Figure 3.7. In this way the standard steel blades were used as a local measurement reference against which the performance of the various test materials could be evaluated.

Since different materials may react differently to varying intensities of abrasion, it was further decided that the test materials should be positioned in regions where both high and low stress intensities were experienced. The range of materials and coatings used in this series of testing are shown in Table 1. Candidate materials selected included corrosion resistant steels, proprietary wear resistant steels and surface coatings in the form of metal hardfacing weld overlays, composite ceramic polymeric coatings and ceramic tiles.

The test procedure followed was to measure the area of each blade through a digitising method both before and after testing for a total of 2 160 hours. This method of measurement was preferable to an assessment by mass loss, since a number of blades were of a composite nature either in the form of an overlay or surface treatment. The material loss was then compared to the material loss of the standard steel blades on either side of its position in the conditioner. The relative wear resistance (RWR) was then calculated as shown below:

$$RWR = (A_{z-1} + A_{z+1})/2A^{t}_{z}$$

where z = position in mixer

A = loss of area for reference blade

A^{t} = loss of area for test blade.

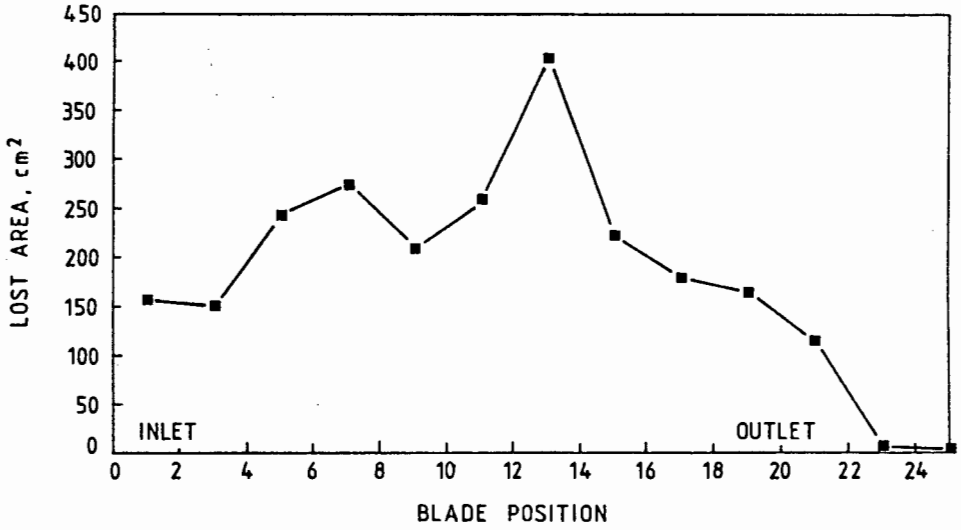

Figure 3.6 Wear of medium carbon steel blades as a function of position in the ash conditioner.

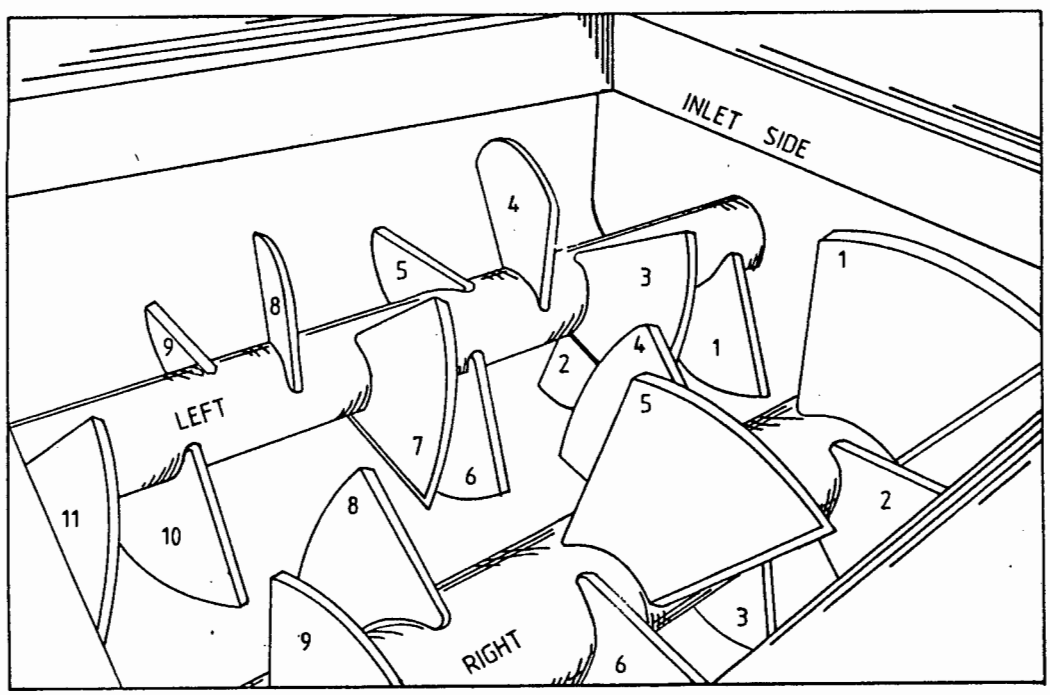

Figure 3.7 Schematic diagram of ash conditioner showing positioning of test and reference blades.

3.2 Results and Discussion

The results of the test programme in which a variety of generic materials were subjected to abrasive wear testing in an ash conditioner are shown in Table 2. The RWR values shown in Table 2 include results for positions of both high and low stress intensity. It can be seen that the relative wear resistance values (RWR) of these test materials, compared to the standard medium carbon blade material, varies from less than unity to approximately twelve for the alumina ceramic tiles.

Both the corrosion resistant steel (Alloy A) (Fig 3.8) and the stainless steel (AISI 304) have RWR values less than unity and thus perform worse than the standard roller quenched and tempered medium carbon steel (Alloy C). (Fig. 3.9) Such a result indicates that the synergistic action of corrosion during the operation of the conditioner does not play a significant role in the total wear process. Whilst there is strong evidence that corrosion of the steel mixing blades does occur, (Fig. 3.5), the loss of material due to abrasion completely overshadows any loss of material brought about by corrosion.

All the proprietary abrasion resistant alloys (Alloys B,C,D) (Fig. 3.10) showed similar performance in service with a RWR values ranging from 0.90 to a maximum of 1.36. The measured RWR values for these alloys is a function of carbon content and bulk hardness of the steels which ranged from 190HV30 (Alloy C) to 570HV30 (Alloy D). Such a result is not unexpected since other workers have found a similar relationship during the abrasive wear testing of metals and alloys, [5,6]. There are of course limits to increasing the hardness of steels to improve wear resistance since it generally leads to a decrease in toughness and the possibility of premature failure of components through brittle fracture.

Conversely, surface treatments on steel can provide high surface hardness or wear resistance whilst maintaining a tough and strong underlying material. In the present work it has been shown that such an approach can result in significant improvement in wear resistance when applied to steel mixing blades in the ash conditioner. The treatments used ranged from one

in which a 0.6 mm thick superhard (2000 HV) iron boride layer is applied to the steel surface, (Fig. 3.11) to various 8 mm thick weld overlays (Alloys E, F and G). Alloy E has a martensite/austenite/carbide structure with a hardness between 650 - 700 HV. (Fig. 3.12)

Alloy F has an austenitic matrix containing extremely hard chromium carbides (Fig. 3.13) whilst Alloy G is a similar weld overlay to Alloy F but is produced as plate by an automated welding process which produces a more uniform distribution of fine chromium carbides. (Fig. 3.14) Such surface treatments can be seen from Table 2 to improve the life of the normal steel mixer blades by fifty percent through boronising to over four hundred percent in the case of the Alloy G coating.

Coating the steel blades with ceramic bead impregnated epoxy resin also provides a substantial improvement in wear resistance. (Fig. 3.15) Relative wear resistance values approaching six were obtained with such coatings. This coating consists of alumina beads, 2 - 5 mm in diameter, impregnated into a silicon carbide filled epoxy. The extremely high hardness of both the alumina (1800 HV) and silicon carbide (2700HV) clearly provides excellent wear resistance to the composite material.

These results should however be viewed with caution. Since the wear of the mixer blades occurs essentially at the blade tip then any advantage provided by a surface layer is substantially lost once this protective coating is worn away. Thus with increasing time the relative wear resistance of coated steel blades would be expected to decrease if the coating was not renewed. Furthermore, wear rates in general decrease with time as the blades themselves become smaller and the peripheral blade speed decreases. Note that the particle history on one blade is not the same for an adjacent blade hence the use of alternate reference blades can only be used for estimating the wear intensity at the location of a test blade. Thus the RWR values are not absolute but indicate a trend in performance.

The highest relative wear resistance of approximately twelve was provided by a ceramic tile coating. These 2 mm thick alumina tiles were bonded to the steel mixer blades with epoxy resin and far outperformed all other materials or coatings.

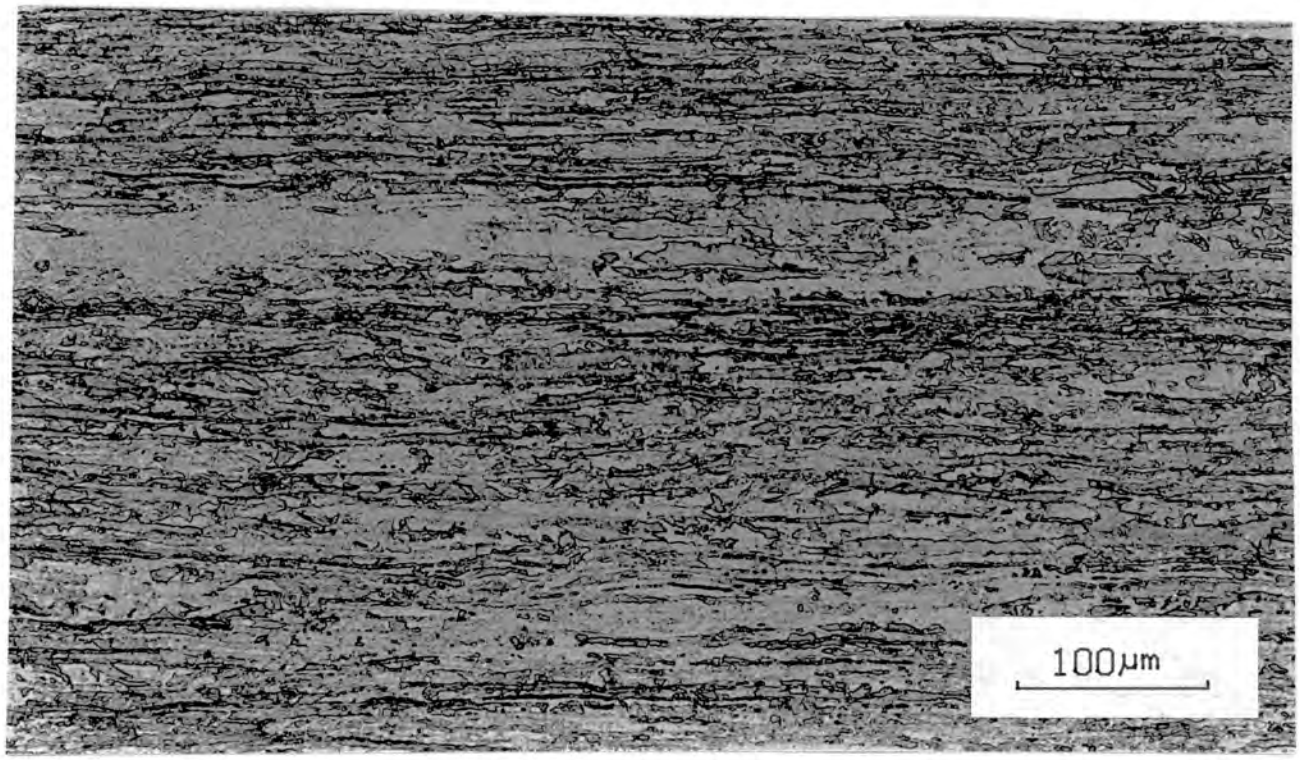

Figure 3.8 Microstructure of corrosion resistant steel (Alloy A). Elongated islands of martensite in ferrite.

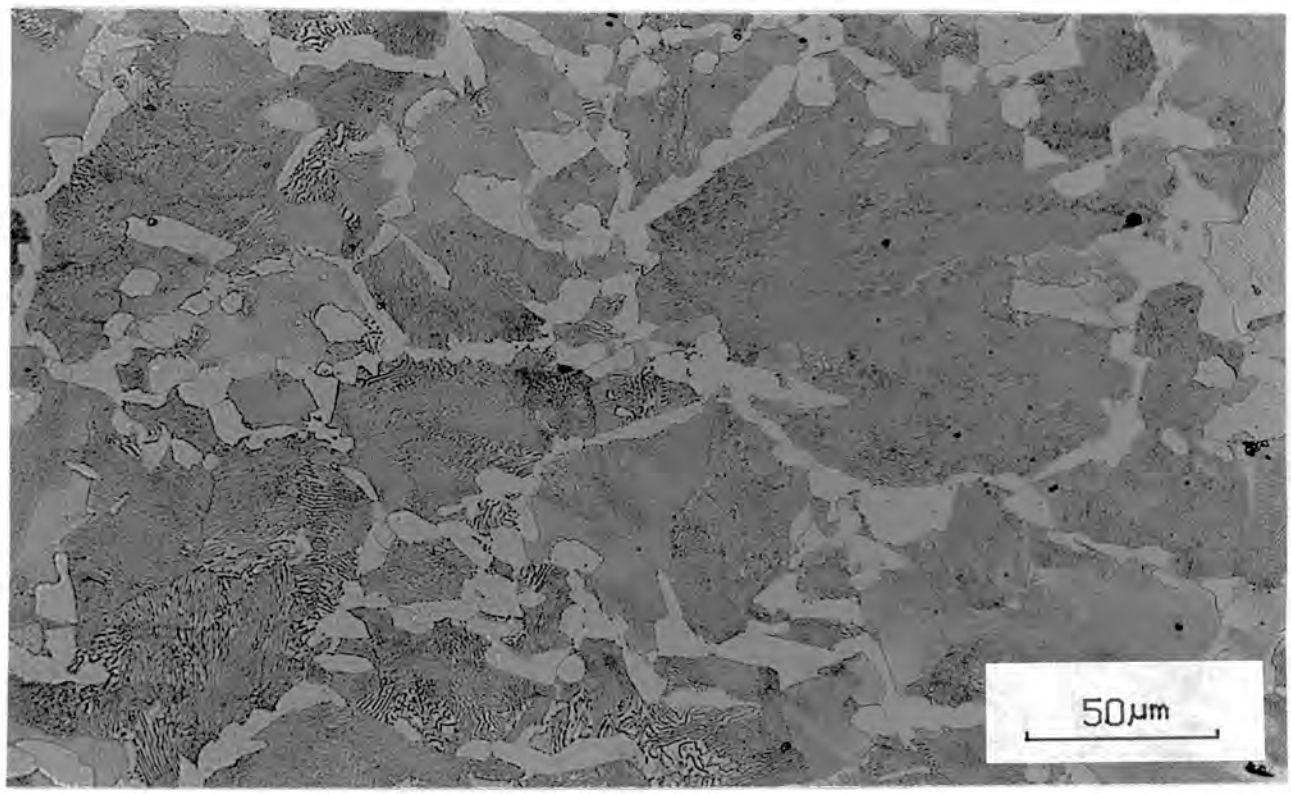

Figure 3.9 Microstructure of roller quenched and tempered medium carbon steel specified as standard material for the blades. Ferrite and pearlite.

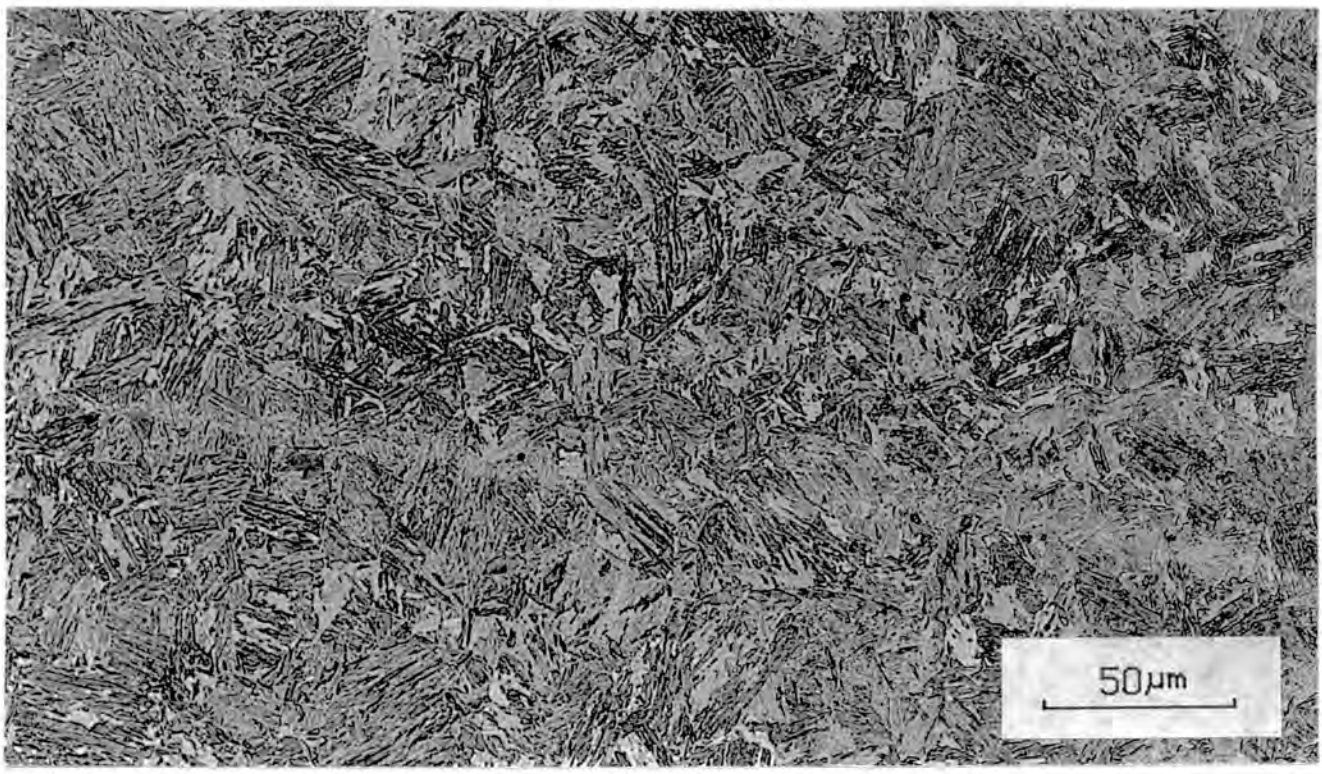

Figure 3.10 Microstructure of a proprietary abrasion resistant alloy having a tempered martensite structure (Alloy D)

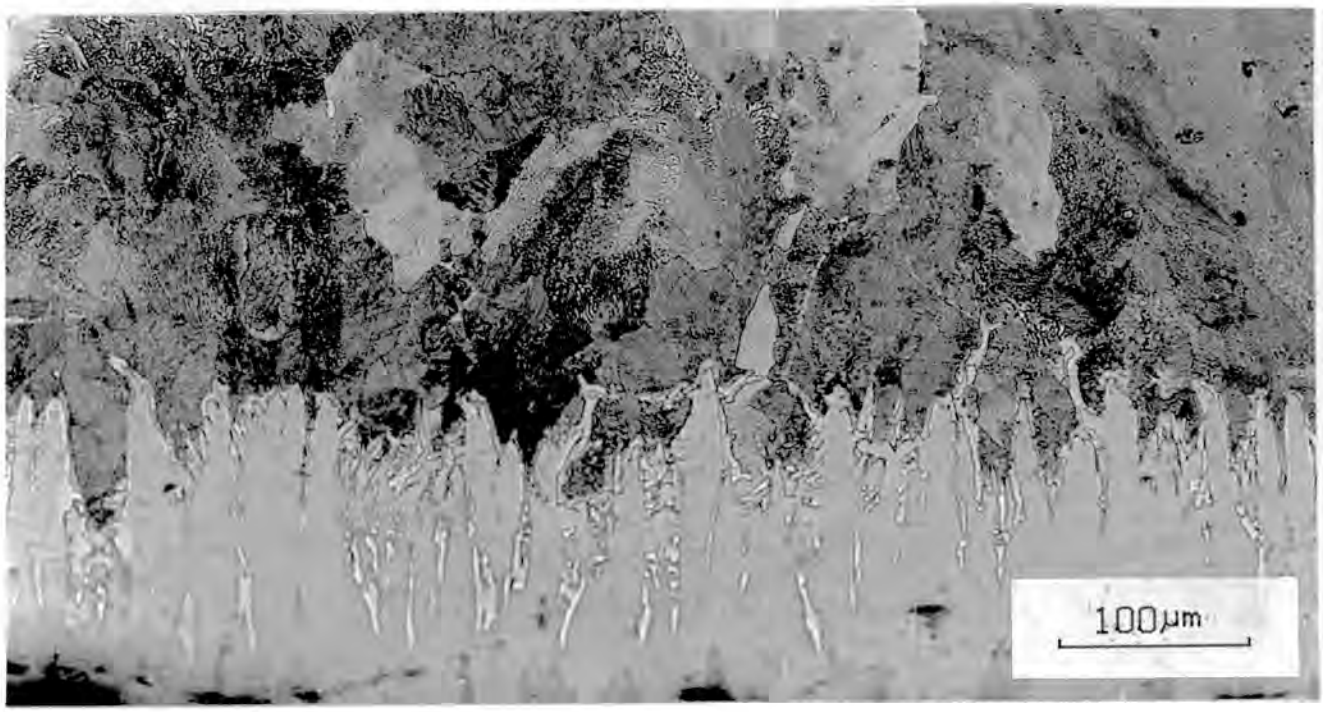

Figure 3.11 Boronised surface showing iron boride layer on a pearlitic core structure.

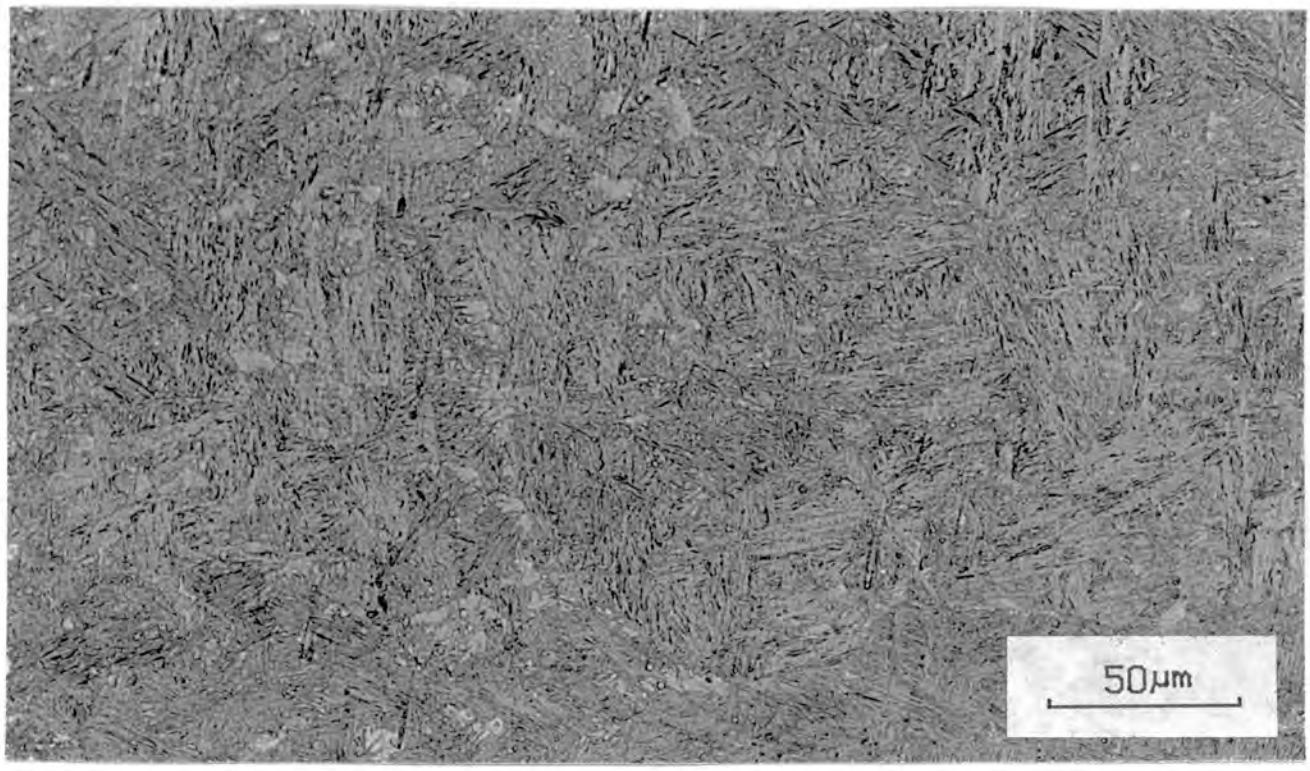

Figure 3.12 Microstructure of Alloy E, showing martensite fine carbides and isolated areas of austenite.

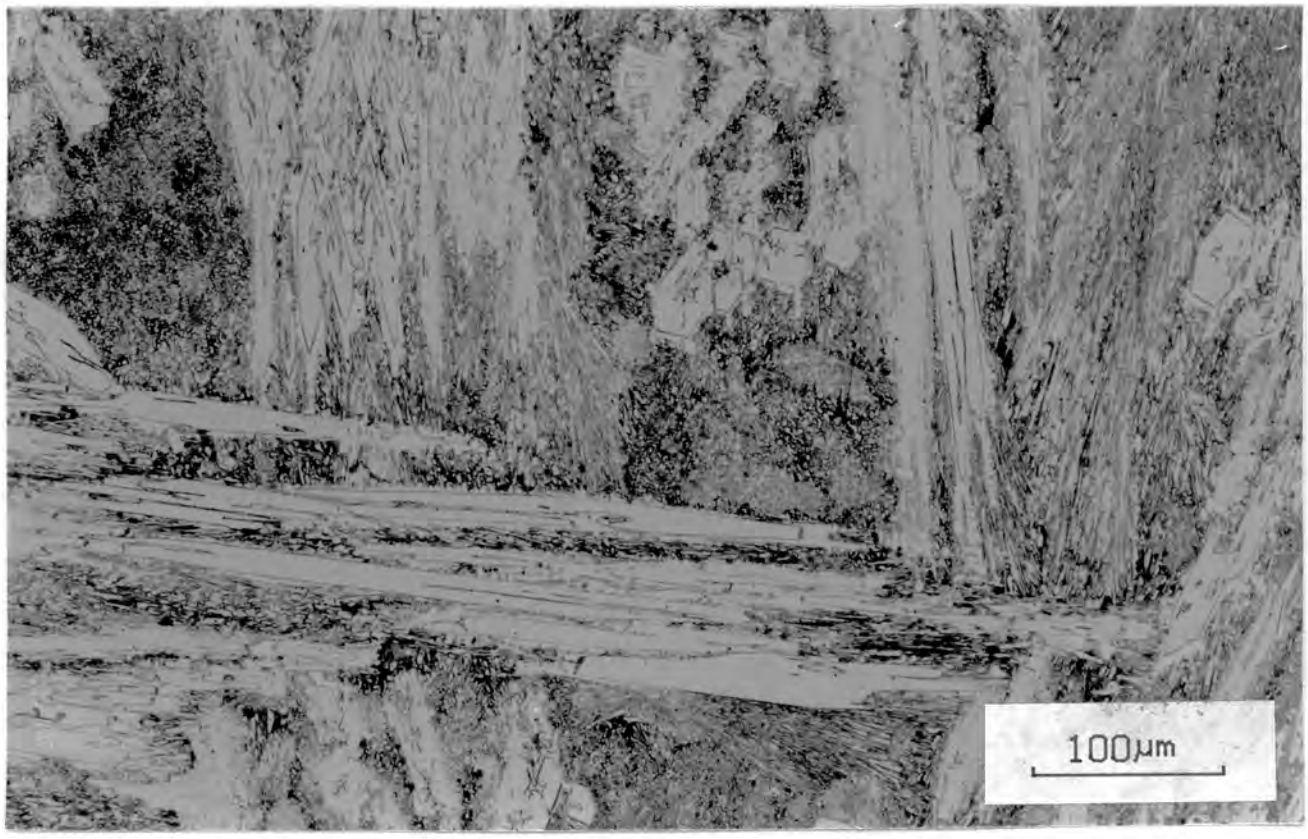

Figure 3.13 Microstructure of Alloy F, showing large carbides in eutectic of carbide and austenite.

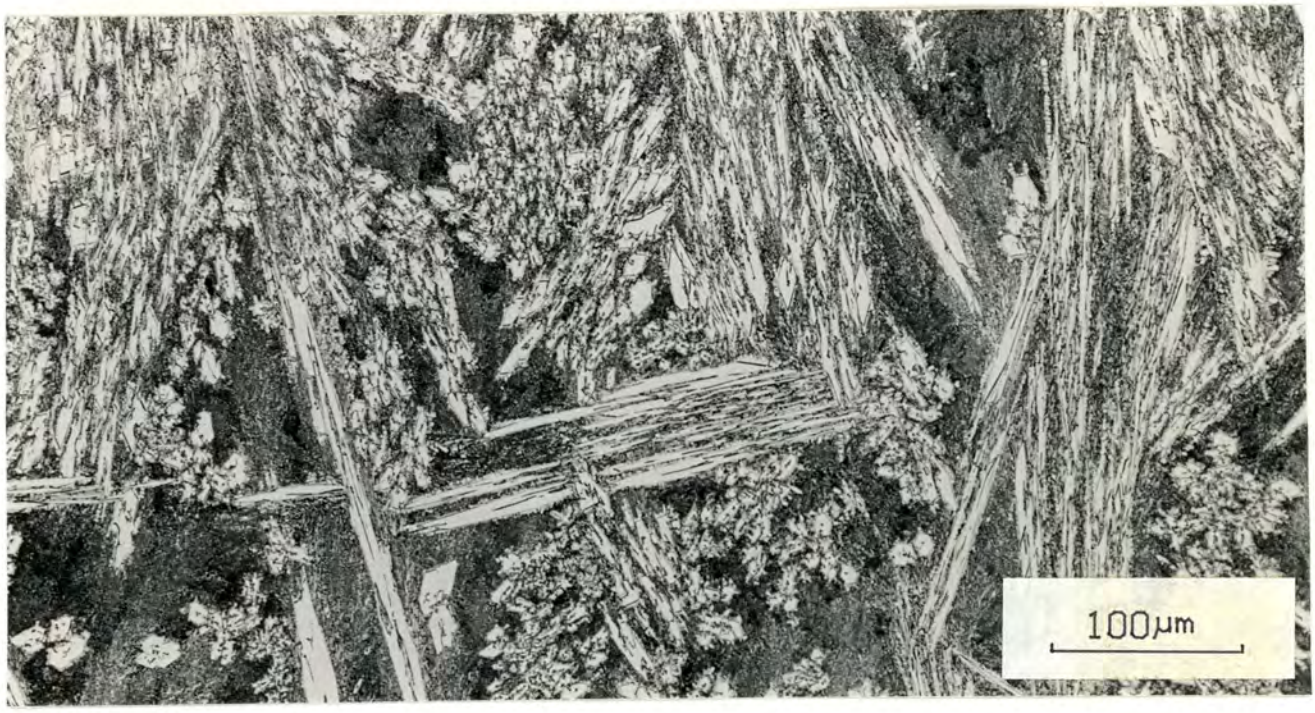

Figure 3.14 Microstructure of Alloy G. Similar to alloy F but somewhat finer.

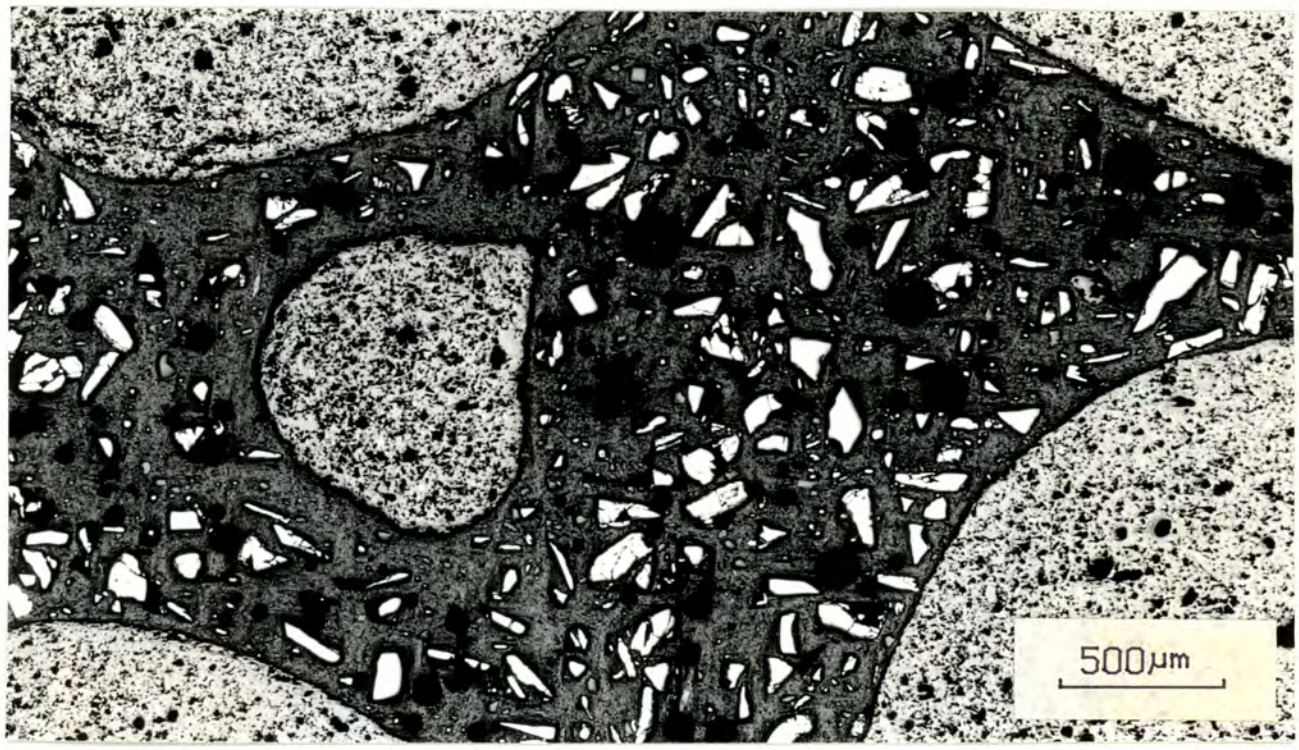

Figure 3.15 Structure of ceramic (white spheres) bead impregnated epoxy. Note the presence of silicon carbide crystals in the epoxy.

3.3. Macroscopic Characterisation of Wear Surfaces

A macroscopic examination of the blade tip (periphery) revealed the presence of wide wear tracks. The angle between these wear tracks and the blade face was constant. This angle was measured at 18° which corresponds to the helix angle blade to the shaft. Hence it follows that since these tracks run true to the direction of rotation of the blade they must result from wear against the encrusted ash on the containment bin. Corresponding ridges were visible in the encrusted ash on the bin wall. Examination of one such ridge revealed spherical ash particle agglomerations of the order of 100 - 200 micrometers in equivalent diameter. Due to the friable nature of these agglomerations and their increased density in an area near the start of a ridge it is likely that they may be the product of a considerably larger conglomerate. (Fig. 3.16)

These tracks were not arrested by any surface irregularities such as tile joints or interlayers between coatings and base metal. (Fig. 3.17) From figure 3.17 it is also clear that not all the blades displayed such prominant wear tracks. However tracks were in greater evidence in the central portion of the mixer which suggests that a compacted encrustation of ash on the bin promotes their formation.

The depth of these tracks increases with time with an incubation period of approximately 48 hours. The tracks are maintained with time but may shift their position along the blade tip with time as the blades shorten. The depth of these tracks was found to be similar for all ductile materials and appreciably less for the alumina ceramic. (Fig. 3.18) Clearly, the superior wear resistance of the ceramic results in less pronounced wear tracks.

3.4 Microstructural Characterisation

Microstructural examination of the ductile materials revealed the mechanism of wear to be a combination of microcutting and microploughing. The microploughing is evident by the presence of a ridge on either side of the wear tracks. (Fig. 3.19) illustrates a track with significant plastic

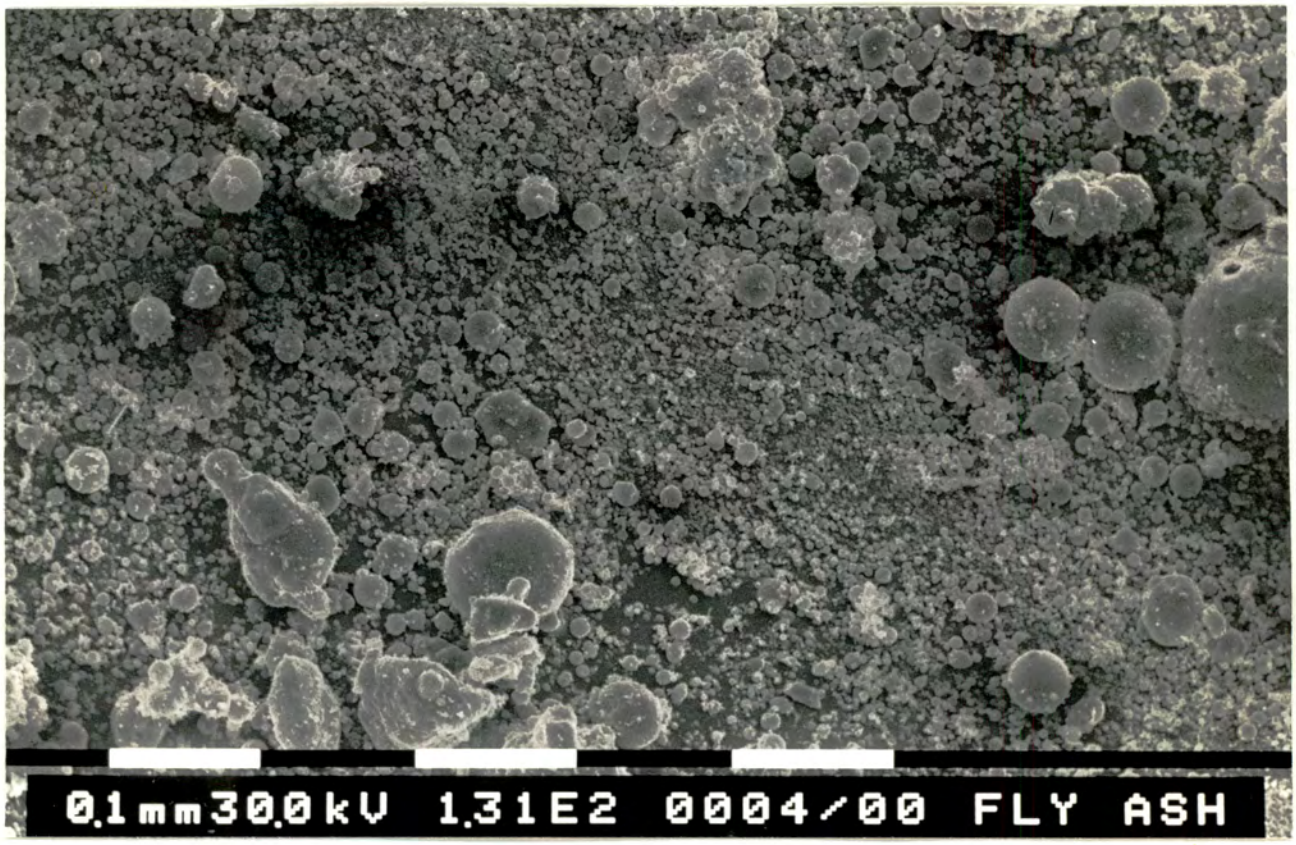

Figure 3.16 Microstructure of friable fly ash agglomerations which have been broken down by the movement of mixer blades.

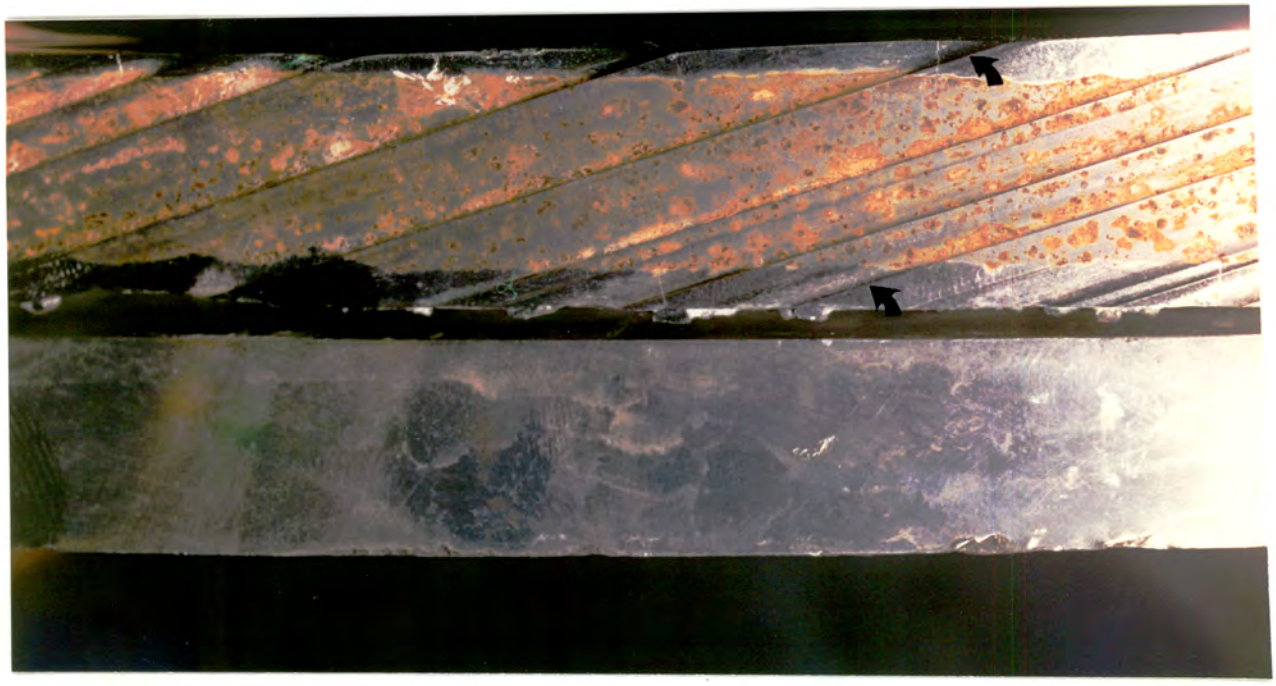

Figure 3.17 Presence of wear tracks on the tip of a mixer blade. Note that the hard facing, even though more wear resistant did in no way arrest the formation of these wear tracks.

Figure 3.18 Comparison of the presence of wear tracks on alumina ceramic and steel on a blade tip.

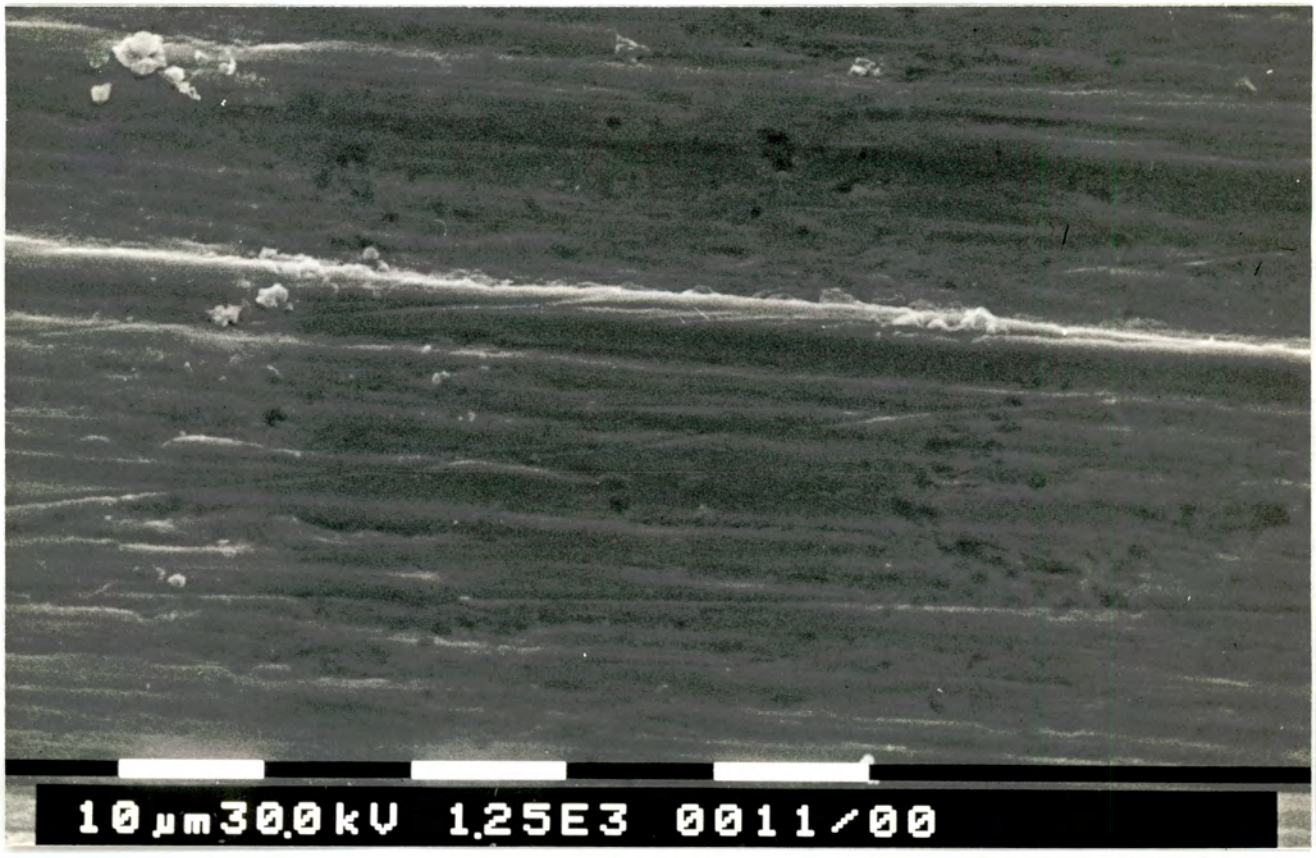

Figure 3.19 Evidence of plastic deformation and micro cutting was typical of the wear surfaces of the ductile materials tested.

deformation of the adjacent material. The raised material in the figure has clearly been subjected to multiple repeated actions once displaced. Fragments of this material are dislodged and lost as a consequence of repeated deformation and ductile tearing. There is also evidence of material removal due to microcutting similar to that found in machining processes.

The presence of free quartz (SiO_2) grains was detected in corrosion products which had adhered to the metal surface which was confirmed through EDAX analysis in the scanning electron microscope. (Fig. 3.20) The conchoidal fractures and sharp edges which characterise the particles would contribute to a high degree of penetration into the softer counterface material, resulting in microcutting during normal operation of the blades.

A study of the wear surface of the alumina ceramic tested reveal a sequence of events which can be seen in Figure 3.21. Initially grain boundary microcracking manifests itself in the wear track (a) leading to the removal of discreet grains, and (b) enhanced removal pursues at these sites resulting in cavities. Intergranular fracture takes the easiest route through the glassy binder and is the predominant mechanism of steady state wear. Since intergranular fracture results in poorly supported grains, the material loss is often orders of grain sizes. The grain structure of the alumina used for the test consists of equiaxed grains of approximately 1 - 2.5 micrometers in equivalent diameter supported in a glassy binder. These observations are not uncommon with findings by Ajayi and Ludema [12] who confirmed that the scale of fracture on a sliding surface is of the order of grain sizes. The workers cited, performed sliding tests with a spherical diamond tip of 100 micrometers radius against freshly prepared ceramics including sintered alumina. Hence it is considered that their findings are valid support to the observations made here.

3.5 Presence of Corrosion

On many of the steel blades general corrosion was visible. Ash conditioners are run by shift operators who occasionally switch off the conditioners in order to stockpile ash in the fly ash bunkers and to remove occasional blockages which build up in the outlet chutes due to poor

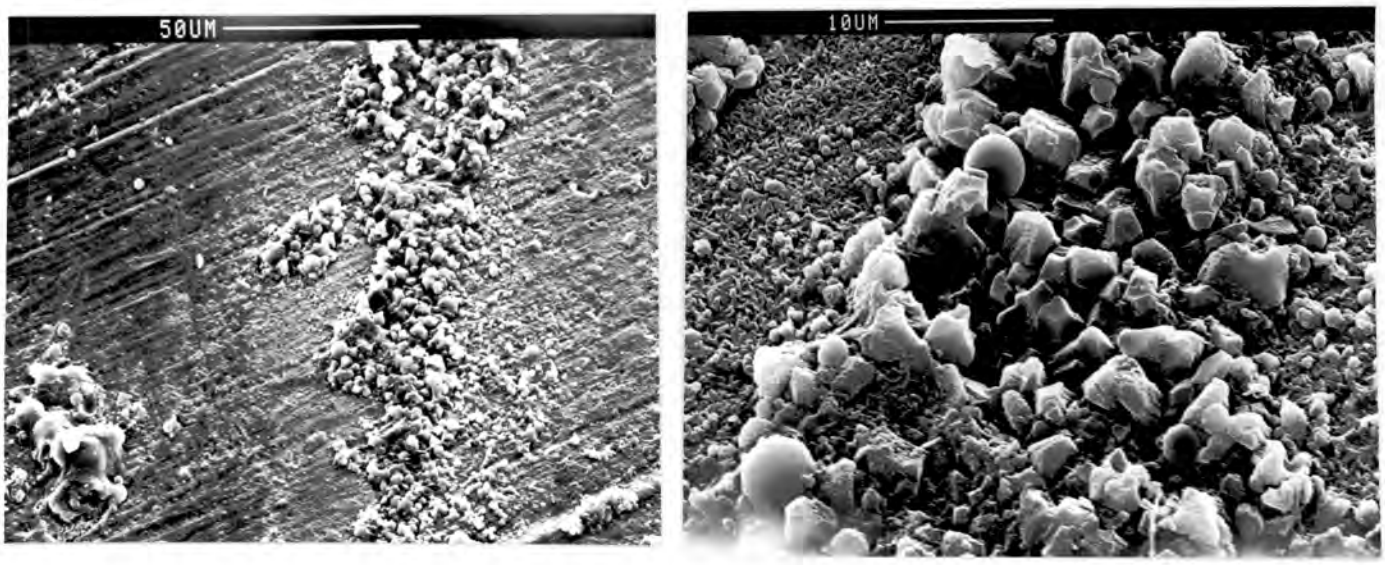

Figure 3.20 Presence of free quartz grains adhering to corrosion products on the tip of a blade.

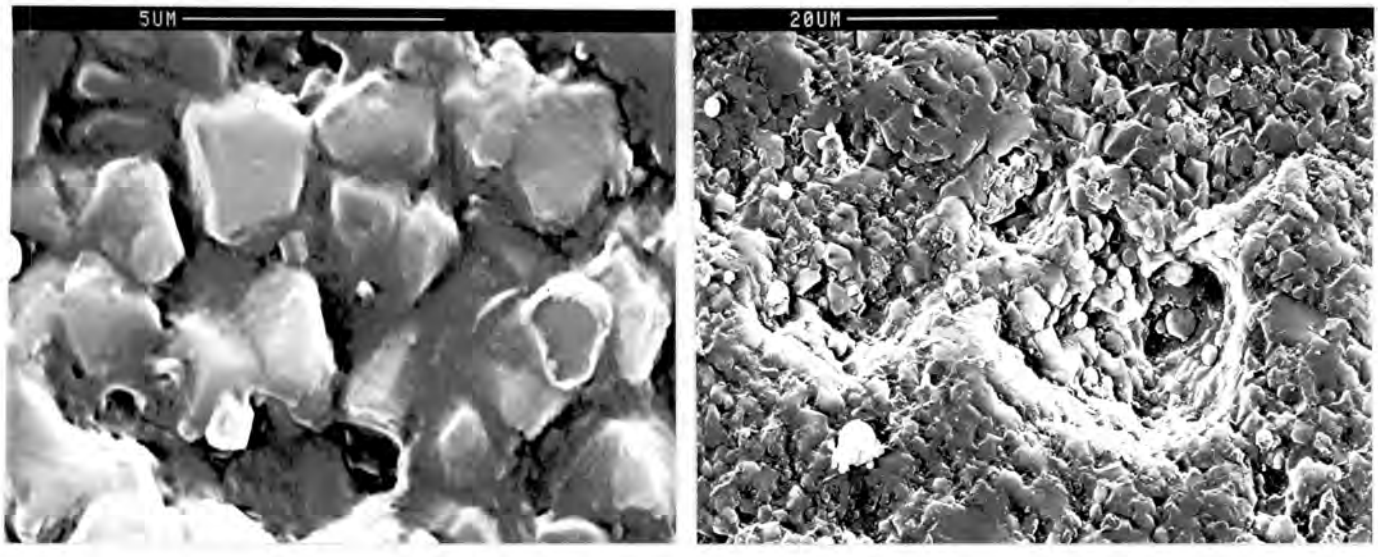

(a) (b)

Figure 3.21 Sequence of events leading to degradation of the surface of a fine grain alumina ceramic by abrasion: (a) Grain boundary micro cracking, leading to the removal of discreet grains; (b) enhanced removal persues at sites of grain removal, resulting in formation of surface cavities.

moisture control. During these stationary periods the high humidity and aggressive aqueous ions present in the containment bin promote general corrosion. Strong evidence of the formation of corrosion pits is also present. (Fig. 3.5) However, both the corrosion resistant steel (Alloy A) and the stainless steel (A1S1 304) have RWR values less than unity (Table 2) and thus perform worse than the standard roller quenched and tempered medium carbon steel (Alloy C). Such a result indicates that the synergistic action of corrosion during the operation of the conditioner does not play a significant role in the total wear process for these materials. Hence it is apparent that the loss of material due to abrasion completely overshadows any loss of material brought about by corrosion. In addition there is no conclusive pattern relating the presence of corrosion pits to location in wear tracks. In systems where other workers [4] have proven a strong case for synergism between corrosion and abrasion, it was observed that corrosion was confined preferentially to the vicinity of a wear track and that removal of the corrosion product revealed an array of corrosion pits along the scratch. These workers showed that there was an observed increase in total wear loss when corrosive and abrasive treatments were more frequent for a given total exposure time. Since the frequency of abrasive contacts and exposure to corrosive environment is high in this study, strong synergistic action would be expected if corrosion was significant. Since this is not the case it is further evidence that corrosion is not significant.

3.6 Assessment of Results

It should be borne in mind that while material replacement may improve blade life, it must also be cost effective. Costs arise from various sources such as original material cost, manufacturing cost, installation and labour costs. When these costs are taken into account, a more valued judgement can be made on the desirability of material replacement.

A relative cost index for the wear of the various test materials compared to the standard steel mixer blades is shown in Table 2. This cost index is the ratio of the relative cost of the blade divided by the relative wear resistance. The standard steel blade, alloy C, is given a nominal value of unity for both cost and relative wear resistance. The costs used to compile this index were obtained from the supply of quotations from industry for the manufacture and installation of blades. These costs are based on prices as at November 1987. It is immediately apparent that the majority of candidate materials and coatings show a higher cost index than the standard steel. Marginal improvements can be obtained by improving the hardness of the standard steel (Alloy C) or by using Alloy F.

Much greater improvements are achieved by using hard facing Alloy C, the alumina bead epoxy coating, or ceramic tiles. The alumina ceramic tiles show the best economic advantage with a cost index only 16 per cent of the original standard.

Since the sintered alumina ceramic used in this test far outperformed all other materials or coatings in the test it was considered that the performance of wear resistant ceramics and cermets should be studied more closely as they hold the most potential for application.

However a disadvantage found with the use of ceramic tiles was that the method of application was not altogether satisfactory, leading to tile loss and impaired performance as indicated in Figure 3.22. Hence design and method of application should also be given attention.

Figure 3.22 Degradation of underlying metal once protection by ceramic tiles is lost.

CHAPTER 4

4. METHOD AND DESIGN OF APPLICATION OF CERAMICS

4.1 Application of Ceramics

Four general designs in which ceramic tiles were affixed to steel blades were evaluated in situ [18]. These were as follows:

(a) One large tile covered the upper half of the blade and protruded 20 mm past the blade in the form of an overhang. The tile is attached to the blade by means of a water resistant epoxy and four weldable inserts which pass through a hole in the tile and are welded to the metal base. These inserts keep the tile attached to the blade in the event of epoxy failure. (Fig. 4.1)

(b) An array of tiles 6 mm thick were attached to the areas of the blade exposed to significant wear by means of a water resistant epoxy. This design also included the application of 2 mm thick, 10 mm by 10 mm square tiles set on a rubber backing which is vulcanised onto the blade. (Fig. 4.2 and 4.3).

(c) A single row of tiles covered the outer section of the front of the blade and extended 10 mm beyond the periphery of the blade, such that they scraped the encrusted ash from the side of the containment bin. (Fig. 4.4)

(d) A fourth design consisted of applying custom shaped 40 mm-thick ceramic cappings to the free ends of the mixing blades [19]. The cappings comprise a number of individual segments each containing a slot within which a portion of the blade is receivable. These segments are attached to the blades by means of heat-resistant and water-resistant epoxy adhesive. A weldable insert is also used to hold the corner pieces firmly in position and thus further prevent the middle two edge tiles being dislodged during use. Mild steel is used for the blade construction. The blades are profiled such that the

Figure 4.1 Single large ceramic tile covering upper half of a blade.

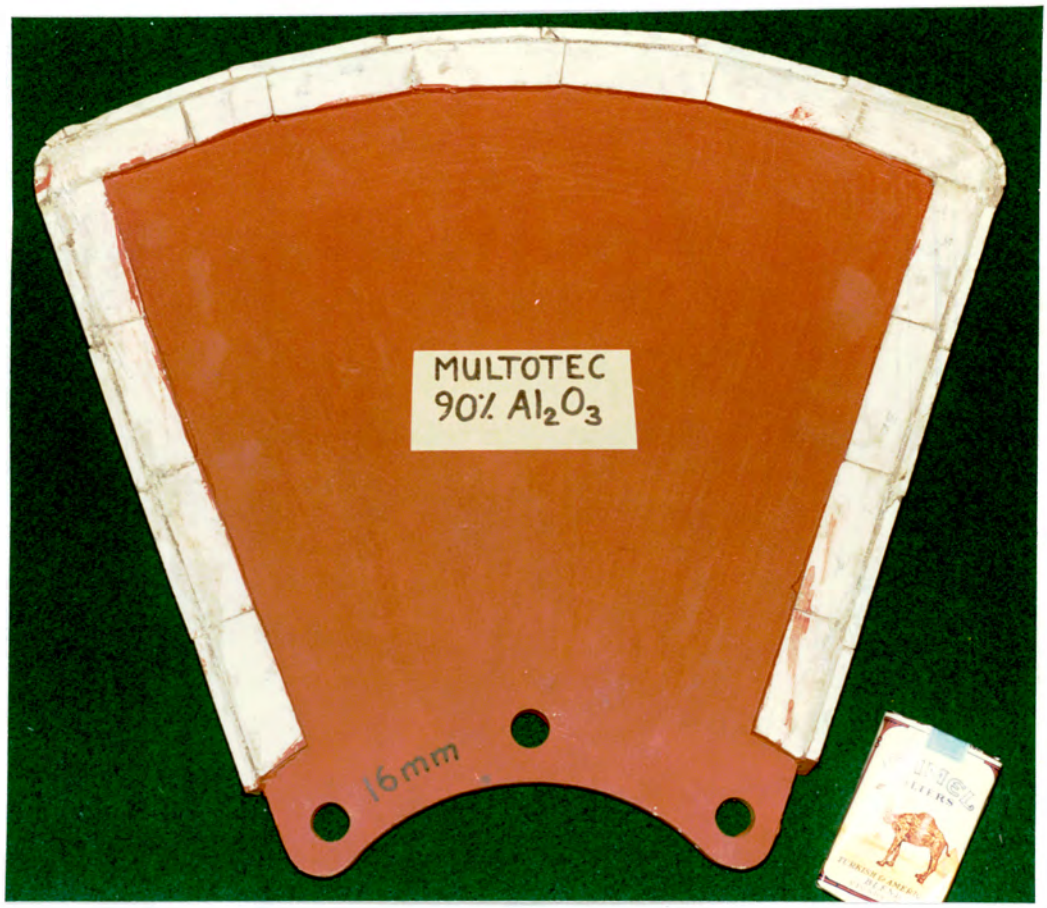

Figure 4.2 Ceramic tiles attached to areas of the blade exposed to significant wear.

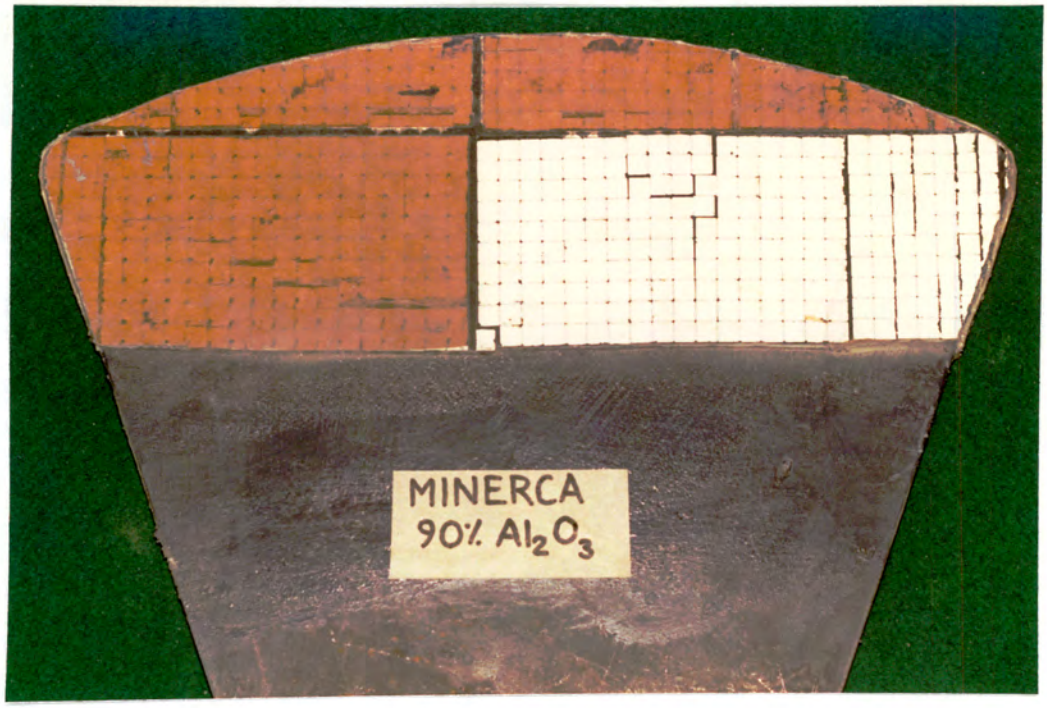

Figure 4.3 A mat of small ceramic tiles vulcanized onto a blade.

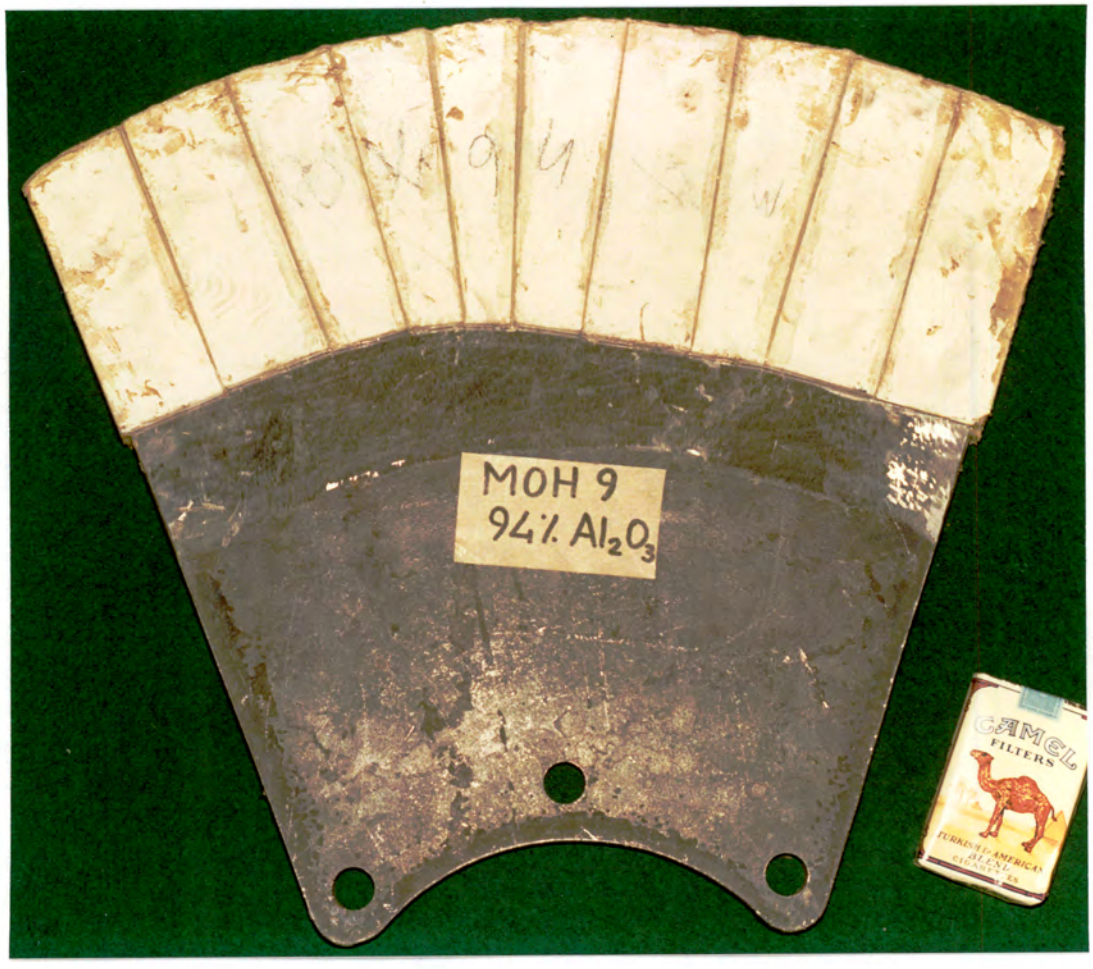

Figure 4.4 Single row of tiles covering the outer section of the front of a blade.

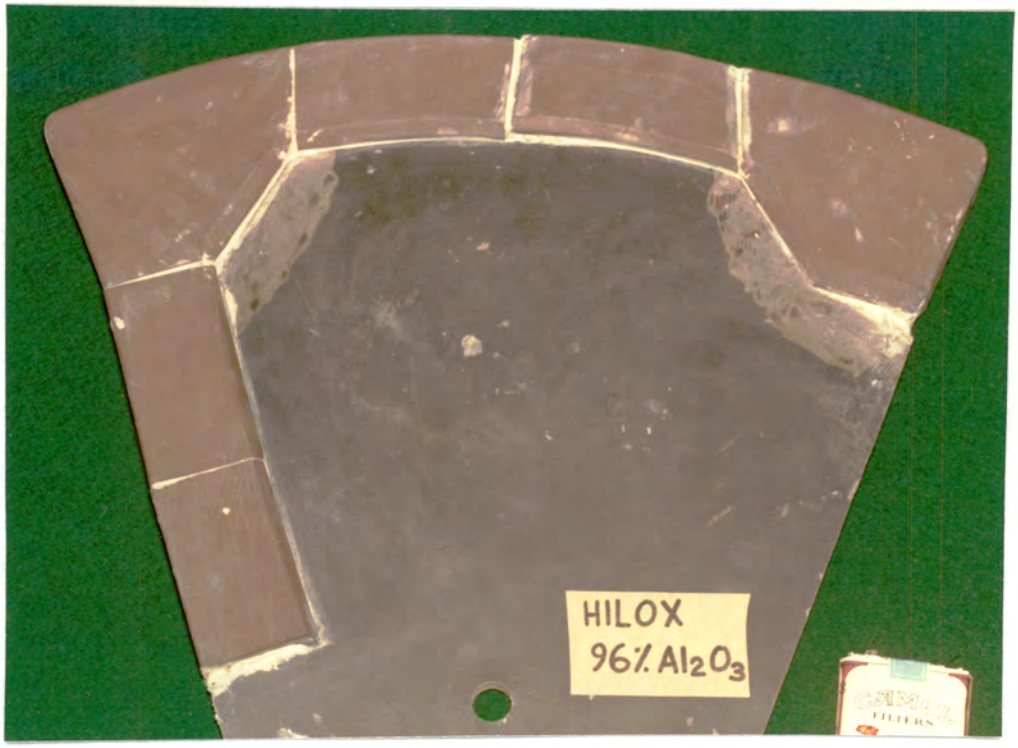

Figure 4.5 Protective ceramic cappings fitting onto a steel blade.

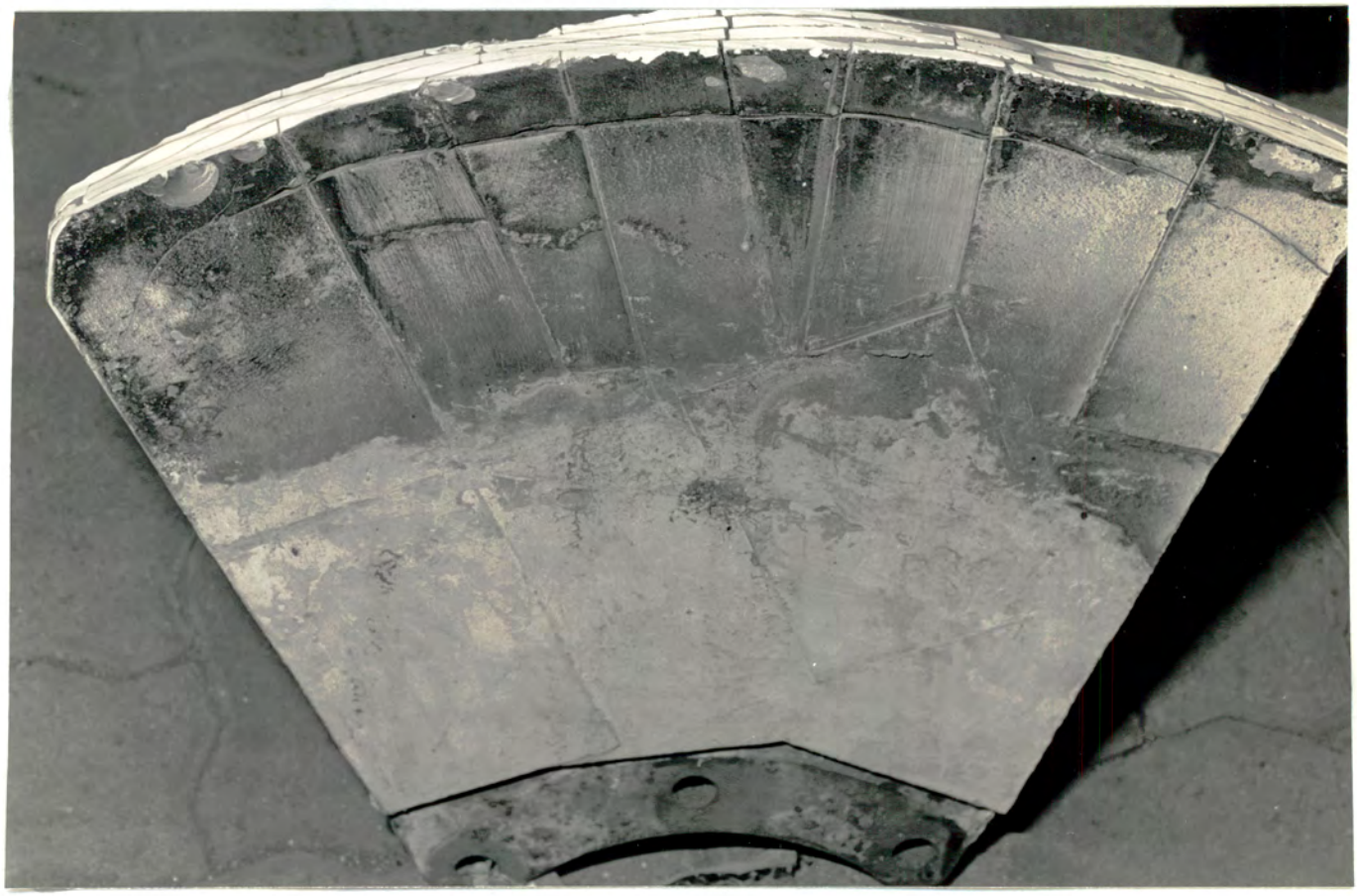

Figure 4.6 Cracking of tiles which protrude past the periphery of the blade.

cappings do not increase the face area of the original blade dimensions. (Fig. 4.5)

4.2 Method of Design Evaluation

It was considered that the most meaningful method of determining the suitability and performance of a design would be to conduct wear testing in situ. The test design consisted of placing a complete set of test blades in an ash conditioner and monitoring their performance. The dimensions and masses of each blade were recorded prior to being placed in service. The various test designs and their derivatives were placed in a sequence that was repeated within the conditioner, so that seven blades of each design or derivative were distributed. This ensured that each blade was subjected to a range of wear intensities. This was necessary in view of the variability of the wear gradient in the conditioner. (Fig. 3.6) The blades were left in the conditioner for a period of service of 6 600 hours which is approximately double the useful lifetime of the original steel blades.

4.3 Observations and Discussion

Following testing, the blades were examined for wear, service cracks and loss of tiles. The wear on the periphery of the tiles varied from approximately 1 mm to 25 mm loss of ceramic thickness from the free end of the blade.

The amount of wear varied for each blade of a particular design. Variations in wear intensity were consistent with the wear gradient established in Figure 3.6. The purpose of this test, however, was not to determine the wear resistance of the blade but to evaluate the design potential for application. The tiles used for the test were all manufactured from sintered alumina ranging from 88 per cent to 94 per cent alumina. This variable in alumina content could not be excluded as three different manufacturers of sintered alumina were involved in the assembly of the blades. However, the strength, hardness and toughness of the three grades employed were similar.

The integrity of the application of ceramic is more readily measured by the extent of service cracks in the tiles and the number of tiles that have become disbonded. Service cracks generally arise when unskilled operators damage the blades when cleaning the conditioner after a long idle period. This occurs when operators break up the cemented sludge with crude implements such as poles. Impact on the ceramic tiles may result in chipping or cracking of the tiles. This problem can be solved by specifying tougher grades of ceramic and cleaning the conditioner prior to stopping it for long periods.

The resistance of a tile to cracking is a material parameter in which design may play a role. Tiles which protrude past the periphery of the blade (Fig. 4.6) are very susceptible to cracking. Large singular tiles are most susceptible to crack propogation and through a single impact can loose a considerable portion of their coverage. (Fig. 4.1) A cracked tile can be retained on the blade for a period of time. However the crack adds an additional route to the epoxy which the water degrades with time. An arrangement of smaller tiles is more resistant to cracking as the cracking only propogates to the tile edge after which it arrests. Figure 4.7 illustrates a crack that has arrested at the capping edge.

Tiles can become detached from the blade with time as the epoxy degrades due to breakdown caused by humidity and the occurence of an expansive corrosion reaction under the tile. To prolong adhesion, water-resistant epoxies are specified. Epoxy is applied evenly to clean, degreased surfaces that fit well in order to obtain a continuous bond between tile and base metal. This limits the formation of corrosion products under tiles which cause them to peel off the base metal. In any adhesive system or application, peel forces should be minimized. Figure 4.8 illustrates the loss of a tile from one blade after a forced outage period. These tiles were knocked off the blade during the cleaning operation that followed the outage of 5 days.

Figure 4.7 A crack which has arrested at the joint between two tiles illustrating the benefit of tile joints.

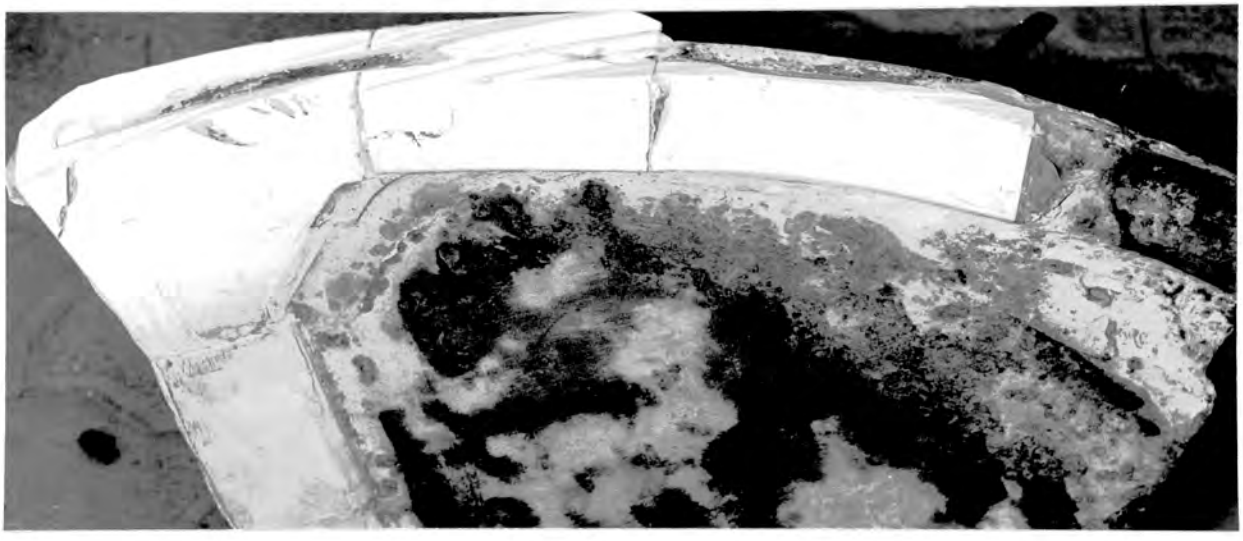

Figure 4.8 Loss of a tile from a blade due to mechanical damage during cleaning of the conditioner after a period of service.

4.4 Conclusion

The design (d) shown in Figures 4.5 and 4.9 provided the lowest amount of tile loss of the designs tested. Implementation of the alumina ceramic tile design discussed is estimated to save approximately R20 000 per annum per conditioner on the basis of this initial testing. At present this design is implemented at two large power stations and is gaining acceptance. By the early 1990s, Eskom will have 36-40 ash conditioners in operation which will clearly result in exceptional total savings in excess of R800 000 annually. Furthermore, consistent mixing of the ash is anticipated, which should reduce cleaning costs attributed to dust emissions from poorly conditioned ash transported on open conveyor belts.

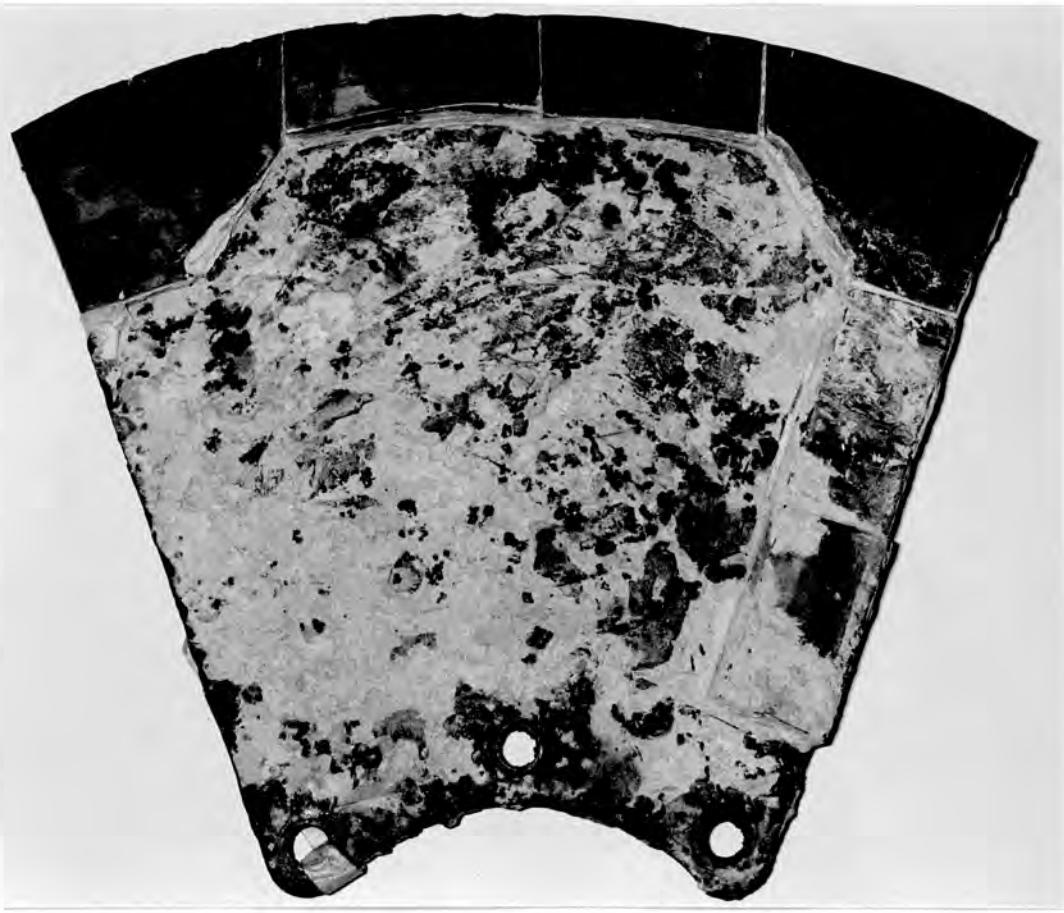

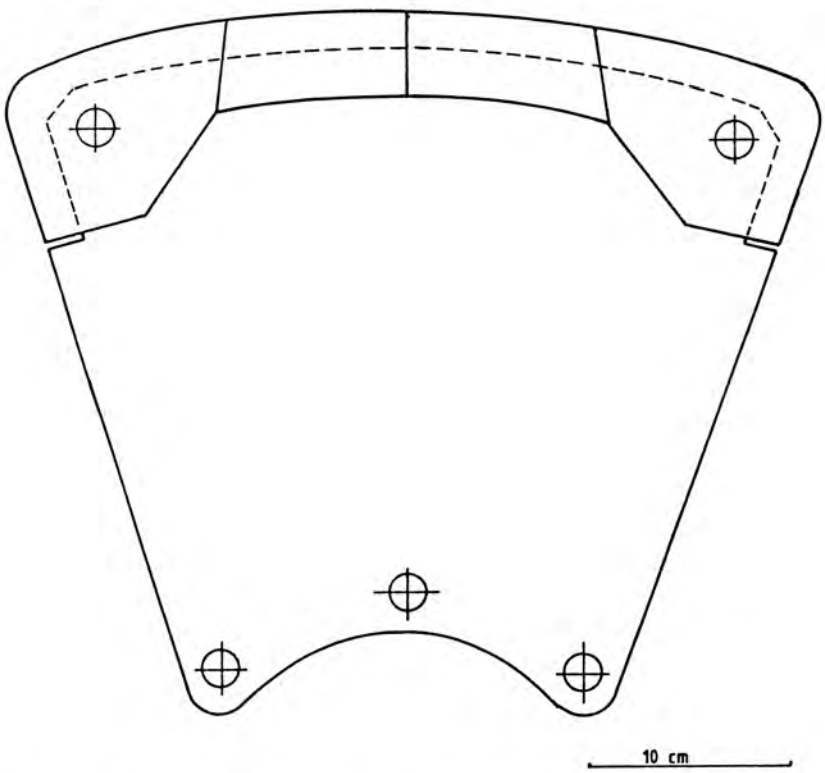

Figure 4.9 (a) The design which provided the most satisfactory performance after 6600 hours of service.
(b) A schematic diagram of final design for ceramic protective cappings on steel mixing blades. The middle segments lock against the outer segments, which are fixed to the blade by means of welded inserts. All segments are attached to the blades by means of epoxy adhesive.

CHAPTER 5

IN SITU TESTING OF CERMETS

Introduction

It was clear from the initial testing programme that ceramic materials performed extremely well in the ash conditioner. Furthermore it was demonstrated that through proper design of mixer blades the brittle nature of ceramic materials can be negated, giving rise to a cost effective solution. On the basis of these results it was decided to test a greater range of ceramic materials than carried out in the initial study. It was anticipated that more quantitative data would be produced as a result of such a programme of work which would distinguish and isolate specific materials for further use in ash conditions. It was also considered that a broader range of test materials could be examined in more detail and help to establish the important material parameters contributing to the wear process. In this way an understanding of the wear process would be realised with consequent important implications for the study of wear in other applications.

5.1 Test Design

One conditioner blade was selected as a test site as this was considered to facilitate better control of applied conditions within the ash conditioner. All test grades were placed alongside each other on the periphery of the blade. (Fig. 5.1) The order in which test grades were placed follows the order shown in Table 3. This series of grades was repeated three times in order to obtain three sets of data for each grade, the purpose of which was to establish the reproducibility of the test method employed. This necessitated the use of two blades for test purposes in order to accommodate all the test grades. The row facing the ash as the blade moves consists entirely of a single batch of reference pieces. The row immediately behind the references consists of a repetition of the test grades.

The test and reference pieces are triangular in geometry (Fig. 5.2). This test geometry was chosen since it was clear that the wear tracks which develop across the blade could cause a wear gradient to be established across the blade tip. To take account of this, a continuous row of reference pieces is required against which the wear losses of different test grades can be normalised.

The test and reference pieces were pressed and compacted in a purpose-made die set, upon which they were sintered [20]. (Fig. 5.2) A threaded stud was soldered to each piece in order to facilitate attachment onto brackets.

The brackets consisted of angle sections with holes bored into the top face through which the studs pass and are fastened by means of a nut. Angle section used for the brackets was effective in preventing ash from attacking the mechanical fasteners. The brackets and studs employed were manufactured from AISI 304L. This compatability and choice of material was necessary in order to prevent galvanic corrosion between the mechanical fastener and bracket. Each bracket held two test pieces and two reference pieces immediately to the fore of the test pieces. The brackets were attached to the top third of a blade which was removable. This facilitated rapid exchange of test blades. (Fig. 5.1)

The wear surfaces of the test and reference pieces were polished with diamond paste down to one micrometer to remove any surface oxidation that could have occurred on soldering studs to the pieces.

Attention was also paid to the direction of wear. To ensure that the test piece allocated to a certain reference piece receives the same abrasive particles across its surface, a suitable reference and test piece geometry is required. It is demonstrated by the triangular geometry shown in Figure 5.3, that, by placing material pieces adjacent to each other this can be achieved. From this schematic it is clear that a more wear resistant grade would not afford protection to a less wear resistant grade adjacent to it.

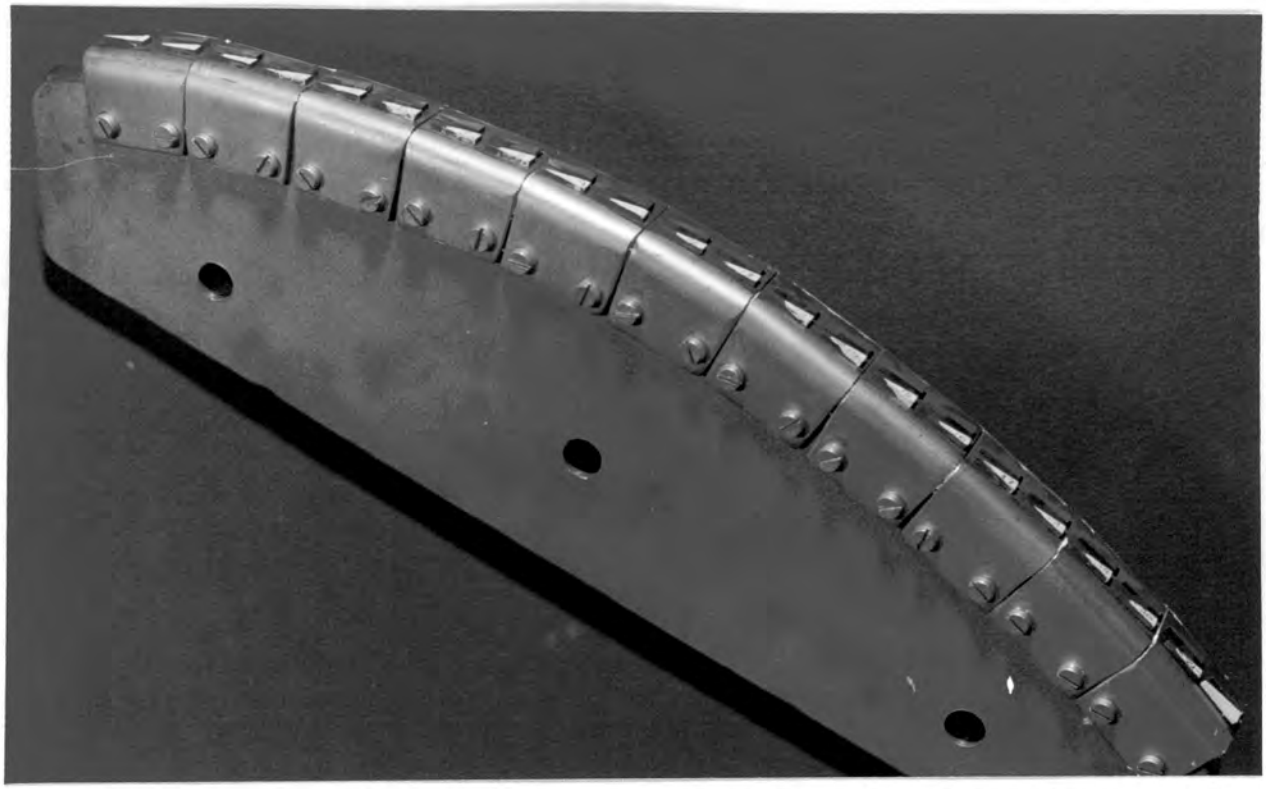

Figure 5.1 Test blade showing positioning of test grades and references.

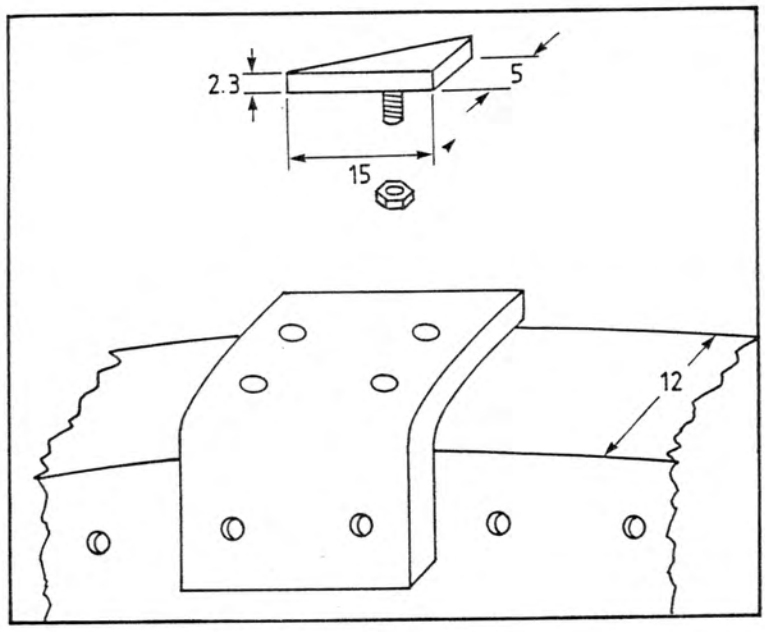

Figure 5.2 Detail of test and reference piece geometry. Dimensions in millimetres. Test and reference pieces are fastened onto a angle shaped bracket which is fastened to the test blade.

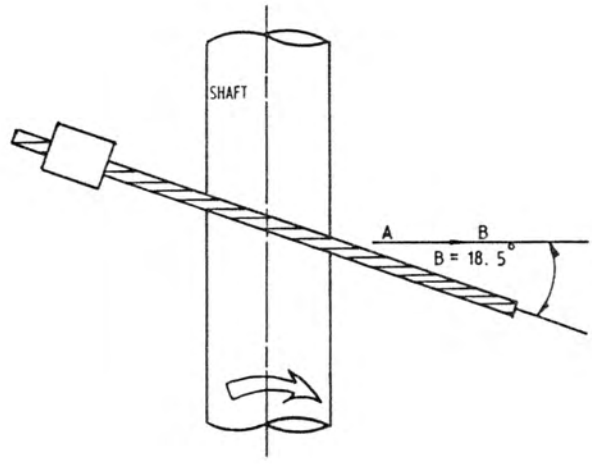

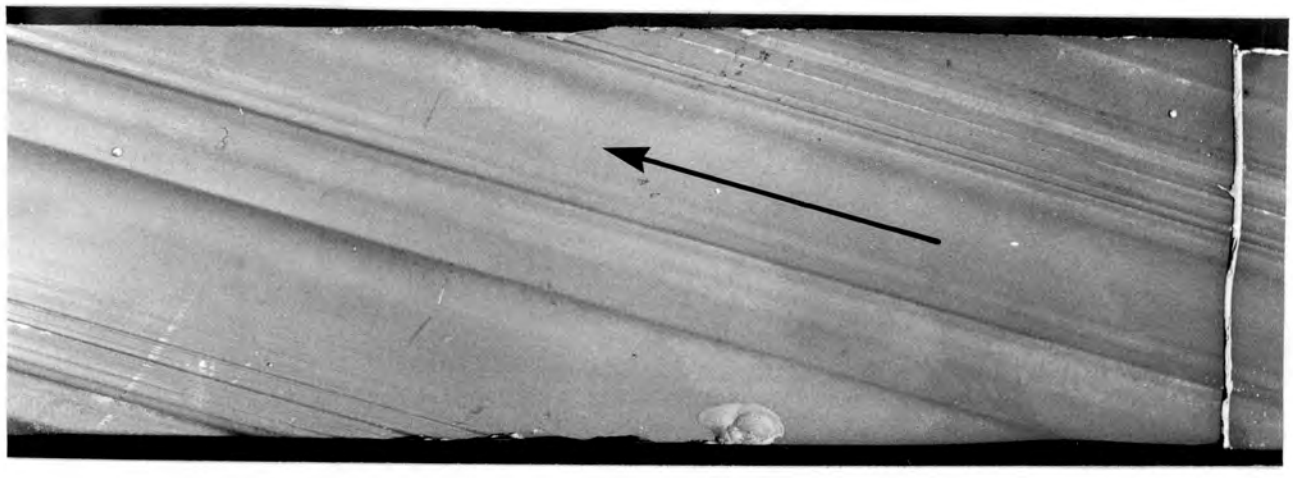

Figure 5.3 (a) Orientation of wear tracks on a blade tip.
(b) Positioning of test pieces to account for orientation of wear tracks.

This design was demonstrated to the local cermet industry [20], who suggested that a low wear resistant grade be used for the reference material. This would ensure that the reference pieces did not protect the more wear resistant test grades. From experience derived from lining the front tip of a spiral clay auger used in the brick industry, it was recommended to use a 20% Co-WC grade which would afford significantly less resistance than the test grades but still significantly more resistance than a roller quenched and tempered steel. If steel were to be used as a reference material this would require the constant monitoring and replacement of reference material pieces.

A preliminary run which compared a medium carbon, roller quench and tempered steel to 20% Co-WC, demonstrated that the cermet reference would afford some 4-5 times greater wear resistance than the steel. Hence it was forecast measurements need only be made approximately every 48 running hours.

Measurements were by mass loss and measured to four significant places on a Mettler laboratory scale. Densities and mechanical properties of all grades and reference pieces were supplied by the manufacturer along with test certificates. These were randomly checked and found to be in good agreement. (Table 3)

The test materials selected cover a well characterised range of strength, hardness and toughness values. (Table 3)

Test grades were selected on the basis of their microstructural characterisation. Researchers have found that the wear characterisation of WC-Co cermets is related to two particular parameters, namely grain size and binder content. [21, 22, 23] These materials consist of equiaxed tungsten carbide (WC) grains in a ductile binder (Co). Grades were selected so that for an average grain size of 4 microns, the binder content ranged from 11.3 to 32 volume percent. In addition to this grades were selected so that for a binder content of 17.5 volume percent, grain size ranged from 1.5 micrometers to 8 micrometers. In all, 13 grades of WC-Co cermets were tested. The microstructural characteristics and mechanical properties are listed in Table 3.

Table 3

Description and in situ wear rates for WC-Co alloys tested.

Grade	Vol % Co	Density	HV 30	Transv. Rupt. Strength*	Av. grain size	steady state wear rate	
		g/cm^3		MPa	µm	$10e-3mm^3/h$	Variance ± %
S6	11.3	14,93	1550	1520	2	2.387	3.7
T6	11.3	14,93	1450	1590	3	2.362	3.4
G6	11.3	14,93	1350	1660	4	2.889	2.9
K10	11.9	14,89	1575	1250	1.5	2.654	1.0
S10	17.5	14,51	1335	1640	2	3.705	4.1
G10	17.5	14,51	1230	2000	4	19.286	3.6
J10	17.5	14,51	1120	2260	8	57.197	6.9
H7	13.4	14.79	1310	1690	4	4.260	3.2
H8	14.6	14.71	1275	1860	4	9.177	3.0
H9	16.2	14.60	1205	1930	4	25.251	4.2
H12	20.6	14.30	1130	2070	4	132.206	4.6
G15	25.0	14,00	1100	1920	4	166.283	5.8
S20	31.5	13,56	1030	2050	2	112.50	11.5

* Based on 4 point load

Note: Steady state wear rate for Medium Carbon Steel : 551 X $10^{-3} mm^3/h$ ± 11%

5.2 Results and Discussion

5.2.1 Wear Gradient

It is clear from Figure 5.4 that the wear on the blade periphery varies as a function of position across the blade. Mass loss measurements of the reference pieces located across the blade, after cumulative intervals shown on the figure, provide an indication of the wear gradients across the blade periphery. This can be attributed to the formation of wear tracks on the blade periphery. Clearly from Figure 5.4 once the tracks initiate they maintain their course, approaching a steady state during 48 to 100 hours service. After this incubation period a steady state wear rate manifests itself and the gradients remain stable. However a disturbance of the encrusted ash on the bin wall may upset this equilibrium and the wear gradients across the periphery may alter as new wear tracks form.

Note that the data presented in Figure 5.4 is in terms of cumulative wear volume loss which were derived from measured mass losses.

5.2.2 Wear Rates of References

The wear losses may be presented as cumulative volume losses with respect to time, as seen in Figure 5.5. Two stages of events are clear from the trend, firstly a period of bedding in and secondly a maintained steady state. It appears that once this course of events have set in, constant wear rates prevail. After 100 hours, once a steady state is reached the wear rates of all the reference materials are very similar. The gradients of the steady state wear losses with respect to test time are constant for all the reference pieces.

This conclusively shows that once a wear track has initiated and stabilised, equivalent amounts of wear occur in the track, on the sides of the track and on the ridges adjacent to the track.

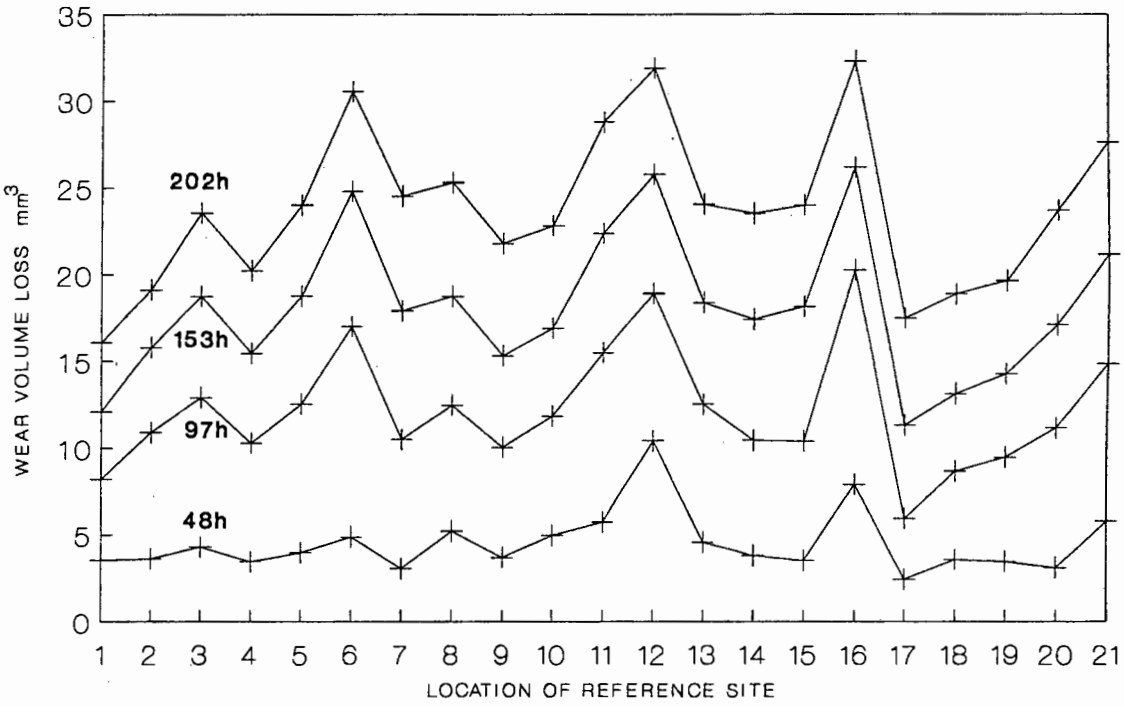

Figure 5.4 Variation in wear intensity as a function of position across the test blade periphery.

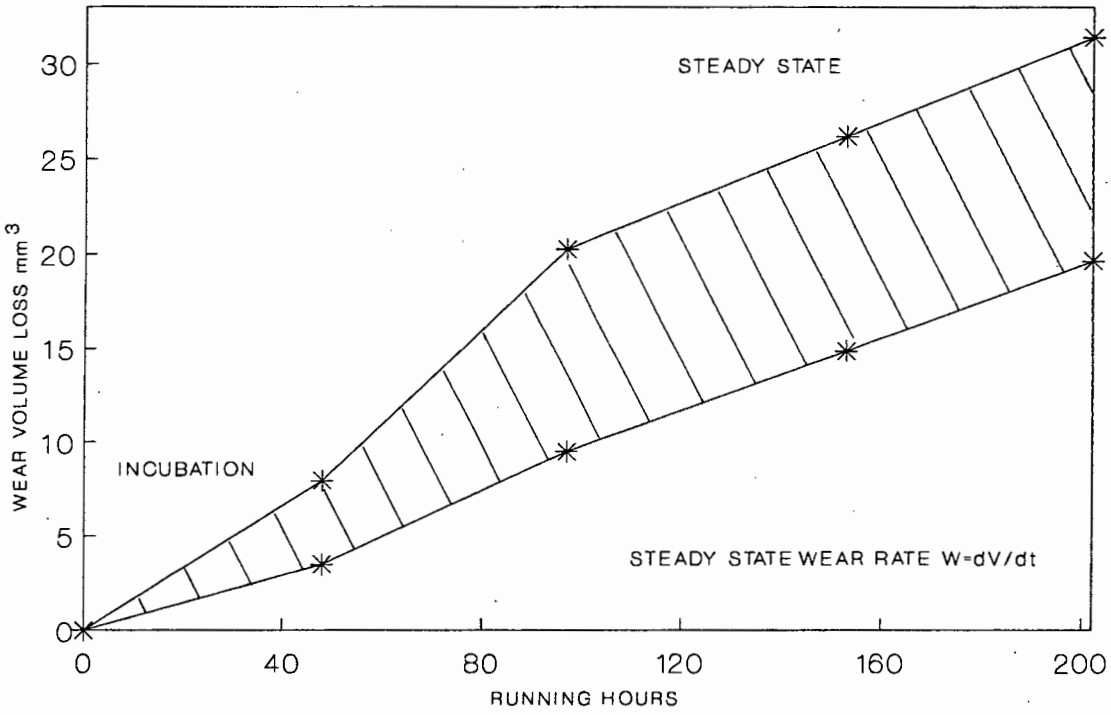

Figure 5.5 Cumulative volume losses with respect to test time for test pieces. Note the presence of incubation and steady state regimes. All test grades displayed trends falling within the shaded area.

Hence a clearer method of presenting the data would be to relate the steady state wear rate of the references to position of reference pieces across the blade periphery. (Fig. 5.6) The steady state wear rate is very consistent across the blade, with a variance of +- 11.6 percent, which is quite acceptable for an in situ test, bearing in mind that control of ash throughput and moisture content in the conditioner, fluctuates all the time. This observation relates well to past experience gathered from inspection of worn blades. It has been observed that the rate at which the blades wear down decreases linearly with the decrease in blade length. That is, the decrease in sliding distance covered by the blade periphery as the blade wears down causes a correlated decrease in wear rate. In addition to this, the blades maintain concentricity with the path of rotation. (Fig. 3.4)

The relationship between steady state wear rate and position across the blade can now be used to normalise data obtained by mass loss measurement of the test grade pieces.

5.2.3 Wear Rates of Test Grades

Volume losses with respect to time of the test grade pieces assumed the same behaviour as characterised by the reference pieces. This is not surprising as all the test grade pieces experience movement against the same encrusted ash as do the reference pieces. The high and low close values for the calculated wear rates were very narrow ranging from less than +- 1 percent up to +- 7 percent for some grades. (Table 3) Wear rates for the various grades differ significantly with a factor of difference in performance of 70 times between best and worse. In Figure 5.7, grade S20, a 20 weight percent Co grade with 2 micrometre sized equiaxed grains represents the performance of the reference material. The prefix K denotes a grain size of 1.5 micrometers, S denotes 2 micrometers, T denotes 3 micrometers, G denotes 4 micrometers and J denotes 8 micrometers. The numbers which follow the prefix indicate the weight percent cobalt binder. The relative wear resistance (RWR) term in Figure 5.7 refers to the reciprocal of wear rate which are normalised by setting the RWR of S20, the reference material to unity. The reference used in this test, S20, outperformed the medium carbon steel previously used for

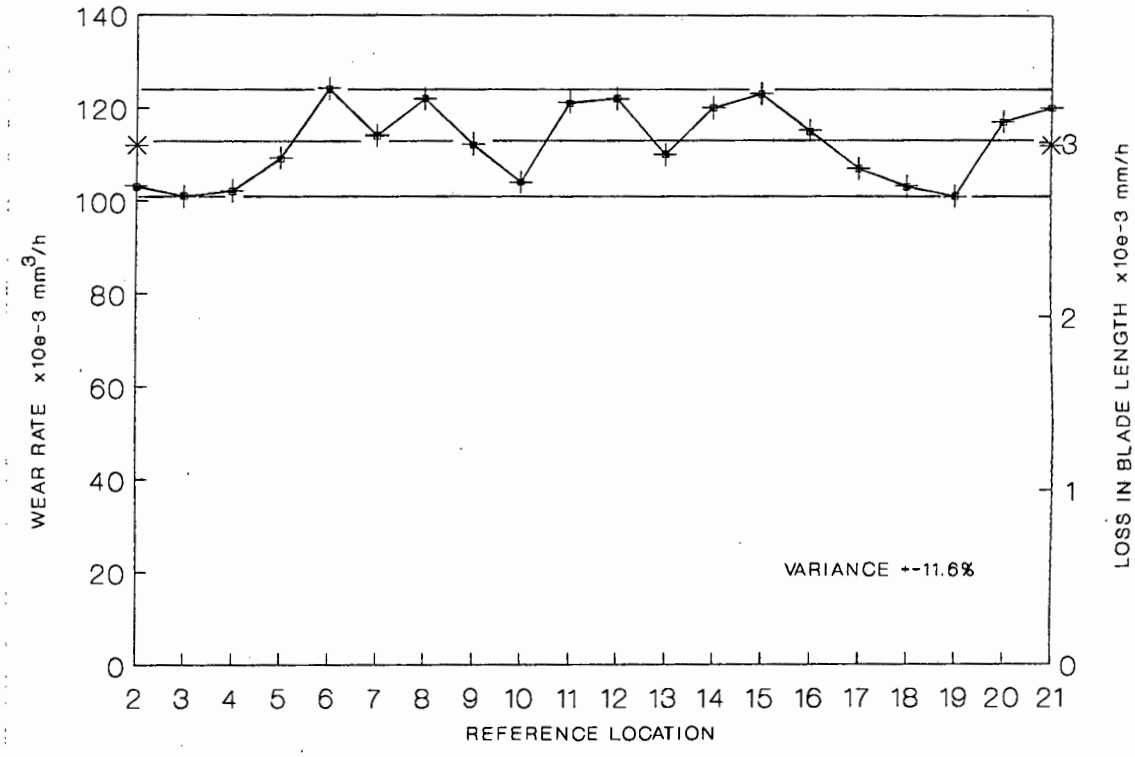

Figure 5.6 Steady state wear rates for the reference pieces as a function of position along the blade periphery.

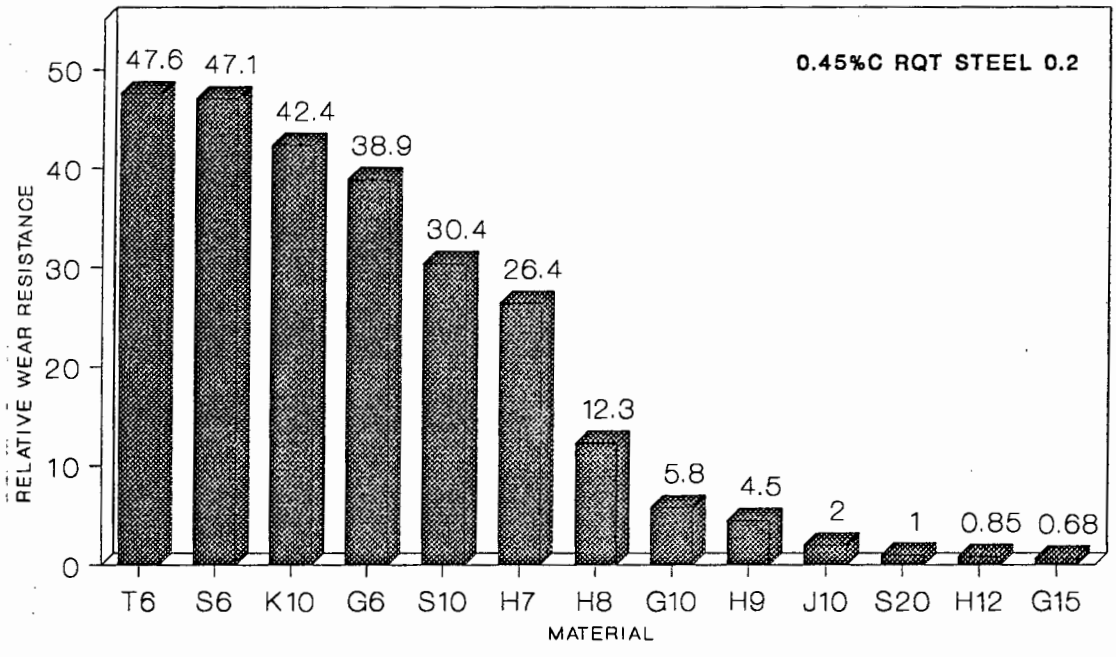

Figure 5.7 Relative wear resistance values for the test materials normalised against the reference material, S20.

the blades by a factor of 4.9 times. In a value judgement that follows, this factor can be used for relating performance to the baseline established through past experience with the medium carbon steel. From the results it is clear that the grades S6, T6, G6 and K10 provide the highest performance. The reasons for the significant differences in performance between the various test grades are related to a mechanistic responce to microstructural characteristics and mechanical properties.

5.3 Performance and Microstructure

Cermets can be described as aggregates of carbides in which the interstices between carbides are filled with binder matter. The make up of WC-Co cermets consists of tungsten carbides and a ductile cobalt matrix. For high carbide fraction cermets as tested here, the carbide network is essentially continuous, thereby forming a skeleton. The binder provides a mechanical three dimensional vice on the carbides as well as being chemically bound to them [16].

The microstructural parameters central in determining the wear resistance in a particular wear system are mean carbide grain size, volume fraction of cobalt and contiguity of the carbide phase. These factors in turn contribute to the mean free path in the binder content, between carbide grains.

The steady state wear rates for a well defined family of WC-Co alloys as a function of volume percent Co binder are presented in Figure 5.8. It is immediately obvious that the binder content has a strong influence on the wear performance of these alloys in this particular environment. This is reinforced by the log-linear relationship between binder content and wear rate. In particular a sharp increase in wear rate results as binder content is increased beyond 10% volume percent. Once this transition is passed the wear rate becomes less sensitive to binder content. The binder content in WC-Co alloys has a strong effect on the mechanical properties of these materials. For instance a relation between bulk hardness and wear rate (Fig. 5.9) also reveals a corresponding transision in wear behaviour for WC-Co alloys having a hardness less than 1200 HV30. All the alloys having a hardness less than 1200 HV30 have a binder content in excess of

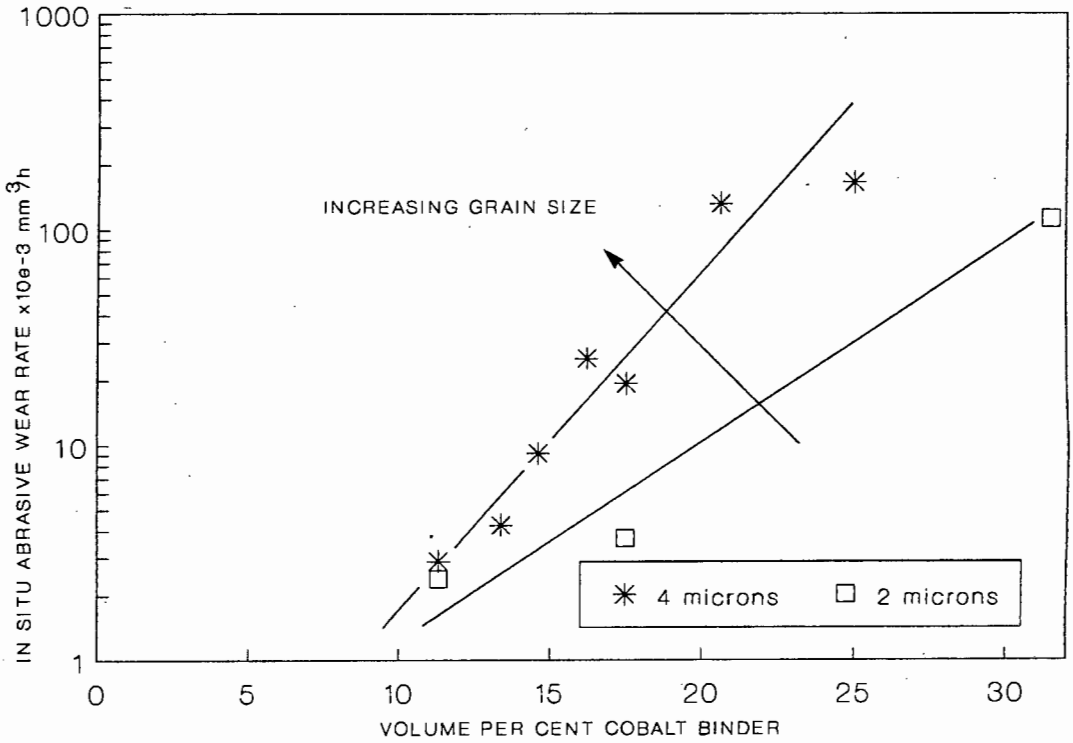

Figure 5.8 Steady state wear rates for the test materials as a function of volume percent Co binder.

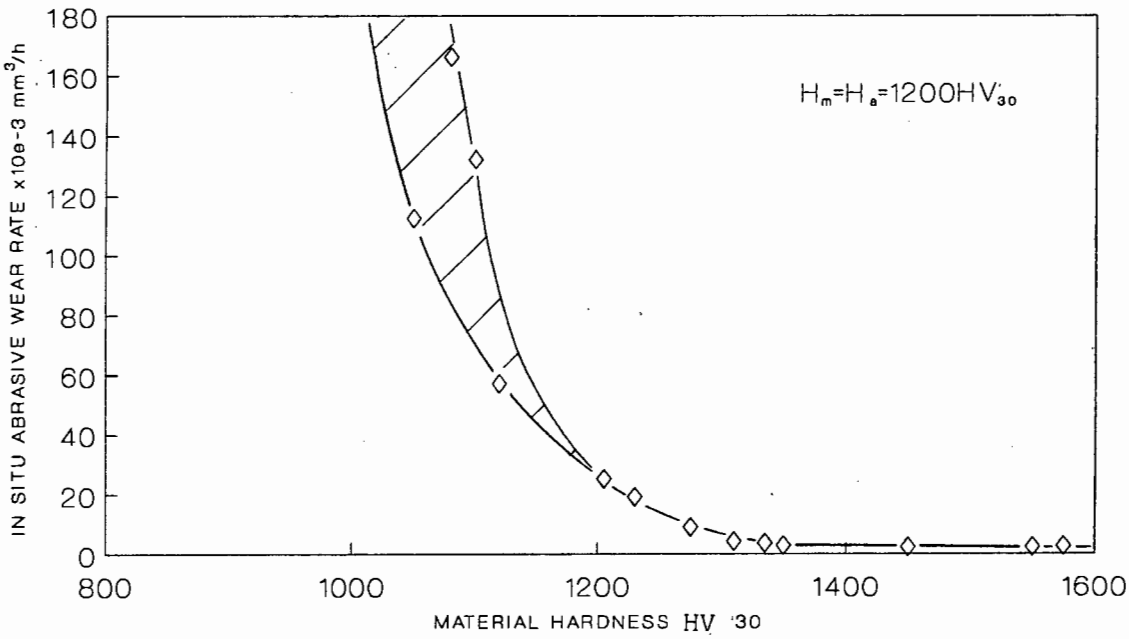

Figure 5.9 Relation between steady state wear rates for the test materials as a function of bulk material hardness.

17.5 volume percent, with the exception of a very coarse grain, 17.5 volume percent grade.

Not surprisingly carbide grain size also influences wear rate of WC-Co alloys in this system. (Fig. 5.10) An increase in grain size for WC-Co alloys with 11.3 to 17.5 volume percent Co binder is presented as a function of wear rate. Alloys with an average grain size of 3 micrometers and less were found to have similar wear rates despite an increase in binder content. However as the average grain size approaches 4 micrometers there is a discernable increase in wear rate with increasing binder content. This strongly suggests the manifestation of a critical grain size of approximately 3 - 4 micrometers as the binder content increases from 11.3 to 17.5 volume percent. As the grain size is increased yet further to an average grain size of 8 micrometers a high wear rate is maintained.

The free path between the carbide grains is determined by the binder content carbide grain size and grain phase contiguity. The mean free path increases with increasing grain size and volume percent binder, and decreases with increasing contiguity. Hence it is to be expected that the mean free path contributes to playing a role in determining the wear rate for a particular WC-Co alloy.

As the mean free path increases, the wear rates for the WC-Co family of alloys tested, increases to a maximum at a mean free path of approximately 1.2 micrometers. (Fig. 5.11) Beyond this value the wear rate decreases noticeably. This transition in behaviour suggests a mechanistic change in the wear process at microstructural level. The degradation mechanisms at play have been studied under the scanning electron microscope in order to elucidate the events that lead to the described behaviours and are refered to in the discussion on wear mechanisms in section 5.5.

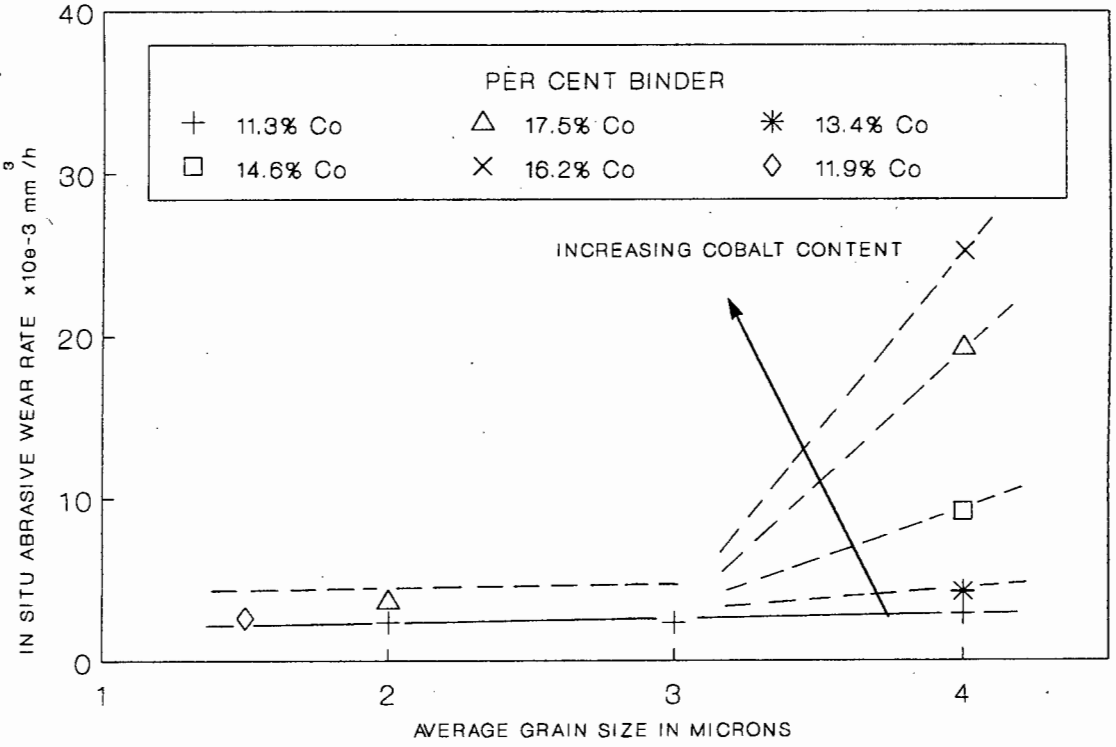

Figure 5.10 Effect of carbide grain size on steady state wear rates. Note the effect of increasing Co binder content.

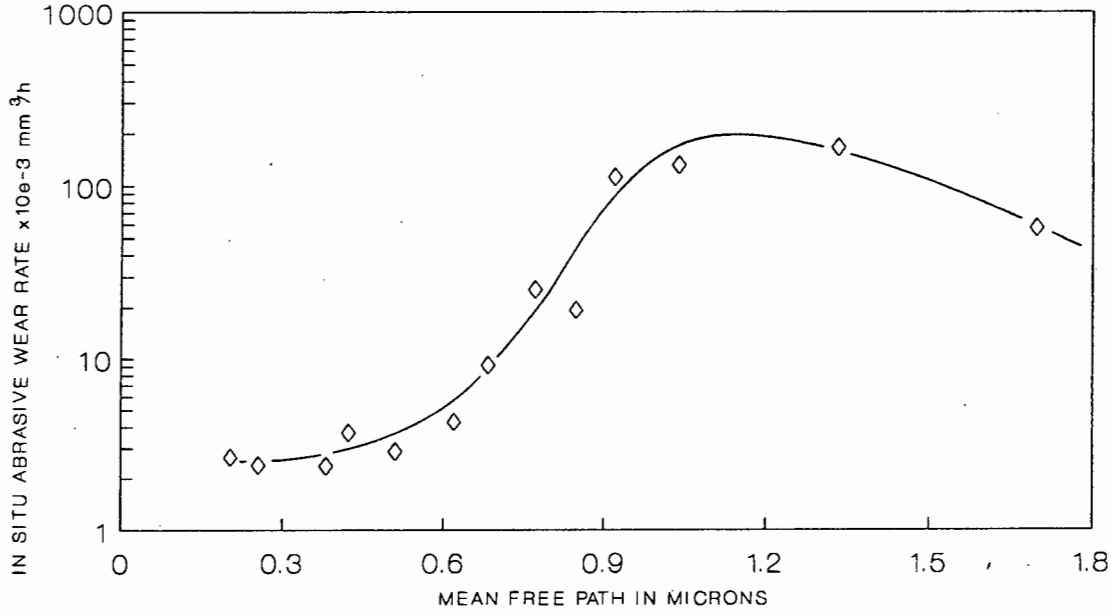

Figure 5.11 Effect of mean free path between carbide grains on steady state wear rates.

5.4 Performance and Mechanical Properties

5.4.1 Effect of Hardness

A transition in wear rate has been demonstrated in the past for metals and alloys sliding against abrasives of low hardness. [7, 25] The difference in hardness between the surface material and the abrasive particle mainly determines the resulting abrasive wear of the surface. The transition occurs in a band where the abrasive is too soft relative to the material to cause sufficient penetration and consequent material removal due to sliding between penetrated particle and material surface. For a homogeneous material the change from low wear to high wear level occurs in a narrow hardness interval of the abrasive. This transition corresponds to a situation where the two opposed surfaces in contact have about the same hardness. For a heterogeneous material like cemented carbide, the interval is broader as an integrated result of the different constituents [21]. (Fig 5.12) For most steels and alloys the transition is of little importance, since commonly occuring abrasives are for the most considerably harder than the material. However in this particular system the hardness of the abrasive 1200 HV30, falls in the range of hardnesses for the WC-Co test materials, 1000 - 1600 HV30. This means that the fly-ash particles, the abrasive in this case, will have a very pronounced effect on the ranking for abrasion resistance of the WC-Co alloys tested. If the abrasive was hard relative to all the test materials, the abrasion resistance would be similar. [22] In Figure 5.9, describing WC-Co test material hardness relative to wear rate, a clear transition occurs at 1200 HV30. This corresponds directly to the hardness of the abrasive fly-ash particles, thereby being in good agreement to existing theory. From the above discussion it appears that the most lucid interpretation for wear performance in this case is addressed at a microscopic level. Hardness, which appears to be purely a mechanical property, when related to micro-events occuring at the surface, assists in a qualitative description of the material removal mechanism. This is discussed under section 5.5.

5.4.2 Effect of Toughness

Toughness can be interpreted as the ability to withstand fracture. Toughness steadily increases with increasing cobalt content and increasing WC grain size in WC-Co cemented carbides. The fracture mechanisms in WC-Co cemented carbides are transgranular cleavage fracture of WC particles, intergranular fracture of WC-WC grain boundaries, and finally ductile shear fracture of the binder phase. [16] Although the amount of transgranular carbide fracture increases with increasing carbide grain size, the toughness is primarily dependent on the amount of shear fracture within the binder phase. Both an increase of the carbide grain size and an increase of cobalt content will imply broader interlayers between adjacent carbide grains and thus an increased amount of fracture.

Fracture toughness can be estimated by different methods. One of these methods is to determine the integrated product of force and deformation up to fracture when determining transverse rupture strength. The physical dimension for toughness will then be energy. The determination can be carried out on a ground 4-point loaded test specimen. Since the values are dependant on specimen dimensions, values are only relative, and suitable only for comparison. (Fig.5.13) By comparison to wear rate as a function of binder content and grain size (Fig. 5.8) there is no justification in using toughness as a lucid explanation for the wear behaviour since the noticable transition in wear rates has no parallel in the relation between toughness and binder content. Since the increase in wear rates with increased binder content are in loose agreement to increase in toughness with binder content, it may be stated that toughness does not imply improved wear resistance. Increased toughness may however have cause and effect for the maximum in Figure 5.11. The WC-Co alloy falling past the maximum in Figure 5.11 has a very coarse grain structure and a high binder content. The real toughness of this material may in some part, start playing a role in the wear performance by compromising the strength but resisting ductile shear fracture in the binder.

It can be argued that in a transverse rupture energy test, Charpy impact test or linear elastic fracture mechanics approach (K_{Ic}), fracture is macroscopic and controlled by a predominant fracture mechanism over a

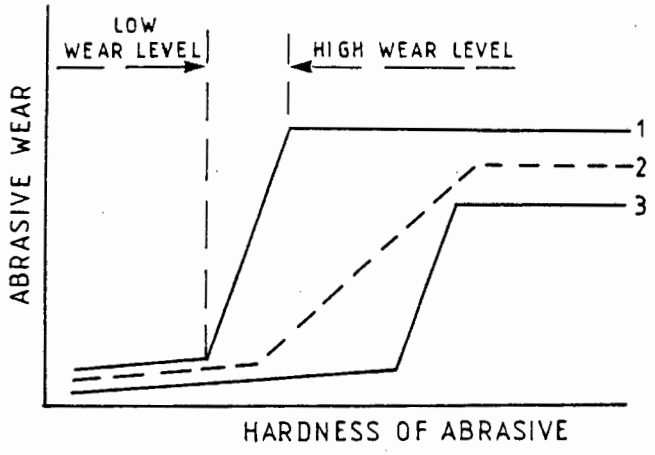

1 SOFT HOMOGENEOUS MATERIAL
2 INHOMOGENEOUS MATERIAL
3 HARD HOMOGENEOUS MATERIAL

Figure 5.12 Influence of abrasive hardness on the abrasive wear behaviour of homogeneous and heterogeneous materials.

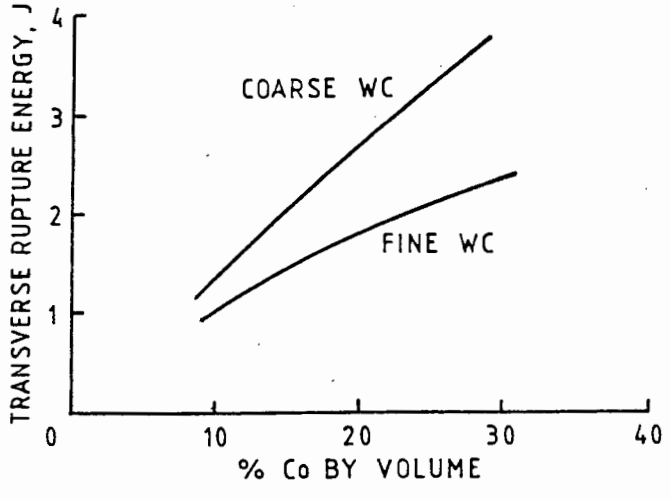

Figure 5.13 Influence of cobalt content and grain size on the toughness of WC-Co alloys as determined by transverse rupture tests. After Sanvik [21].

volumetric span of material, whereas in a surface wear process, many mechanisms may prevail simultaneously often acting synergistically. To compound this, in a heterogeneous material system, fracture on a microscopic scale caused by wear on the surface may follow a very different sequence of events to fracture encountered in a bulk material state [12]. It is likely that more progress is to be made by qualitatively describing the wear process in terms of material microstructure, in an attempt to elucidate the behaviour.

5.5 Discussion on Degradation Mechanisms

5.5.1 Mechanical Degradation

Preferential binder removal is observed in all the WC-Co grades tested. Binder is removed between grains leaving them poorly supported. Where a number of grains are in very close packing, indicative of low binder content grades having high contiguity, binder removal has been retarded. (Fig. 5.14) The plastic constraint in the binder is significant in such a packing arrangement and hence the extrusion of binder caused by relative movement of grains, is limited. In alloys where the contiguity is considerably lower, binder removal has been more noticeable . (Fig. 5.15)

Alloys with high binder content show evidence of relative movement of grains resulting in ductile shear of binder between grains. Forces which arise in this displacement even result in transgranular fracture of carbide grains. (Fig. 5.16) Deformation tracks of approximately 20 micrometers in diameter were also observed which correspond well to the diameter of large fly-ash particles. This provides support to the discussion on the affect of abrasive hardness relative to bulk material hardness put forward in section 5.4. As the bulk hardness of the material becomes similar to that of the fly ash particles, these particles become effective in causing significant material displacement comprising of binder and carbide grains.

This can be contrasted by the removal of discreet grains in grades of WC-Co having hardness significantly greater than that of fly ash particles. (Fig. 5.17)

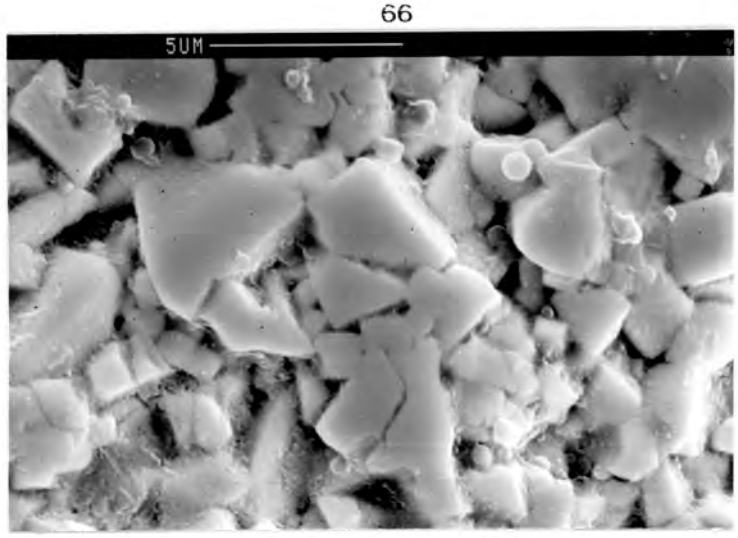

Figure 5.14 Retarded binder removal in a low binder content WC-Co alloy having high contiguity.

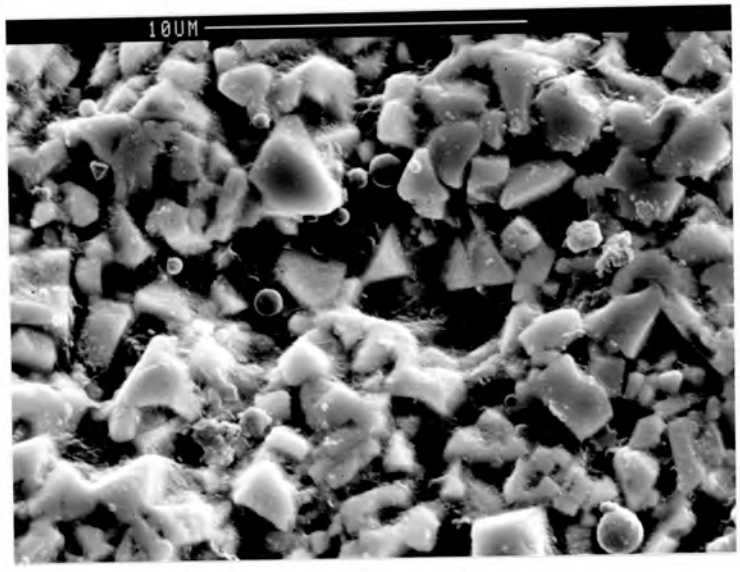

Figure 5.15 Significant binder removal in a high binder content WC-Co alloy having poor contiguity.

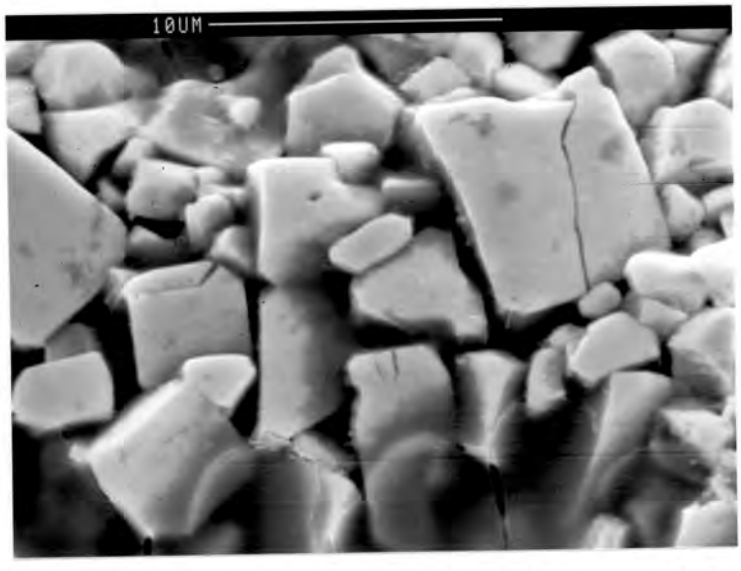

Figure 5.16 Relative displacement of carbide grains resulting in transgranular fracture of grains.

A feature typical of the low binder content alloys is the presence of potholes of the order of a discreet grain size, where a grain has been plucked from the binder. This would result from carbide grains which are only bound on some of the grain sides, which are then torn loose by the movement of relatively large abrading particles, or torn out by frictional forces arising at the grain surface and moving particles. (Fig. 5.17) This is particularly noticeable in low binder content alloys which provide a greater number of contact points which are very rigidly constrained resulting in intergranular WC-WC grain fracture and plucking out of grains. As adjacent grains are now less firmly supported this grain hole becomes a site for enhanced removal of further grains. (Fig. 5.18)

As binder content and grain size are increased, ingress of ash particles between grains is observed. (Fig. 5.19) Hence very fine spherical ash particles help in removing the supporting binder phase which in turn may assist in crack initiation of grain boundaries.

In a very coarse grained, 17.3 volume percent grade, a considerable amount of binder smearing was evident. Shear caused by friction between ash particles and the binder, results in tearing of the binder from the surface. Removal of a layer of binder extracts a large amount of grains from the subsurface. (Fig. 5.20) Crack initiation and propagation in the cobalt with an increasing amount of ash particles sliding over the surface results in the removal of a cobalt laminate to which grains are adhered.

5.5.2 Chemical Degradation

Since binder phase depletion at the surface was common to all the WC-Co grades tested, it is logical that a degree of corrosion may have occurred. Examination of a daily log of water chemistry kept over a period of six months for the effluent water used in the ash conditioning plant confirms this. Acidic pH values were recorded on 36 percent of the total analyses. The pH on occasion has been as low as 1.7. The pH value is one of the most important parameters when determining the corrosivity of a medium, but other factors also have a strong influence. Temperature and the amount of dissolved salts, indicated by electrical conductivity, are

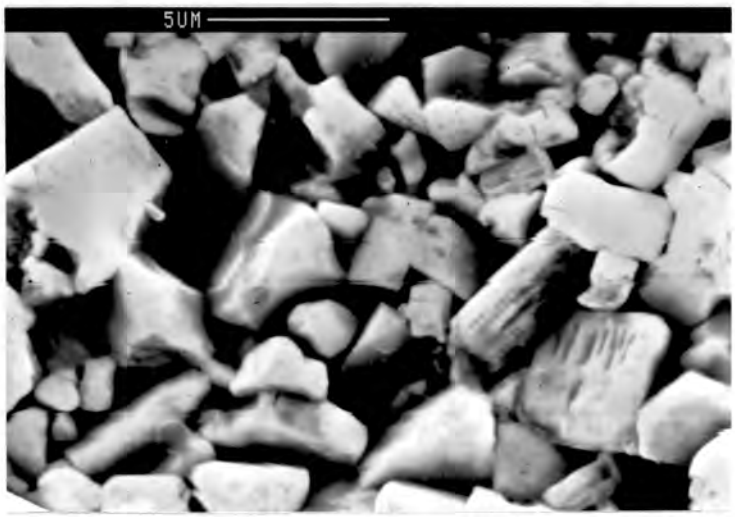

Figure 5.17 Removal of a discreet carbide grain.

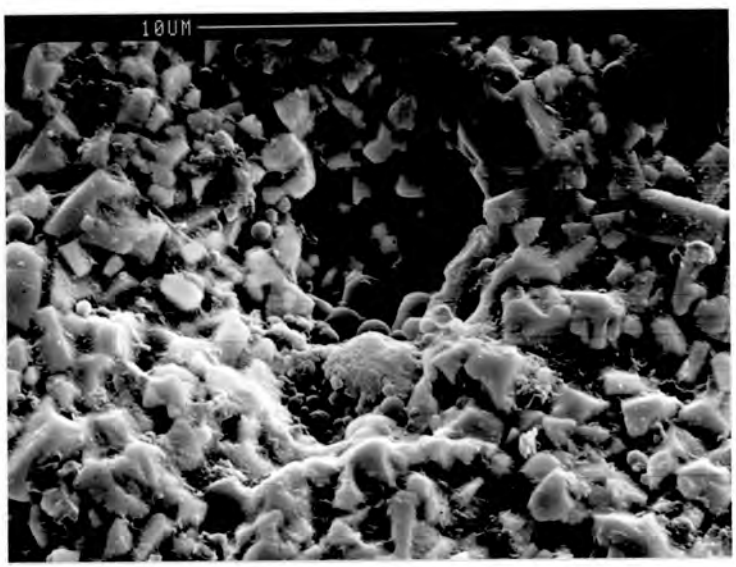

Figure 5.18 Enhanced removal of grains resulting in a cavity.

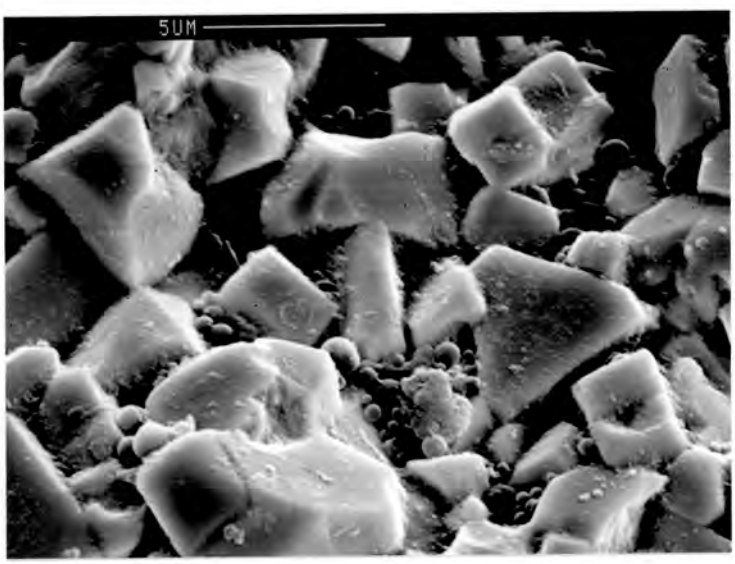

Figure 5.19 Ingress of ash particles between grains giving rise to wedging during subsequent abrasive contacts.

also of prime consideration. The temperature in the ash conditioners is approximately 70°C. Corrosion rates are noticeably higher at temperatures above room temperature for WC-Co alloys in some aqueous solutions [21].

The corrosion rate as a function of the pH value for different types of cemented carbides tested by Sandvik in buffered solutions is presented in Figure 5.21. These tests include a final surface wear treatment by tumbling in order to obtain a true value for the corroded surface zone. As can be seen in the figure straight WC-Co grades are resistant down to pH7. Hence it is certain that corrosion leading to surface depletion of the binder phase occurs in this system.

High concentrations of nitrates, sulphates and chlorides amongst others are present in the effluent water used for blending with the fly-ash. The WC-Co cemented carbides have little or no resistance to attack by sulphate ions [21].

In view of the above findings it is clear that corrosion has occurred, leading to surface depletion of the binder phase and thus the surface region will remain only as a carbide skeleton. The bonds between adjacent carbide grains are, compared to uncorroded conditions, rather weak and the deterioration rate will increase accordingly. It is possible that when the two effects, abrasion and corrosion occur simultaneously, some synergism may occur. The two effects would have to be separated and quantified by means of laboratory testing and compared to the composite effect gained in situ in order to establish this [15, 16]. This programme concentrates on in situ testing in an environment where water chemistry is widely divergent. Hence it is beyond the scope of this work to investigate potential synergism.

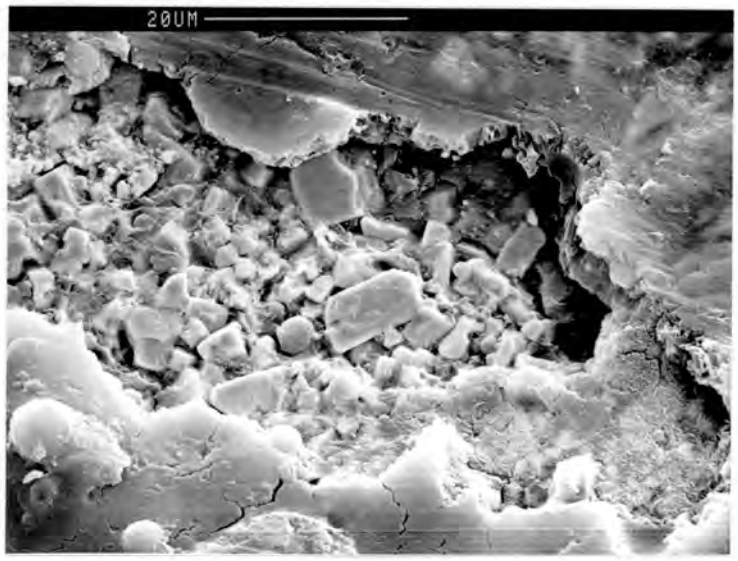

Figure 5.20 Removal of a layer of binder from the surface resulting in removal of many grains.

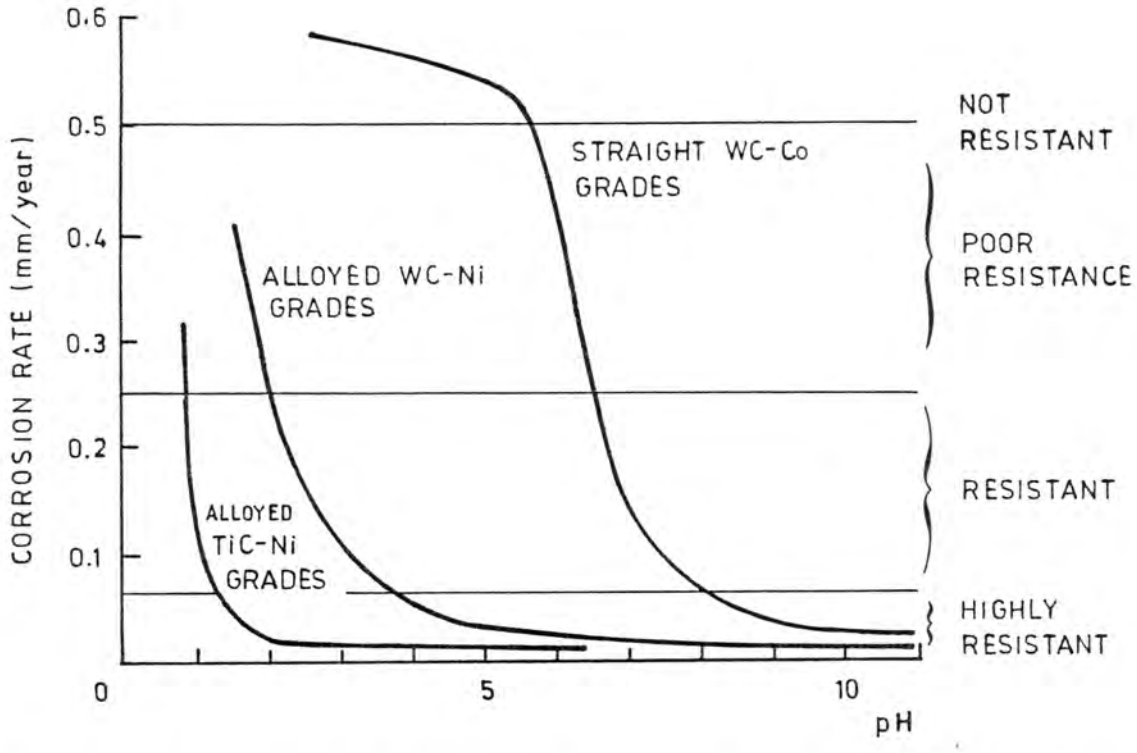

Figure 5.21 Effect of pH on general corrosion rates for cermets. After Sanvik [21].

At low binder phase contents the carbide skeleton is more developed and accordingly such grades exhibit a somewhat higher combined wear and corrosion resistance than corresponding grades with higher binder phase contents. A well developed carbide skeleton imparts rigidity to the carbide grains by mechanical locking at grain interfaces. Reduced free path between grains, also charateristic of low binder content WC-Co grades results in increased plastic constraint at grain-binder interfaces, thereby strengthening the material structure. It has been found that this is central in providing good wear resistance to WC-Co cermets. [26; 27, 28,]

5.6 Schematic of Corrosion - Wear Behaviour

The corrosion-wear behaviour pertaining to WC-Co alloys prevalent in the in situ test environment can be schematically illustrated. (Fig. 5.22) Decreasing strength and rigidity of the carbide grain skeleton and increasing free path between carbides, as the binder content and grain size increase, govern the increase in susceptibility to corrosion and abrasion. At low binder contents and to a lesser extent fine grain size the degradation is characterised by localised intergranular fracture of WC - WC grain boundaries and removal of discrete grains, which is repeated at the removal site. At high binder contents and coarse grain structures, the controling mechanism of abrasion is the ductile shear occuring in the binder phase as abrasive particles have sufficient compressive strength (related to ratio of hardness of abrasive to bulk hardness of material) to resist fragmentation and consequently plough aside furrows of carbide and binder. Corrosion of the resulting weakened binder phase then results in accelerated loss of carbide grains. This is assisted by transgranular fracture of carbide grains which occurs in this process due to the constraint imposed upon grains during ductile shear of the binder.

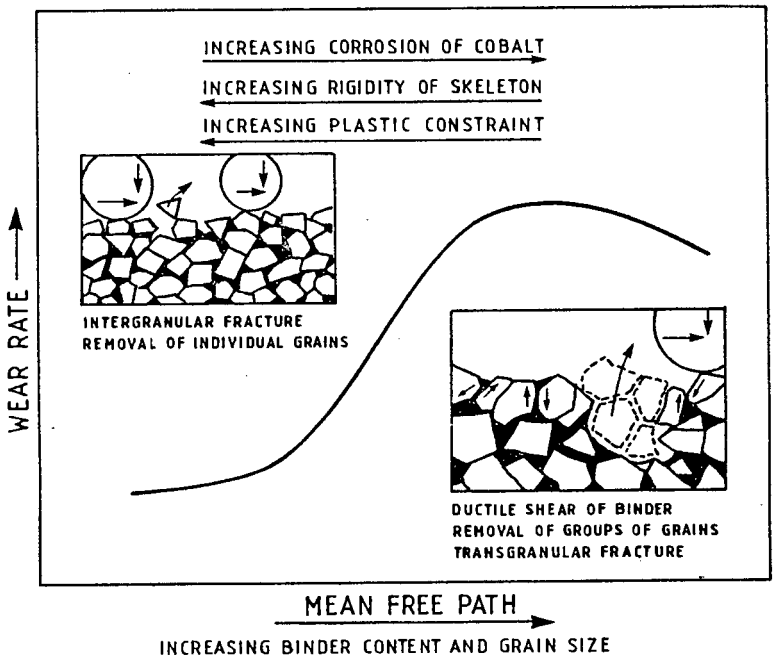

Figure 5.22 Schematic illustration of the corrosion - wear behaviour for WC-Co alloys employed in wet fly ash systems.

Conclusion

Of the grades tested low binder, fine grain size WC-Co cemented carbides are the most suitable for this particular application. Suitable designs of application and cost analyses are presented in Chapter 6. These WC-Co materials are compared to the performance of structural ceramics evaluated in the following chapter.

CHAPTER 6

IN SITU TESTING OF STRUCTURAL CERAMICS

A variety of structural ceramics have been tested in situ by means of a similar test design employed for testing WC-Co cermets, described in the previous chapter. The test materials include eight grades of sintered alumina, with alumina content ranging from 88 percent to 99.9 percent. Very fine grain and a coarser grain Y_2O_3 stabilised TZP (Tetragonal Zirconia Polycrystal) were also tested along with sintered silicon carbide. Wear rates are presented for the test materials and a performance ranking discussed in terms of microstructure, mechanical properties and abrasion mechanisms.

6.1 Test Design

A test design very similar to that employed for the testing of WC-Co cermets has been used. (Fig. 6.1) The test pieces are shaped in the form of circular discs. This was the most practical shape for cutting the test specimens. Specimens were cut using a cored drill and diamond ground to provide a disc diameter of 10mm. The surfaces were then ground and polished to a finish of 1 micron, using diamond paste. The use of circular specimens meant that the test specimens had to be separated in order to prevent shielding of less wear resistant specimens.

Each test specimen was provided with a reference disc of the same geometry. All references were cut-off from a bar machined from a medium carbon steel plate that represents the material previously employed for the construction of the conditioner blades. The steel bar was cut so that the face of the reference discs were perpendicular to the rolling direction. This corresponds to the periphery of a blade which is exposed to wear. The reference discs were ground and polished to remove any work hardened material. Each ceramic test piece was allocated a reference piece. Positioning of the reference piece relative to the ceramic test piece ensured that both reference and test pieces would receive the same particle abrasion events.

Figure 6.1 Lay out of ceramic test pieces and medium carbon steel references.

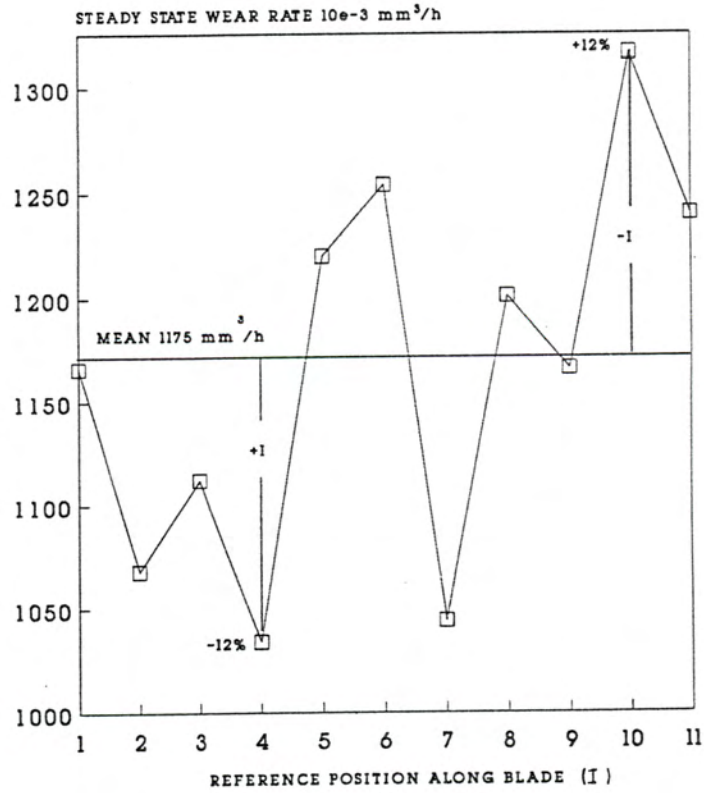

Figure 6.2 Steady state wear rates for the references as a function of position across the test blade.

Test specimens and reference pieces were accurately weighed at intervals of service to determine wear rates for the various test materials. The test was not repeated as it had been established from similar testing of WC-Co cermets that this method of testing yielded good reproducibility.

The microstructural parameters and mechanical properties of the test materials are presented in Table 4.

6.2 Results and Discussion

Steady state wear rates for the medium carbon steel references can be presented as a function of position across the test blade periphery. (Fig. 6.2) On this figure position I_1 through to I_{11} are used as wear intensity factors for normalising the test material results. If the wear rate shown at any position I is below the mean the correction factor for normalising the test material result will be >1 and if above the mean, will be <1. The variance for the reference wear rates is +- 12 per cent which is reasonable for in situ testing considering the difficulties in controlling all parameters.

The normalised cumulative volume losses for a family of alumina ceramics, two TZP's and a sintered SiC are presented in Figure 6.3. The sintered alumina ceramics which performed best had either a fine grain size or a high alumina content. Where a particular alumina has a combination of both these microstructural aspects, as in the case of 88% alumina, Table 4, superior wear resistance results. This is explained in terms of the discussion on wear mechanism in section 6.3. All eight grades of alumina have a bulk hardness significantly greater than that of the abrasive fly ash particles. Hence from observation in Chapter 5, it is not expected that abrasive hardness would cause any noticeable transitions in wear performance. There is no linear correlation between material hardness and wear performance for the aluminas tested, rather there is a band of similar performance for the aluminas as hardness increases. (Fig. 6.4) The two grades of alumina which provided the best performance had good toughness relative to the other aluminas. (Table 4) This suggests that a degree of toughness is required, in addition to certain microstructural parameters, in order to

Table 4

Description and in situ wear rates for structural ceramics tested

material	$HV_{0.5}$	K_{Ic}	density	av. grain size	morphology	steady state wear rate	
		MPa $\sqrt{m}$	g/cm^3	µm		$10e-3mm^3/h$	test position
88% alumina	1650	-	3.46	1.5	equiaxed	7.8405	1
90% alumina	1750	3.8	3.68	2.5	equiaxed	7.3210	5
90% alumina	1500	3.9	3.60	6	lenticular + equiaxed	14.8951	7
94% alumina	1510	-	3.62	7	equiaxed	13.4980	8
97% alumina	1600	-	3.72	4.5	equiaxed	10.0376	4
97.5% alumina	1630	4.6	3.80	7	equiaxed	11.9491	3
99.5% alumina	1550	5.0	3.89	20	equiaxed	6.1274	6
99.9% alumina	1700	4.5	3.92	1	equiaxed	4.5601	11
SiC	2400	3.2	3.14	10	platelet	7.6348	2
5m%Y_2O_3-TZP	1350	6.0	6.05	0.35	spherical	18.8122	9
5m%Y_2O_3-TZP	1250	10.0	6.05	1	spherical	21.5703	10

* S.E.N.B.

Note: Steady state wear rate for Medium Carbon Steel : 1175 X 10^{-3} mm^3/h $\pm$ 12%

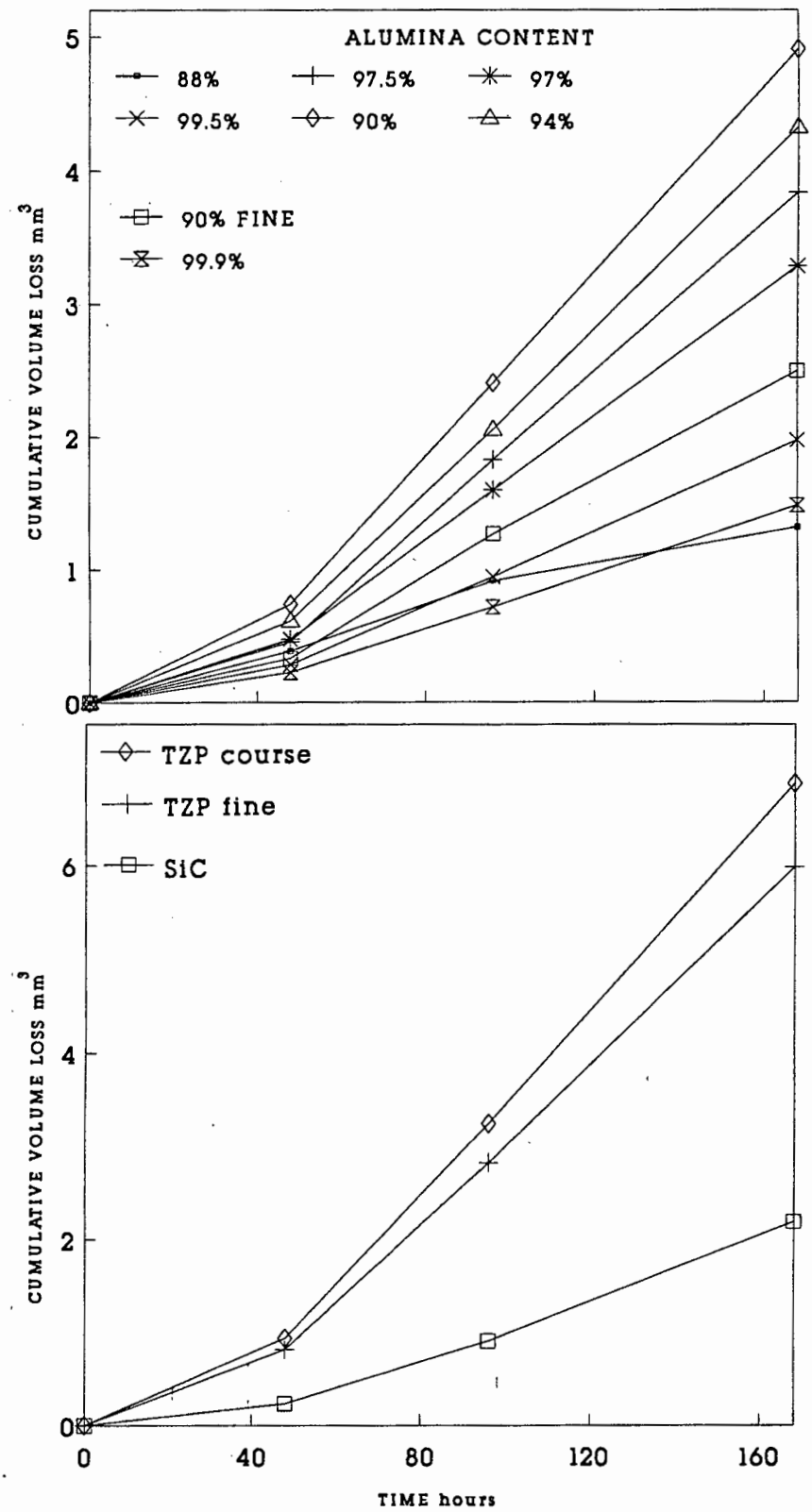

Figure 6.3 (a) Cumulative volume losses for a family of alumina ceramics tested.
(b) Cumulative volume losses for sintered SiC, and two Ytria stabilised Tetragonal Zirconia Polycrystals (TZP).

provide superior performance. However there was no clear linear correlation between wear rate and toughness. Sintered silicon carbide provided performance comparable to that of the best performing grades of alumina. While SiC has greater compressive strength and hardness than the top grades of alumina, some toughness is compromised, which may be responsible for some loss of performance.

At this point it is necessary to note that some workers [12, 29] have found that the fracture toughness approach to wear modeling for ceramics does not materialise as the assumed linking of radial and lateral cracks does not occur in most wear events. Rather the scale of fracture is of the order of grain sizes whereas the radial and lateral cracks from which toughness is determined, are of the order of size indentations.

The two TZP's tested provided noticeably poorer performance than the other ceramics tested. The grade with the higher bulk hardness but lower toughness provided better performance, than did the other TZP grade. It is to be noted that the bulk hardness of TZP is approximately the same as that of the abrasive fly ash. This could explain the noticeable decrease in performance afforded by TZP. As the transition to the hard abrasive area (Fig. 5.12) is approached increased wear is expected. This is in agreement to findings of this test.

It is notable that of the two grades of TZP tested, improved wear resistance is afforded by the grade having a finer grain size and higher hardness. As the toughness is lower, it is arguable that fracture does not predominate in the wear process for TZP's in this particular system. For the aluminas toughness is seen to be an important property, suggesting that fracture predominates in the wear process of aluminas.

Hence it is proposed that the ratio of material hardness to abrasive hardness is most significant in determining the mechanisms of wear occurring in the TZP samples.

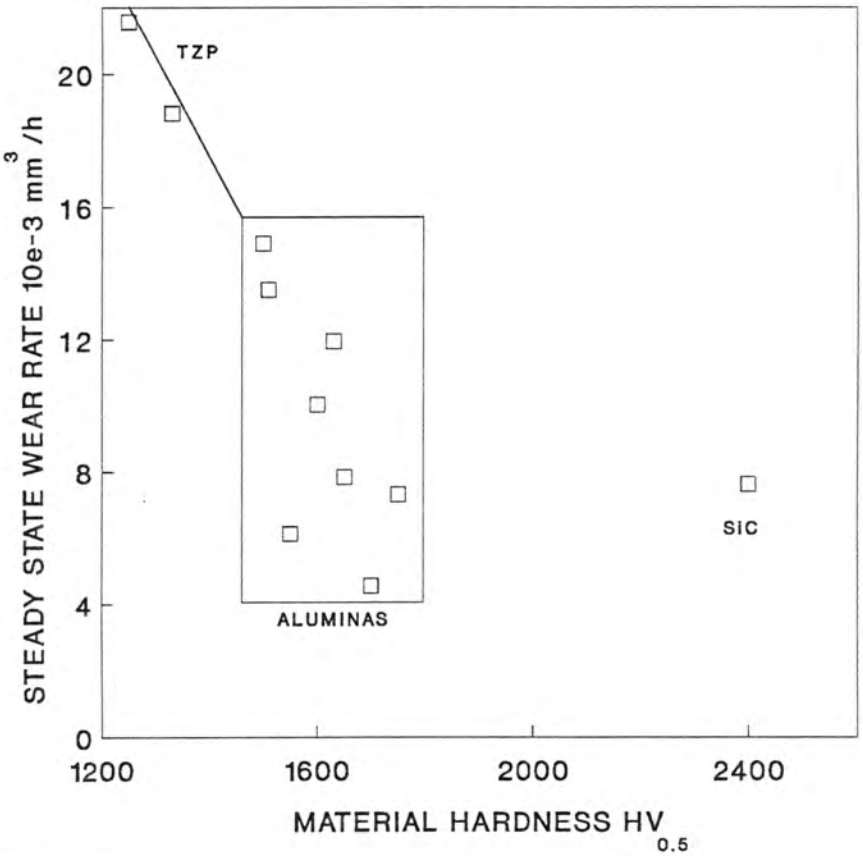

Figure 6.4 Relation between bulk material hardness and steady state wear rate.

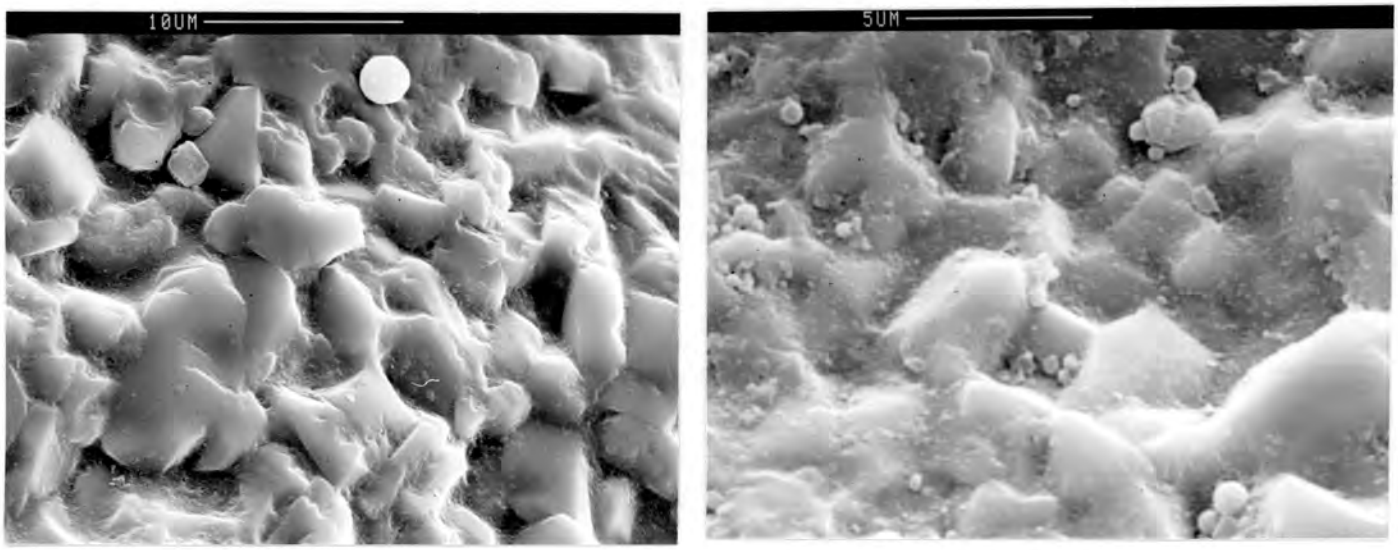

Figure 6.5 Intergranular fracture of alumina grains.

6.3 Wear Mechanisms

Steady state abrasion surfaces generated by in situ testing were examined in the SEM in order to establish the mechanisms of material removal.

Typically the alumina surfaces all displayed grainy regions with isolated flat regions having underlying intergranular fracture. The steady state wear surfaces in all grades tested was consistent and can be viewed as intergranular crack propogation, leading to removal of grains. (Fig. 6.5)

In view of the above mechanism it is expected that grain size would influence the wear performance of aluminas. The effect of grain size on grain removal is contrasted by Figures 6.6 and 6.7. Simply, the removal of a large grain constitutes significantly more material removal than does the removal of a fine grain. A microstructure having fine equiaxed grains has greater ability to absorb energy from cumulative wear events, in the form of intergranular fracture, over a small localised area, by virtue of its high grain boundary surface area.

The abundance of flat areas were more abundant in SiC and the best performing aluminas. Underlying intergranular fracture was present in these flat areas. (Fig. 6.8) Fracture is resisted until the damage produced by sufficient cumulative wear events, in this case sliding and fragmenting ash particles, result in the connecting up of cracks and the subsequent removal of grains.

Srinivasan and Scattergood [26] have recently established that the relative hardness values of erodent particles and target material, in an erosion system, play a significant role in the erosion rates of brittle materials. It was found that for erodents softer than the target material, erodents fragment on impact. In a steady state behaviour it appeared that lateral crack based erosion mechanisms do operate, but on the scale of grain sizes. For softer erodents (relatively hard materials) damage accumulation is necessary to build up requisite stresses in order to produce lateral cracks.

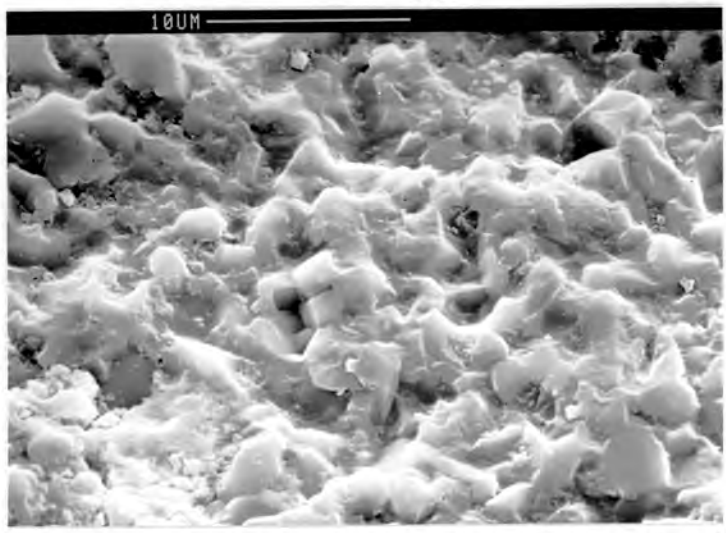

Figure 6.6 Removal of discreet grains in a fine grain alumina ceramic.

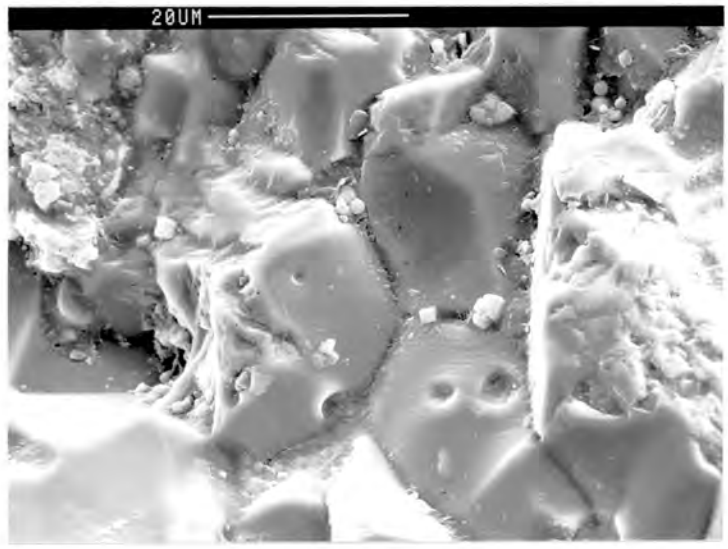

Figure 6.7 Removal of a large grain from a coarse grain alumina.

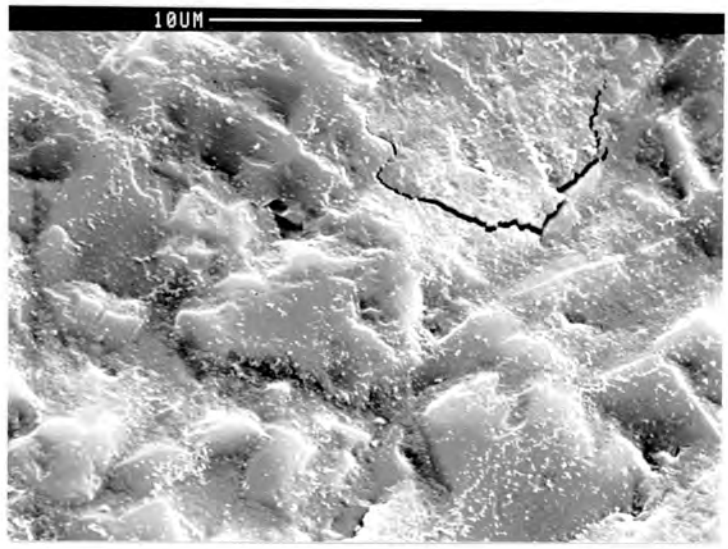

Figure 6.8 Underlying intergranular fracture propogating in a flat surface in SiC.

Evidence of plastic deformation and micro cutting (Fig. 6.9) caused by sliding ash particles were typical features on the surfaces of the two TZP's tested in this programme. Sliding ash particles lead to the formation of wear tracks causing cutting of material and plastic chip formation and removal. Multiple sliding contacts result in fatigue initiation in the wear track leading to delamination and flake removal. The removal of a flake (Fig. 6.10) results in the loss of large amount of material. Hence it is clear that as the hardness of the abrading particles become comparable to that of the test material hardness, a change in mechanism becomes evident. This is supported by the smoothed out appearance of the wear surfaces. It is also likely that the inherent toughness of TZP resists the formation of lateral cracks, and as the hardness is compromised the effect of wear track formation by particles of comparable hardness results.

In summary, superior wear resistance is obtained from aluminas having a high alumina content and fine grain size. This is related to the removal of smaller quantities of material during steady state wear events than would result in coarse grain structures. Silicon Carbide also provided good wear resistance. Clearly the hardness of the wear surface relative to the abrasive particles is important in determining the mechanism of material removal. Where the hardness of the wear surface is significantly higher than that of the abrading particles, intergranular crack propagation depends on cumulative damage from sliding contacts resulting in low steady state wear rates.

6.4 Cost analyses of designs of application

Having obtained time based wear data from in situ testing, it is possible to make value judgements resulting in the optimum selection and specification of suitable materials and designs of application.

An index of wear resistance for the WC-Co cermets and the structural ceramics tested by means of controlled in situ test design, is derived. The medium carbon steel previously used for the manufacture of blades, can be used as a baseline by setting its performance to unity. From past experience, value judgements can then be made concerning the cost effective

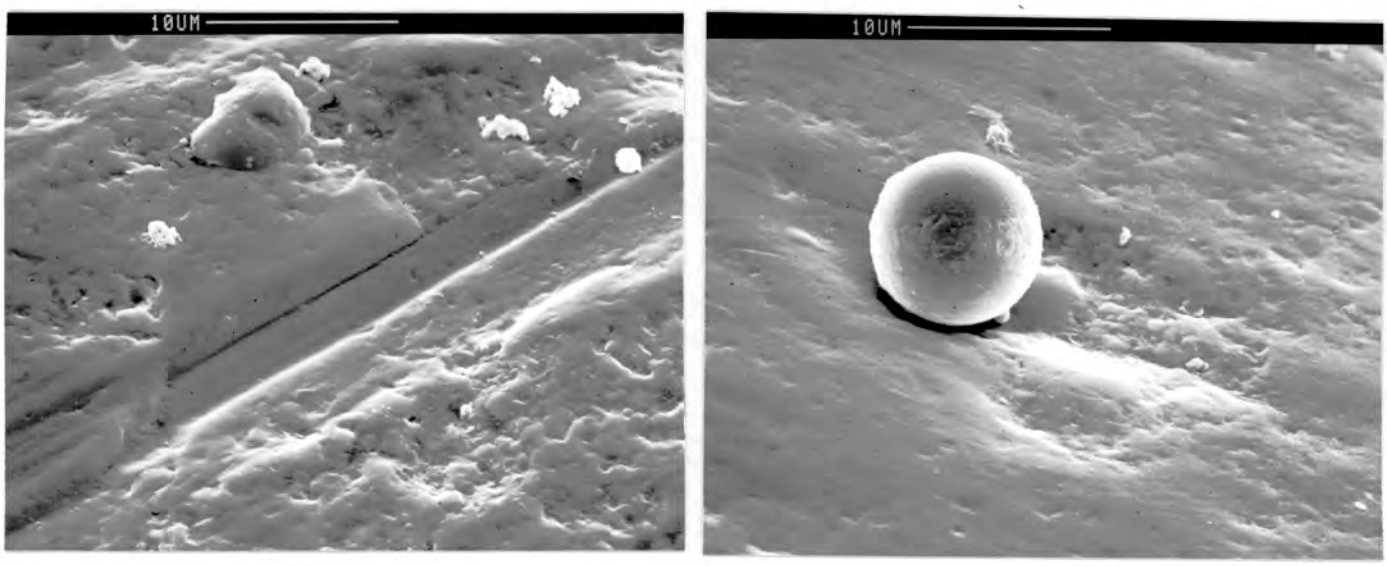

Figure 6.9 Micro cutting on the wear surface of TZP.

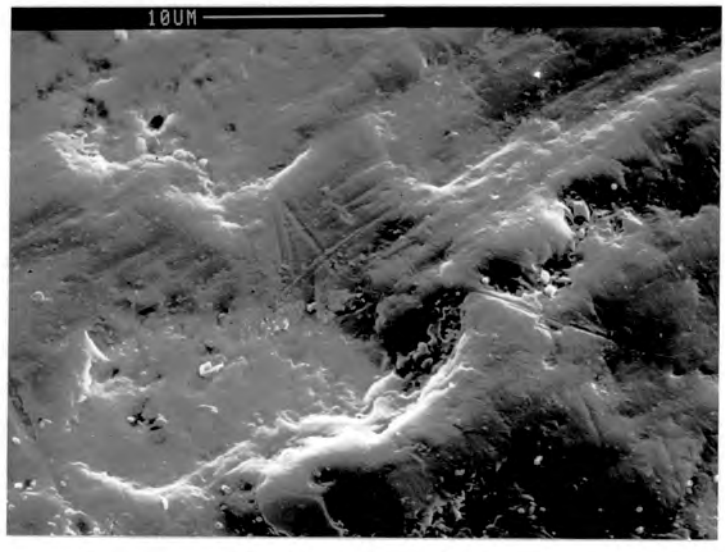

Figure 6.10 Delamination on the surface of TZP resulting from a number of sliding contacts with ash particles.

wear performance of candidate materials. This was made possible by always including the described steel in the in situ test designs. The wear resistance values of the test materials were obtained from the reciprocal of steady state wear rate. By normalising these values relative to the baseline, a ranking of relative wear resistance (RWR) is established. (Fig. 6.11)

In view of performance, the optimum materials for application are, in the first instance, high alumina sintered ceramics having a fine equiaxed grain structure; and secondly, fine carbide grain size, low binder content WC-Co cermets.

To a large extent the service reliability of the material is determined by its design of application. By means of in situ testing it has been shown that a design suitable for application of ceramics could consist of custom shaped cappings which fit over the periphery of the blade and held in position both mechanically and by means of suitable epoxy adhesive. (Fig. 4.9b)

The WC-Co cermets can be suitably applied in the form of tiles which are brazed onto the blade face, in an arrangement which would cover the significantly wearing areas. (Fig. 6.12)

The above designs were submitted to the appropriate industries in order to derive quotations for completely assembled blades. The quantities quoted on, reflect the annual demand for blades within Eskom. The amounts are large and hence the cost of a die set required for manufacture of the WC-Co tiles is low in relation to the unit price of a blade, since this cost is amortised into the total amount of blade required over one year, viz 0.1 percent of the unit price of a blade.

The unit cost for purchasing a WC-Co protected blade which would include complete assembly by brazing the tiles to a steel blade as per Figure 6.12 amounts to approximately R605,00 per blade.

At this stage availability become pertinent to the analyses. High alumina content sintered aluminas having a fine equiaxed grain structure of the

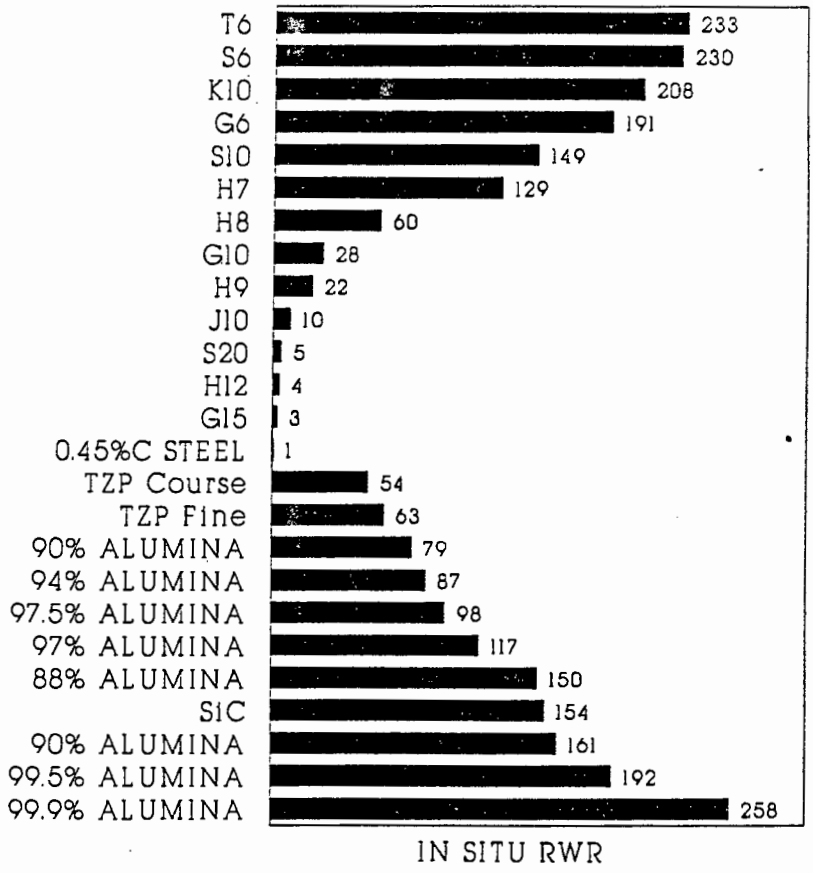

Figure 6.11 Relative wear resistance of all ceramics and WC-Co cermets tested. A Medium carbon steel previously employed is used as a baseline reference i.e. equal to unity.

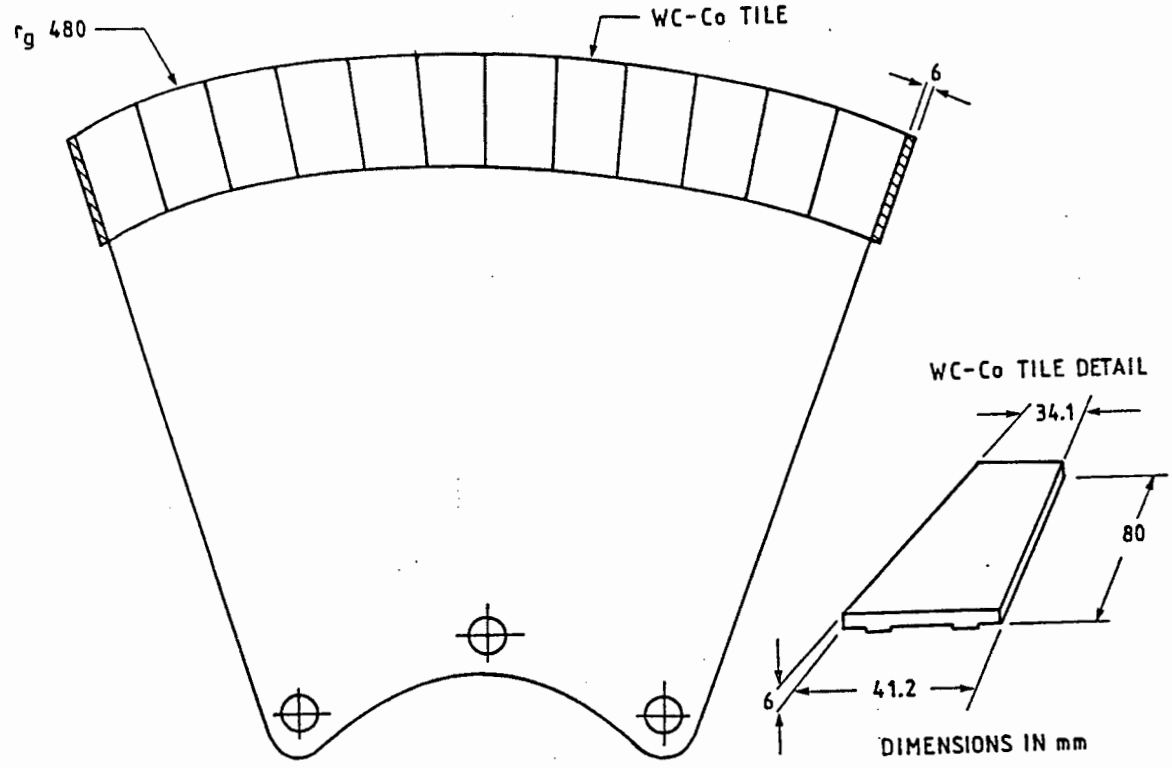

Figure 6.12 Geometry and dimensions of suitable tiles for application on mixer blades. Dimensions in millimetres.

type described by Al_2O_3 grade 8 are not locally manufactured. It is corporate policy in Eskom to replace imported items with as much local content as possible. The reasons for this in this situation are firstly availability and secondly for cost. If blades could not be timeously obtained the availability of a generating unit requiring ash conditioner refurbishment could be jeopardised. To avoid such a catastrophe maintenance personnel will in all probability revert back to the use of steel blades. This would nullify the efforts promoted by this programme of work. For the same reasons no cost analysis was conducted for SiC and TZP materials. However it may be mentioned that the landed cost of imported aluminas of the quality described are approximately four times that of the cost of local aluminas. This scenario worsens considerably for SiC which places the material out of consideration. No material costs were obtained for TZP.

The best performing locally available grade of alumina is characterised by low alumina content and fine equiaxed grain structure. (Al_2O_3, test position 1 in Table 4). The performance of this material relative to the best performing locally available grades of WC-Co cermet (T6 and S6 in Table 3) amounts to 65%.

The unit cost for purchasing a completely assembled ceramic capped blade ready for use as per Figure 4.9 manufactured from the described local grade of Al_2O_3 amounts to approximately R200,00 per blade. (Prices as at December 1988)

Hence the life cycle cost effective benefit of using the described alumina capped blade over the WC-Co protected blade amounts to a factor of two. Due to the large amounts of blade purchases anticipated, other local manufacturers may be approached. (Al_2O_3 3, 4, 5 in Table 4). Use of these materials in the illustrated fashion would only result in cost benefit factors of between 1.06 (3) and 1.55 (5) over that of WC-Co cermets.

Hence it is clear that WC-Co cermets would provide cost effective performance of the same order as that of some locally available alumina ceramics. Therefore it is quite feasible that WC-Co be considered for application in the event of poor availability of Al_2O_3.

6.5 Specification guidelines for ash conditioner blades.

6.5.1 Design

The design of blades for ash conditioners shall consist of a steel blade, 12mm in thickness to which custom shaped ceramic cappings as per Figure 4.9b are attached to the free end.

The cappings shall comprise a number of individual segments each containing a slot within which a portion of the blade is receivable. [19]

6.5.2 Dimensions

The blades are to be profiled such that the cappings do not increase the face area of the original blade dimensions.

6.5.3 Materials and Assembly

The blades are to be plasma cut from 12mm gauge mild steel. The surfaces of the blades to which cappings are to be attached shall be free of irregularities, grease and dirt. These surfaces are to be given necessary surface preparation as stipulated in the instructions for the application of suitable epoxy adhesives.

The cappings are to be attached to the profiled steel blades by means of a water resistant epoxy which is capable of withstanding sustained temperatures of above 70 degrees centigrade.

Care is to be taken that faces between the cappings and steel blades are packed with epoxy to prevent the ingress of water. This may require the use of additional sealants.

The fixing method employed shall accommodate mechanical fastening of suitable form which will ensure that cappings remain secure in the event of epoxy failure.

Suitable installation contractors who are accustomed to handling and installation of ceramics are to install the blades in the ash conditioners.

6.5.4 Operation

Prior to stopping an ash conditioner for long periods, all remaining ash in the bin is to be washed out in order to prevent siltation and blockages. It must be emphasised that ceramics are susceptible to impact resulting from damage that may occur during the removal of ash from the conditioners.

CHAPTER 7

Conclusions

The specific objectives of this programme of work were to:

(a) Evaluate a range of potential materials for use in ash conditioning plant through in situ testing.

(b) Relate wear performance to material constitution.

(c) Produce a ranking order of wear resistance based on cost.

It has been demonstrated that WC-Co cermets and alumina ceramics provide excellent wear resistance in the described application. The wear performance of these materials has been found to increase with decreasing carbide grain size and decreasing binder content in the case of WC-Co cermets; and increase with decreasing alumina grain size and increasing alumina content in the case of alumina ceramics.

Noticeable transitions in the wear mechanism for these materials occurred as the bulk hardness of the material was increased past that corresponding to the hardness of fly ash particles, the abrasive in this particular system. For materials of high relative hardness, wear rates were low and were typified by removal of discreet carbide grains in WC-Co cermets and intergranular fracture resulting in loss of grains in the case of the alumina ceramics. It has been observed that chemical attack of the cobalt binder in WC-Co cermets results in depletion of the binder, thereby assisting the abrasion process. As the material hardness falls below the abrasive hardness, the predominant mechanical degradation mechanism occurring in WC-Co cermets is one of ductile shear of binder located between grains, resulting in the weakening of adhesion of tracks of grains, ultimately leading to loss of groups of grains.

A ranking order of wear resistance based on cost for locally available aluminas and low binder content, fine grain WC-Co cermets establishes these materials in the same order of merit. Suitable methods of application have been proposed for the manufacture of blades utilising the superior wear resistance of these materials.

Extensive improvements in the lives of steel mixer blades in ash conditioning plant can be achieved through the use of ceramic cappings and WC-Co tiles applied to the high wear areas of the blades. Significant cost savings, improvement in availability and performance, through use of the findings of this programme, are envisaged.

REFERENCES

1. Cuddon A, "The abrasive wear of ash-handling plant at Lethabo Power Station". Proc. 2nd Nat. Conf. on Tribology, Johannesburg (1988), 278-290.

2. Moore MA, "Abrasive Wear", paper presented at the Fundamentals and Friction and Wear of Materials, Materials Science Seminar, ASM Mat. Sci. Seminar, (1980).

3. Rabinowicz E, "Friction and Wear of Materials", Wiley, New York, (1965).

4. Ball A, "The mechanisms of wear, and the performance of engineering materials", J.S. Afr. Inst. Min. Metall., Vol. 86, no. 1 (Jan. 1986), 1-13.

5. Krushchov MM; Babichev MA, "Resistance to Abrasive wear of structurally Heterogeneous Materials", Friction and Wear in Machinery, (1958), 12-26.

6. Mutton PJ; Watson JD, "Some effects of microstructure on the abrasion resistance of metals", Wear, 48, (1978), 385-398.

7. Richardson RCD, "The wear of metals by relatively soft abrasives", Wear, 11, (1968), 245-275.

8. Hokkirigawa K; Kato K, "An experimental and theoretical investigation of ploughing, cutting and wedge formation during abrasive wear", Tribology International, Vol. 21, no. 1 (Feb. 1988), 51-57.

9. Mulhearn TO; Samuels LE, "The abrasion of metals: A model of the process", Wear, 5, (1962), 478-498.

10. Murray MJ, Mutton PJ; Watson JD, "Abrasive wear mechanisms in steels", Conf. Proc. on Wear of Materials, Michigan, (1979), 257-265.

11. Zum Gahr KH, "Modelling of two-body abrasive wear", Wear, 124, (1988), 87-103.

12. Ajayi OO; Ludema KC, "Surface damage of structural ceramics: Implications for wear modelling", Wear, 124, (1988), 237-257.

13. Moore MA; Douthwaite RM, "Plastic deformation below worn surfaces", Metallurgical Transactions, 7A, (1976), 1833-1839.

14. Moore MA; Richardson RCD; Attwood DG, "The limiting strength of worn metal surfaces", Metallurgical Transactions, 3 (1972), 2485-2491.

15. Noël REJ, "The abrasive-corrosive wear behaviour of metals", MSc Eng. thesis, Univ. of Cape Town (1983).

16. Barker KC; Ball A, "Steel in an abrasive-corrosive mining environment", Proc. Int. Antiwear 88 Conf., Inst. Metals, London (1988), 22.

17. Lesch W; Cornell DH, "The mineralogy and morphology of fly ash from South African stations", Conf. Proc. on Ash - a valuable resource, CSIR, Pretoria (1987), Vol. 3-13.

18. Cuddon A, "Ash conditioner wear investigation", Eskom Report TRR-T87/022, (1987).

19. RSA Registered Patent No. 87-6173 RSA.

20. Meeting with Boart International, Springs, RSA, (1988).

21. Sandvik, "The properties of cemented carbides".

22. Larsen-Basse J, "Effect of composition, microstructure, and service conditions on the wear of cemented carbides", Journal of Metals, (Nov. 1983), 35-42.

23. Keshavan MK; Jee N, "Abrasion and erosion of WC-Co alloys", Met. Powder Rep, Vol. 42-12 (1987), 866-869.

24. Pickens JR; Gurland J, "Relation of strength, composition and grain size sintered WC-Co alloys", J. Mat. Sci and Eng., Vol. 33-135, (1978).

25. Nathan GK; Jones WJD, "Influence of hardness of abrasives on the abrasive wear of metals", Lubrication and Wear, 5th Conv. Proc., Inst. Engrs., Vol. 181 (1967), 215-226.

26. Ball A; Paterson AW, Proc. 11th Int. Plansee Seminar, Reutte, Austria, Vol. 2 (1985), 377-391.

27. Pennefather RC, "The solid particle erosion of WC-Co alloys", MSc thesis, Univ. of Cape Town (1986).

28. Hankey SE, "Cavitation erosion of WC-Co", MSc thesis, Univ. of Cape Town (1987).

29. Sprinivasan S; Scattergood RO, "Effect of erodent hardness on erosion of brittle materials", Wear, 128, (1988) 139-152.